HARTREE-FOCK CALCULATIONS

RESTRICTED HARTREE-FOCK CALCULATIONS IN LIGHT NUCLEI

by

MARTIN RICHARD DERMOT PATRICK MANNING, M. SC.

A Thesis

Submitted to the Faculty of Graduate Studies

in Partial Fulfilment of the Requirements

for the Degree

Doctor of Philosophy

McMaster University

October 1967

DOCTOR OF PHILOSOPHY (1967) McMASTER UNIVERSITY
(Physics) Hamilton, Ontario.

TITLE: Restricted Hartree-Fock Calculations in Light Nuclei

AUTHOR: Martin Richard Dermot Patrick Manning, B.Sc. (Victoria University, Wellington, New Zealand)
M.Sc. (Victoria University, Wellington, New Zealand)

SUPERVISOR: Professor A. B. Volkov

NUMBER OF PAGES: 213

SCOPE AND CONTENTS:

Restricted Hartree-Fock calculations for light even-even nuclei have been carried out using simple effective interactions. The primary emphasis is on the nature of the intrinsic states, and, in particular, on the deformation of these states. In order to find the equilibrium deformations a representation of deformed cylindrically symmetric states is used. A self-consistent technique for finding the equilibrium size and shape is proposed.

There is a strong secondary emphasis on the role of the effective interaction, and four rather different interactions are used. Two of these incorporate a dependence on the density on the nuclear system, and this density dependence improves the systematic behaviour of the energies and sizes of light nuclei.

ACKNOWLEDGEMENTS

This thesis is part of a continuing study of nuclear structure being carried out by my supervisor, Dr. A. B. Volkov, and by the graduate students working with him. It is natural, therefore, that a large number of the physical ideas which are used in this thesis originate from Dr. Volkov, and many of those which did not arise directly from him, arose during our numerous discussions. I am very grateful to Dr. Volkov for introducing me to this field of physics, and for his encouragement and enthusiasm.

My sincere thanks go also to Mr. R. Leavens whose patient running of my programs produced many of the results quoted, and to the staff of the computer centre at McMaster University who were always prompt and courteous when they could understandably have been otherwise.

This research has been supported by a Commonwealth Scholarship and by the Department of Scientific and Industrial Research, New Zealand, and I am indebted to the relevant authorities for the opportunity to study in Canada.

Miss S. Schonfeld has very capably and cheerfully typed the final draft of a difficult manuscript and I thank her very much for this.

Last but by no means least, I would like to thank my wife for her continual encouragement, for keeping my feet on the ground, and for her very patient typing of a rough draft of this thesis.

TABLE OF CONTENTS

LIST OF TABLES

CHAPTER 1

INTRODUCTION

The study of the structure of nuclei has been dominated for many years by the shell model. In this model it is assumed that the effect of the interactions between pairs of particles can be approximated by a simple local potential acting on the individual particles. In the simplest form of the model the complicated Schrodinger equation for the nuclear system is replaced by a set of Schrodinger equations, one for each nucleon moving independently in a harmonic potential. It is well known that the many-body wave functions, which are solutions to this set of equations, are antisymmetrized products of single-particle wave functions. The single-particle wave functions are just the eigenstates of the Schrodinger equation for the harmonic well, and the many-body wave functions which they produce are called configurations. Normally a single-particle spin-orbit force is included with the harmonic potential, and, with this modification, the model can explain many of the gross features of nuclei. The experimental evidence in favour of such a model has been reviewed many times (e.g. Elliott and Lane 57).

One of the drawbacks of this approximation is that it is not connected with the actual two-nucleon interaction, and because of this it is not possible to obtain self-consistent nuclear energies or sizes. One way of relating the model wave functions, to the two-nucleon interaction, is to regard them as approximations to the true nuclear wave functions. A better approximation can be obtained by taking linear combinations of configurations, obtained by a variational procedure of the form

$$\delta \langle \Psi | H | \Psi \rangle = 0$$

$$\Psi = \Sigma_{i=1}^{N} \quad C_i \ \Phi_i$$

This is equivalent to diagonalizing the N x N matrix whose elements are $\langle \Phi_i | H | \Phi_j \rangle$. Mixtures of configurations found in this way contain long-range correlations which are not present in the simple configurations. A problem which arises in this approach is the choice of the incomplete representation of states Φ_i. This problem also occurs in the Hartree-Fock approach, and will be discussed later.

An alternative way of making this type of model self-consistent is to use the two-nucleon interaction to derive the average potential experienced by the individual nucleons. A procedure for doing just this, for the atomic

electron problem, was given by Hartree (1928) and improved by Fock (1930) many years ago. The Hartree-Fock method is based on a variational principle of the Ritz type, and will be discussed in detail in chapter 2*. This method is complicated by the fact that the average one-body potential, which is derived, is in general non-local. Furthermore, the only practical procedure for finding the average one-body potential is an iterative one. Successive iterations must be carried out from some suitably chosen starting point, and there is no guarantee that these iterations will converge to give a self-consistent result. Despite this difficulty, convergence is usually obtained if a good staring point is chosen. Meaningful Hartree-Fock calculations for light nuclei must be carried out with a computer, but these calculations are more tractable than the configuration mixing ones mentioned above. In particular the Hartree-Fock method can be applied to a wider range of nuclei, and consequently it is suitable for studying the systematic behaviour of energies and sizes of light nuclei.

---

*NOTE:

For an alternative derivation see Baranger (1963).

In the type of Hartree-Fock calculation that will be considered here the single-particle wave functions are derived as linear combinations of a finite number of harmonic oscillator states*. These harmonic oscillator states form an incomplete representation for the Hilbert space of all one-body states. Because the representation used is incomplete, the restricted Hartree-Fock (RHF) solutions depend on how this representation is chosen.

Unfortunately, the "realistic" two-nucleon interactions, which can be derived from scattering experiments, appear to be strongly repulsive at short distances. Because of this there are important short-range correlations in the true nuclear wave function. These correlations are not present in the types of wave functions considered above, and because of this such wave functions have very large or infinite energies. In fact the matrix elements of the two-nucleon interaction, which are needed in the configuration mixing and Hartree-Fock calculations, do not exist for most of these "realistic" interactions. This difficulty has been removed, in principle, by the advent of the Brueckner-Goldstone theory (Goldstone 57). This theory showed quantatively how the

---

*NOTE:

An alternative procedure is to use a co-ordinate space representation. For an example of this technique see Vautherin and Veneroni (1967).

strong two-nucleon interaction is effectively damped, in a many-body system, as a result of the exclusion principle which prevents two nucleons from occupying the same state. Brueckner proposed an alternative form of the Hartree-Fock theory in which the strong two-nucleon interaction is replaced by a complicated reaction matrix. The reaction matrix expresses the damped interaction and is dependent on the many-body system in which the interaction takes place. It was further shown by Moszkowski and Scott (1960) that the reaction matrix could be approximated quite well by an effective potential. From these ideas it appears that the Hartree-Fock method can be used if the "realistic" interaction is replaced by an effective interaction. Such an approach has also been used in configuration mixing calculations (e.g. Kallio and Koltveit 64), and more recently this type of calculation had been carried out with reaction matrix elements derived directly from "realistic" interactions (e.g. Kuo and Brown 77). The effective interaction to be used in this work is not taken from a "realistic" interaction, but rather is derived from physical properties which the effective interaction should have.

The modified form of the Hartree-Fock method obtained from the Brueckner-Goldstone theory, is expected to give the binding energies of nuclear many-body systems

quite well, even though the short-range correlations are still absent in the wave functions used. It can be shown from the Bethe-Goldstone equation that the relative wave function for two particles "heals" outside a small region which is directly affected by the short-range correlation. That is, except when two particles are very close together, they behave as if they were independent. It is reasonable to expect that this long-range independent behaviour of the particles is expressed by the wave function arising in the modified Hartree-Fock approach. Thus the size and shape of the Hartree-Fock wave function can be compared with the size and shape of actual nuclei.

The earliest Hartree-Fock calculations for light nuclei were carried out by Kelson et. al. (Kelson 63; Kelson and Levinson 64; Bassichis, Kelson and Levinson 64). In these calculations the representation was taken to be a single shell of oscillator states belonging to a spherically symmetric harmonic potential. A large part of the one-body potential was inferred from the experimentally observed single-particle energies. Because these energies vary with the size and shape of the nuclear state in a more complete calculation, it was necessary to "freeze" the nucleus at the experimentally observed size. Furthermore the effective two-body interaction used could not be

related directly to a "realistic" interaction. In this way much of the self-consistent nature of the Hartree-Fock calculation was destroyed. Ripka (1966) has studied the effect of increasing the representation to include more than one major shell of oscillator states. An increase of the size of the representation in this way always improves the Hartree-Fock calculation.

In the recent work of Davies, Krieger and Baranger (1966), of Muthukrishnan (1967), of Bassichis, Kerman and Svenne (1967), and in this work, the average one-body potential is derived consistently from some simplified form of effective two-body interaction. Davies et. al. use a representation of four major shells of spherical oscillator states. There is one degree of freedom in this representation, which is the size of the harmonic well which generates the oscillator states. In principle the Hartree-Fock calculation will always seek the equilibrium size of the nucleus, but in practice the size of the RHF solution varies almost linearly with the size of the representation states. For this reason it is necessary to vary the representation size until a minimum energy is found; this minimum point gives the equilibrium solution. In the work of Muthukrishnan a representation of four major shells of cartesian oscillator states was used. This representation has three degrees

of freedom, one for each of the three axes of the asymmetric harmonic potential used to generate the oscillator states. If these three degrees of freedom are used, not only the size but also the shape of the RHF solution is changed. Once again an equilibrium point should be found by minimizing the energy of the RHF solution. In neither of these two works just mentioned is it clear exactly how this type of variation was carried out, or the extent to which it was carried out.

In the work of Bassichis, Kerman and Svenne a representation of four major shells of oscillator states generated by a spherical well was used. The representation was kept at a fixed size but the nuclear system under consideration was forced to deform by using a constrained form of the Hartree-Fock method. There does not seem to be so clear a theoretical justification for this technique, as there is for the method used here to find the equilibrium deformation. One of the important points made by Bassichis et. al. is the magnitude of the second-order correction to the energies found in the Hartree-Fock method. The authors find that the energies decrease (i.e. become more negative) by about 17% of the total potential energy, when the second-order term is taken into account. This represents a large correction in terms of the binding energy. If the second and higher order corrections are

as large for the forces used in this thesis, then the discussion of the systematic behaviour which is taken up in chapter 7 must be modified.

In this thesis a representation of three major shells of cylindrical states will be used. Such a representation has basically two degrees of freedom. However one of the original features presented here is to allow the different oscillator states in the representation to come from harmonic wells of different sizes and deformations. The effect of this is examined in chapter 5. In most of the previous RHF calculations that have been reported, some symmetry has been imposed on the single-particle states. No such impositions are made here and it is shown that in some cases spurious solutions are created by symmetry requirements which effectively relate the single-particle states to preferred axes in space.

In the second chapter the RHF method is explained, and a closely related approximation is defined. The third chapter is concerned with the development of the four different effective forces to be used. It is shown in this chapter that the parameters of a certain analytic form of effective interaction can be almost entirely determined by imposing natural requirements. The fourth chapter presents the technical details of the RHF

calculation, which are too important to be confined to an appendix. The results which follow cannot be fully understood unless the techniques and their limitations described in this chapter are understood. Some problems connected with the convergence of the Hartree-Fock iteration procedure are also discussed at this stage. A detailed examination of the influence of the shape of the representation on the RHF solution is carried out in chapter 5. In this chapter comparisons are made with some calculations in a representation of cartesian states, and also with some RHF calculations which use a representation of four shells of cylindrical oscillator states. A standard procedure for obtaining an approximate equilibrium RHF solution is defined in chapter 2 and examined in chapter 5. In chapter 6 this procedure is used to examine the even-even nuclei lighter than ^{40}Ca. All the calculations described in chapters 4, 5 and 6 are carried out with the same simple effective force, force 1. In chapter 7, a survey of results derived from three other effective forces is given. All these three effective forces represent a considerable improvement over the first force, and two of them incorporate a dependence on the density of the nucleus in a manner suggested by Bethe (1966). These density dependent forces are designed to saturate nuclear matter in a

Hartree-Fock calculation. Unfortunately these forces have not been treated exactly in the calculations with finite nuclei, and some of the problems related to this fact are discussed.

The calculations carried out for this thesis do not permit a detailed comparison with experimental spectra. The reason for this is explained in chapter 6. Instead of making such a comparison, we have attempted to understand as fully as possible the nature of the Hartree-Fock solutions, for light nuclei. The comparisons that are made with experimental results are confined to chapter 7, and are made in order to improve the phenomenological force used.

CHAPTER 2

SIMPLE HARTREE-FOCK THEORY FOR WELL-BEHAVED INTERACTIONS

The large number of Hartree-Fock calculations which have been reported for finite nuclei in recent years have employed a variety of techniques. Therefore, it is felt necessary to explain here in a detailed and unambiguous way how the results to be discussed in later chapters were obtained. To do this in a self-contained manner we consider a non-relativistic n-body problem, in which there is a two-body interaction $v(r_{ij})$ for which all the matrix elements we will require are assumed to be well defined. The Hamiltonian for the problem is then

$$H = \sum_i T_i + \sum_{i<j} v(r_{ij}) - T_{cM} \qquad (1)$$

in which T_i denotes the kinetic energy of the i'th particle and r_{ij} denotes all the relative co-ordinates of the i'th and j'th particles. T_{cM} denotes the kinetic energy associated with the motion of the centre of mass, and is subtracted explicitly, so that the Hamiltonian represents only the intrinsic energy of the nucleus. The Schrodinger equation which should be solved is

$$H|\psi> = E|\psi> \qquad (2)$$

and because it is not known how to treat this equation exactly, approximate solutions must be used.

The state vector $|\Psi>$ belongs to an infinite dimensional Hilbert space, and it is well known that the real valued function $<\Psi|H|\Psi>$, confined to the hypersphere defined by $<\Psi|\Psi> = 1$, has stationary values at those points where (2) is satisfied (Messiah 65). To find approximate eigenstates of H some finite dimensional hypersurface S is chosen, and the function $<\Psi|H|\Psi>$ confined to S and to the hypersphere is written as $<\Psi|H|\Psi>|_S$. The presence of an eigenstate of H close to S can be expected to induce one or more stationary values of the restricted function $<\Psi|H|\Psi>|_S$, on S and close to the true eigenstate. If the states on the surface S are paramaterized by a set of real numbers $\alpha_1, \ldots \alpha_m$, then the approximate solutions are given by values of the α's which satisfy

$$\frac{\partial}{\partial \alpha_i} \{<\Psi(\alpha_1, \ldots\ _m)|H|\Psi(\alpha_1, \ldots \alpha_m)>\} = 0;\ i = 1, 2, \ldots m.$$

Points found in this way are regarded as approximate eigenstates. It must be noted that there is not necessarily a one to one correspondence between the true eigenstates and these approximations. In the special case where S is a linear subspace of dimension N of the Hilbert space, and is spanned by a set of states $|\Phi_i>$, i = 1, ... N, then the general form of $|\Psi>$ is

$$|\Psi> = \Sigma_{i=1}^{N} a_i\ |\Phi_i>,$$

and

$$<\Psi|H|\Psi> = \underset{\sim}{a}^{\dagger} H_S \underset{\sim}{a}$$

where $\underset{\sim}{a}$ is the column vector of the a_i, and H_S is the N x N matrix whose elements are $<\Phi_i|H|\Phi_j>$. The function $\underset{\sim}{a}^{+} H_S \underset{\sim}{a}$, whose stationary points are required, subject to the constraint

$$\langle\Psi|\Psi\rangle = \sum_i |a_i|^2 = 1,$$

is the analogue of $\langle\Psi|H|\Psi\rangle$ in an N-dimensional space. So, by the converse of the theorem relating eigensolutions to stationary points, the approximate solutions in S occur at the eigenvectors of H_S. In this way approximate solutions are found by diagonalizing finite matrices.

The Hartree-Fock Approximation.

An approximation of the type outlined above will now be considered for the problem defined by the Hamiltonian (1). The choice of the surface S is dictated, for the case of finite nuclei, partly by mathematical simplicity and partly by experimental results. There is much evidence to indicate that the low lying states of finite nuclei are close to independent particle states, that is to say to states which are formed by forcing individual nucleons into particular one-body states and then taking into account the fermi statistics which the nucleons must obey. If the particular one-body states are indexed by a set of indices $\{\alpha_i : i = 1, \ldots n\}$ and denoted by $|\alpha_i\rangle$ with configuration space wave functions $\psi_{\alpha_i}(r)$, then the n-particle state has the wave function

$$\Psi(r_1, \ldots r_n) = A\cdot[\psi_{\alpha_1}(r_1)\psi_{\alpha_2}(r_2) \ldots \psi_{\alpha_n}(r_n)]$$

Where A is the normalized antisymmetrising operator acting on the generalized co-ordinates r_i. This wave function has the form of a determinant and we will denote it in its normalized

form by $\Psi = \det(\psi_{\alpha_1}, \psi_{\alpha_2}, \ldots \psi_{\alpha_n})$.

We will also denote the n-particle state by

$$|\Psi\rangle = |\alpha_1, \ldots \alpha_n\rangle \tag{3}$$

and the one-body states $|\alpha_i\rangle$ are called the occupied states.

If the wave function $\det(\psi_{\alpha_1}, \ldots \psi_{\alpha_n})$ is to be non-zero, then the one-body wave functions must be linearly independent, and it will be seen below that there is no loss of generality if the states are taken to be orthonormal, so this will be assumed from now on.

The belief that states of this form lie close to the true eigenstates of the problem leads in a natural way to minimizing the function $\langle\Psi|H|\Psi\rangle$ over the hypersurface of such independent particle states.

The most general variation on this hypersurface is

$$\delta\Psi = \det(\psi_{\alpha_1} + \delta\psi_{\alpha_1}, \ldots \psi_{\alpha_n} + \delta\psi_{\alpha_n}) - \det(\psi_{\alpha_1}, \ldots \psi_{\alpha_n})$$

which, when second order and higher terms are ignored, can be separated into the sum of n independent variations of the form

$$\delta_{\alpha_i}\Psi = \det(\psi_{\alpha_1}, \ldots \psi_{\alpha_i} + \delta\psi_{\alpha_i}, \ldots \psi_{\alpha_n}) - \det(\psi_{\alpha_1}, \ldots \psi_{\alpha_n}). \tag{4}$$

The conditions

$$\delta\langle\Psi|H|\Psi\rangle = 0$$

$$\langle\Psi|\Psi\rangle = 1, \tag{5}$$

that $|\Psi\rangle$ be a stationary point of the required form, imply certain conditions on the $|\alpha_i\rangle$, and to express these conditions we consider a complete orthonormal basis of states $|\beta\rangle$, for

the one-body Hilbert space, which include the states $|\alpha_i\rangle$. Then we can write

$$\delta\psi_{\alpha_i}(r) = \Sigma_\beta \varepsilon_\beta^{\alpha_i} \psi_\beta(r)$$

and the variation (4) of the i'th state can be further separated into a sum of independent variations of the form

$$\delta_{\alpha_i,\beta}\Psi = \det(\psi_{\alpha_1}, \ldots \psi_{\alpha_i} + \varepsilon_\beta^{\alpha_i} \psi_\beta, \ldots \psi_{\alpha_n}) - \det(\psi_{\alpha_1}, \ldots \psi_{\alpha_n}). \tag{6}$$

Certain of these variations are identically zero, namely those where $\beta = \alpha_i$ for some i. If the set of occupied states α_i is denoted by A then the remaining non-vanishing variations produce

$$\delta\langle\Psi|H|\Psi\rangle = \sum_{\alpha\varepsilon A,\ \beta\notin A} 2 \times \mathrm{Re}[\langle\Psi|H|\delta_{\alpha,\beta}\Psi\rangle] \tag{7}$$

In order to satisfy conditions (5) simultaneously, a Lagrange multiplier is introduced in the usual way and it is necessary to find states $|\Psi\rangle$ which satisfy

$$\delta\langle\Psi|H-\lambda I|\Psi\rangle = 0 \tag{8}$$

or from (7)

$$\sum_{\alpha\varepsilon A,\ \beta\notin A} \mathrm{Re}[\langle\Psi|H-\lambda I|\delta_{\alpha,\beta}\Psi\rangle] = 0$$

As the ε_β^α coefficients in the $\delta_{\alpha,\beta}\psi(r)$ are all independent and may be real or imaginary, it follows that

$$\langle\Psi|H-\lambda I|\delta_{\alpha,\beta}\Psi\rangle = 0 \tag{9}$$

for all $\alpha\varepsilon A$, $\beta\notin A$.

The conditions (9) are most easily reduced to conditions on the states $|\alpha_i\rangle$ if we resort to the notation of second quantization, and introduce creation and annihilation operators a_α^+, a_α

satisfying $\{a_\alpha, a_\beta\} = \{a_\alpha^+, a_\beta^+\} = 0$

$$\{a_\alpha^+, a_\beta\} = \delta_{\alpha\beta}$$

$$a_\alpha^+|0\rangle = |\alpha\rangle \ , \ a_\alpha|0\rangle = 0$$

and $$a_{\alpha_1}^+ \ a_{\alpha_2}^+ \ldots\ldots \ a_{\alpha_n}^+ \ |0\rangle = |\alpha_1, \ldots. \ \alpha_n\rangle$$

where $\{A,B\} = AB + BA$ is the usual anticommutator.

So that from (6)

$$\delta_{\alpha,\beta} \ |\Psi\rangle = \mathcal{E}_\beta^\alpha \ a_\beta^+ \ a_\alpha \ |\alpha_1, \ldots. \ \alpha_n\rangle$$

and (9) becomes

$$\langle\alpha_1 \ldots \alpha_n \mid (H-\lambda I) \ a_\beta^+ \ a_\alpha \mid \alpha_1 \ldots \alpha_n\rangle = 0. \qquad (10)$$

It is well known that the operator H can be expressed in terms of the operators a_α, a_α^+ as

$$H = T + V$$

$$T = \sum_{\alpha\beta} \langle\alpha|T|\beta\rangle \ a_\alpha^+ \ a_\beta$$

$$V = \tfrac{1}{4} \sum_{\alpha\beta\gamma\delta} \langle\alpha\beta|V|\gamma\delta\rangle \ a_\alpha^+ \ a_\beta^+ \ a_\delta \ a_\gamma \ . \qquad (11)$$

T and V are used here to denote the parts of H which are one and two-body operators respectively. It should be noted that the centre of mass energy affects both terms. As defined above the two-body state $|\alpha\beta\rangle$ is antisymmetric; it will be more convenient in later chapters to use matrix elements between

states which are not antisymmetric, and such states will be written $|\alpha\beta)$. Thus

$$|\alpha\beta\rangle = 1/\sqrt{2}\,[|\alpha\beta) - |\beta\alpha)]$$

and $$\langle\alpha\beta|V|\gamma\delta\rangle = (\alpha\beta|V|\gamma\delta - \delta\gamma).$$

Using (11) equation (10) can be reduced to

$$\langle\alpha \mid T + \Gamma \mid \beta\rangle = 0 \qquad \alpha\varepsilon A,\ \beta\notin A \tag{12}$$

where $$\Gamma = \sum_{\alpha\varepsilon A} a_\alpha\, V\, a_\alpha^{+} \tag{13}$$

or $$\langle\alpha|\Gamma|\beta\rangle = \Sigma_{\gamma\varepsilon A}\, \langle\alpha\gamma|V|\beta\gamma\rangle \tag{14}$$

In (13) and (14) V is the two-body operator defined in (11).

Equations (12) are the required conditions on the one-body states, but it must be noted that the states that are defined by these conditions are not unique. The reason for this is as follows. The many body state $|\alpha_1, \alpha_2 \ldots \alpha_n\rangle$, which is of interest, can be formed just as well from the states

$$|\alpha_i'\rangle = \Sigma_{j=1}^{n} U_{ij}\, |\alpha_j\rangle \tag{15}$$

so long as the n x n matrix U has rank n, and if in addition U is unitary then the $|\alpha_i'\rangle$ are orthonormal. Because of this the many-body state does not define unique occupied one-body states, but instead defines an n-dimensional subspace (the subspace spanned by the $|\alpha_i\rangle$) within the Hilbert space of all one-body states. Any n linearly independent states $|\alpha_i\rangle$ taken from this subspace define the same many-body state and

it is because of this that the n states can be taken as orthonormal. It is customary to characterize the subspace of occupied states by the projection operator onto it i.e.

$$\rho = \Sigma_{\alpha \epsilon A} \, |\alpha><\alpha| \qquad (16)$$

and this operator is called the density matrix. There is now a one-to-one correspondence between many-body states of the independent particle type and their density matrices. The one-body operator Γ is defined uniquely by the many-body state (it is not changed by the transformation (15)) and this can be expressed by writing $\Gamma(\rho)$.

The Hartree-Fock equations (12) are now satisfied by a set of n states $|\alpha_i>$, which form an approximate many-body state, provided the operator $\Gamma(\rho)$ which they produce is such that the operator $T + \Gamma(\rho)$ leaves the subspace spanned by the $|\alpha_i>$ invariant. Because more than one set of one-body states will produce the same many-body state and the same density matrix these one-body states are not unique. However, it is customary to denote the eigenstates of $T + \Gamma(\rho)$ as the Hartree-Fock states of the system. These states satisfy the eigenvalue equation

$$[T + \Gamma(\rho)] \, |\alpha> = \varepsilon_\alpha \, |\alpha> \, , \qquad (17)$$

in which $\Gamma(\rho)$ appears as an average potential felt by the independent particles. The Hartree-Fock state has an energy

$$\langle\alpha_1\alpha_2 \ldots \alpha_n|H|\alpha_1\alpha_2 \ldots .\alpha_n\rangle = \sum_{\alpha\varepsilon A} \langle\alpha|T|\alpha\rangle + \tfrac{1}{2}\sum_{\alpha,\beta\varepsilon A} \langle\alpha\beta|V|\alpha\beta\rangle$$

$$= E_o = \tfrac{1}{2}\sum_{\alpha\varepsilon A} (\langle\alpha|T|\alpha\rangle + \varepsilon_\alpha) \qquad (18)$$

Furthermore the one-particle-one-hole excitation $a_\beta^+ a_{\alpha_i}|\alpha_1 \ldots .\alpha_n\rangle$ of this ground state has an energy

$$\langle\alpha_1 \ldots \alpha_n|a_{\alpha_i}^+ a_\beta H a_\beta^+ a_{\alpha_i}|\alpha_1 \ldots \alpha_n\rangle = E_o + \varepsilon_\beta - \varepsilon_{\alpha_i} - \langle\beta\alpha_i|V|\beta\alpha_i\rangle$$

(19)

When the interactions are small the last term in (19) may be neglected and the energies ε_α appear as single particle excitation energies. In general though these one-particle-one-hole excitations do not satisfy the Hartree-Fock conditions because the density matrix, and hence $\Gamma(\rho)$, is changed when the set of occupied states is changed. This means that the single particle energies ε_α must be recalculated, and even when the one-particle-one-hole states are close to Hartree-Fock solutions there is a rearrangement of the single-particle levels. In even-even light nuclei, where states with high space symmetry are preferred, the low lying excited states are not of the one-particle-one-hole type.

A further important point is evident from an investigation of (13), namely that any unitary transformation which leaves the subspace of occupied states invariant, and which also leaves V invariant, necessarily leaves $\Gamma(\rho)$ invariant.

Consequently, the effective potential Γ has just those symmetries which are common to the set of states $|\alpha_i>$ (i.e. to ρ) and V the two-body interaction.

The Hartree-Fock conditions (12) or (17) do not immediately solve the problem of finding approximate many-body states, because the operator whose eigenstates are required depends, through ρ on the states themselves. For this reason one must find solutions by choosing an initial set of states $|\alpha_i^{(o)}>$ and carrying out successive iterations. In the p'th iteration one replaces the states $|\alpha_i^{(p)}>$ with the eigenstates of $T + \Gamma(\rho^{(p)})$ where $\rho^{(p)}$ is the p'th approximation to the density matrix defined by

$$\rho^{(p)} = \Sigma_{\alpha\varepsilon A}|\alpha^{(p)}><\alpha^{(p)}|. \qquad (21)$$

The iterations should continue until the solutions converge, in particular until successive approximations $\rho^{(p)}$ are equal. Actually the above iteration procedure is not well defined until some prescription is given for selecting which of the infinite number of eigenstates of $T + \Gamma$ are to be occupied. One such prescription would be to select the eigenstates which were closest to the previously occupied states (i.e. to the $|\alpha_i^{(p)}>$). However, it is felt that such a procedure might act as a constraint on the overall convergence of the density matrix. That is by continually forcing the system into single-particle states of the same type, convergence may be prohibited.

A more physical prescription has been used here and is based on arranging the single-particle states so that their eigenvalues are increasing. When this is done the states are occupied according to an occupation vector η which has components

$\eta_i = 1$ if the i'th state is to be occupied

$\eta_i = 0$ if the i'th state is to be empty.

Thus the density matrix $\rho^{(p)}$ is defined for the p'th iteration as

$$\rho^{(p)} = \Sigma_i \, \eta_i \, |\alpha_i^{(p)} > < \alpha_i^{(p)} \, | \, .$$

Unfortunately this method can also lead to serious difficulties in convergence, particularly for odd nuclei. This problem, which seems to have been ignored in previous works will be discussed more fully in chapter 4.

The question of convergence must be examined more carefully in another respect. If the operator $T + \Gamma$ has degeneracies, as is very often the case, then the eigenstates associated with degenerate eigenvalues are not unique and cannot be expected to converge even when the density matrix does.

The Restricted Hartree-Fock Method

Equation (17), which we would like to solve in any given iteration, is of the same form as equation (2). However, we are now in a one-body Hilbert space rather than an n-body

one, and we have paid the price by becoming involved in an iteration procedure in order to find a self-consistent solution. Because of the similarity between (2) and (17), we use the same ideas to solve (17), in any particular iteration. That is we would like to find some finite dimensional hypersurface in the space of one-body states, which lies close to the true Hartree-Fock states. Some caution is needed at this point because, as mentioned before, when a variational procedure is used to find approximate states, there is no guarantee that two or more approximate solutions do not correspond to the same true solution. However if two approximate one-body states, both close to the same true one-body state, are used to construct a density operator it seems clear that this will give a poor approximation. To some extent this situation can be avoided if the approximate one-body states are constrained to be orthonormal. Also it is reasonable to believe that the Hartree-Fock states are quite similar to the single-particle states used in simple shell models, in particular the Nilsson model for deformed nuclei (Nilsson 55). If this in fact turns out to be the case, then we can be fairly confident in our solution. Furthermore since the Hartree-Fock states should be similar to those of the Nilsson model, a reasonable choice for the hypersurface is a subspace spanned by a finite number N, of the one-body

wave functions of this model. Thus recalling the special form of the variational procedure for such a linear subspace, it is seen that a given iteration can be carried out by diagonalizing an N x N matrix with matrix elements

$$H_{ij} = \langle i \mid T + \Gamma(\rho) \mid j \rangle \qquad (23)$$

The states $|i\rangle$ are the harmonic oscillator states appropriate to a cylindrically symmetric harmonic well, and so satisfy the Schrodinger equation

$$\frac{\hbar^2}{2m} [-\nabla^2 + \alpha^2\rho^2 + \beta^2 z^2] \; |i\rangle = e_i \; |i\rangle \; .^{*} \qquad (24)$$

$|i\rangle$ is characterised by 5 quantum numbers as well as the parameters α and β .

Thus, $$|i\rangle \equiv |n_i, m_i, n_{zi}, s_i, T_i; \alpha, \beta\rangle$$

and $$e_i = \frac{\hbar^2}{m} [(2n_i + |m_i| + 1)\alpha + (n_{zi} + \tfrac{1}{2})\beta] \; . \qquad (26)$$

s_i and T_i denote the spin and isospin quantum numbers respectively. The cylindrical harmonic oscillator wave-functions are considered in some detail in Appendix 1.

This then defines our concept of a simple restricted Hartree-Fock (RHF) calculation in a fixed representation of states $|i\rangle$, i = 1, ... N (N must be larger than n the number of particles). If the approximate Hartree-Fock states for the p'th iteration are contained in a row vector $|\underset{\sim}{\alpha}^{(p)}\rangle$ of

---

Note

* This notation is ambiguous as α and β have been used to label single particle states, however no confusion should arise in what follows.

length N, and the representation states similarly in a vector $|\underset{\sim}{i}>$ and if the N x N matrix η consists simply of the occupation numbers η_j, mentioned above, along the diagonal, then the p'th iteration can be defined by the matrix equations

$$|\underset{\sim}{\alpha}^{(p)}> = |\underset{\sim}{i}> \; B^{(p)}$$

$$\rho^{(p)} = B^{(p)} \eta \; B^{(p)\dagger}$$

$$\Gamma_{ij}^{(p)} = \Sigma_{\ell m} \rho_{\ell m}^{(p)} <i\ell|V|jm> \qquad (27)$$

$$E^{(p)} = \tfrac{1}{2} \mathrm{Tr}(T\rho^{(p)}) + \tfrac{1}{2}\Sigma_k \eta_k \varepsilon_k^{(p)}$$

$$[T + \Gamma^{(p)}] |\alpha_j^{(p+1)}> = \varepsilon_j^{(p+1)} |\alpha_j^{(p+1)}>$$

$|\underset{\sim}{\alpha}^{(p+1)}>$ = row vector of the $|\alpha_j^{(p+1)}>$ ordered so that the $\varepsilon_j^{(p+1)}$ are non-decreasing.

The N x N matrix B is unitary, $\rho^{(p)}$ and $\Gamma^{(p)}$ are hermitian, the matrix T remains unchanged, and $E^{(p)}$ is the energy of the many-body state at the end of the p'th iteration. It was stated previously that the effective Hartree-Fock potential $\Gamma(\rho)$ has all the symmetries common to V and to ρ. This is still true in the restricted Hartree-Fock calculation. If the initial states $|\alpha_i^{(o)}>$ have some symmetry, such as cylindrical symmetry or time-reversal symmetry, so that the

density matrix also has this symmetry, then $T + \Gamma(\rho)$ will have the same symmetry. This symmetry is then passed on to the eigenvectors of $T + \Gamma$ which are the next approximate Hartree-Fock states. Therefore, any symmetry in the initial choice of states is passed on to all subsequent approximations. This feature is often used to simplify the calculation by making the matrix $T + \Gamma(\rho)$ split into a block diagonal form, by choosing to impose certain symmetries on the Hartree-Fock states, which are shared by the representation states. In this work no such restrictions have been imposed and the more general range of states was maintained.

The solution obtained by following this procedure is entirely self-consistent except for the choice of representation. Part of this choice is simple because experience with the shell model has shown that the states with the lowest eigenvalues e_i in (24) are the appropriate ones to use. However, the choice of parameters α_i and β_i for each state is not so trivial. In fact the RHF calculation can be carried out for any values of these oscillator parameters and a value for the binding energy E is obtained when convergence is achieved. In this manner E can be found as a function of all the oscillator constants in the representation.

$$\langle \Psi_{RHF} | H | \Psi_{RHF} \rangle = E(\alpha_1 \ldots \alpha_N, \beta_1 \ldots \beta_N). \qquad (28)$$

Since we are essentially involved in a variational procedure,

it is clear that the proper self-consistent values for the α's and β's are those which give the lowest value for (28) subject to the constraint that the representation states are orthonormal.

Larger values of N in this RHF calculation will give more complete representations and so better approximations to the true Hartree-Fock states. Furthermore, the energy (28) will become less dependent on the size and shape parameters α_i and β_i defining the representation. If it were possible to pass to the limit $N = \infty$ and the representation were to become complete, then no matter what parameters α and β were used it would be possible to solve exactly for the true Hartree-Fock states. Thus the need to consider variations of the representation, is simply a consequence of the restricted nature of the calculation.

The General Harmonic Approximation

It is possible to consider an alternative, less general, approximate solution of (17). As has been stated, the states $|\alpha\rangle$ are similar to the solutions $|i\rangle$ of (24) and we might then look for solutions to (17) within the hypersurface of all one-body states of this form, seeking minimum values of

$$\langle i|T + \Gamma|i\rangle = f(\alpha_1 \ldots \alpha_n, \beta_1 \ldots \beta_n). \qquad (29)$$

In this equation it is implied that Γ is derived from the

density matrix for a many-body state $|1,2 \ldots n\rangle$. Because the density matrix for this state depends on the oscillator parameters of all the single particle states, the function to be minimized in (29) also depends on all these parameters. Equation (29) is used to determine the values of these parameters by requiring that the n functions

$$\langle i|T + \Gamma|i\rangle \qquad i = 1,2, \ldots n.$$

are simultaneously minimized. In fact this condition can be derived from the condition that

$$\langle 1, 2 \ldots n |H|1, 2 \ldots n\rangle = E(\alpha_1 \ldots \alpha_n, \beta_1 \ldots \beta_n) \tag{30}$$

be a minimum. The many-body state $|1, 2 \ldots n\rangle$ is simply a determinant of cylindrical oscillator states and, apart from the fact that different oscillator states may have different oscillator parameters α and β, this is just the type of state used in the Nilsson model. For reasons mentioned above the oscillator states used are constrained to be orthogonal, and this is equivalent to constraints of the form $\alpha_i = \alpha_j$ or $\beta_i = \beta_j$ for certain pairs i and j. It should be noticed that in this case only the n occupied oscillator states are varied and constrained, whereas in the minimization of (28) all N oscillator states are varied and constrained. The quantum numbers for all of the states $|1\rangle$, $|2\rangle$ ... $|n\rangle$ determine an n-particle configuration

By minimizing (30), the best parameters for the configuration are obtained and the configuration wave function defined in this way is an approximation to the Hartree-Fock state. This approximation will be called the generalized harmonic approximation (GHA), and has been used in various forms by other authors (e.g. Brink and Boeker 67).

Since the results of the more general Hartree-Fock calculations are usually close to these simple configuration wave functions, we shall adopt the standard procedure of using such configurations as starting points for the RHF iterations. But, in order to break the high symmetry of such states, small random admixtures are introduced into the density matrix before starting. The way this will be done will be considered in detail in chapter 3. Furthermore the function (28) is only slightly dependent on the oscillator parameters of the representation states which were not contained in the starting configuration, at least in the region of the minimum. This leads us to use the same oscillator parameters in the RHF calculation as found from the minimization of (30), together with some reasonable average values for the parameters of those states not occupied in the starting configuration. Later we shall present some evidence that in fact, the best values for the oscillator parameters defined by minimizing (28) are usually close to those found in the GHA by minimizing (30).

CHAPTER 3

CHOICE OF A PHENOMENOLOGICAL POTENTIAL

The discussion of the last chapter can not be applied directly to nuclei if the two-body interaction occurring in the Hamiltonian does not have well defined matrix elements between harmonic oscillator states. Most "realistic" interactions have infinite hard cores, so that such matrix elements do not exist, and these interactions can not be used directly. However, the solution to this difficulty has been known for some years and it amounts to using a reaction matrix G instead of the interaction v (Goldstone 57). G is derived from v by a complicated equation which can be solved by various approximations (Brown 67). This equation will not be discussed here but its significance is that the matrix elements of G, which are required, can be reasonably well approximated by those of a well behaved potential (Brandow 65). This well behaved potential would, in particular, no longer have a hard core and so could be used in an RHF calculation. To compensate for the removal of the hard core the new effective potential would have a definite velocity dependence even if this were not present in v. Thus it is known from the work of Moszkowski

and Scott (1960), that the effect of the repulsive core can be cancelled by the effect of some of the attractive tail, leaving a simple potential which is zero inside some separation distance d. This is shown diagrammatically in figure 1. The resulting long-range part of the "realistic" potential gives, to a reasonable approximation, the same matrix elements as the reaction matrix G. However the amount of the attractive tail region that must be taken to cancel the core varies with the energy of the interacting particles. In fact for a given energy this long-range effective potential is simply chosen to give the correct scattering phase shift. In this way the separation distance d depends on the relative energy (Bhaduri and Tomusiak 65). Simple potentials based on these ideas have been used in many nuclear calculations (e.g. Kallio and Koltveit 64).

The non-central tensor force, which is a component of most "realistic" interactions can be treated in this way, but the corresponding part of the G matrix element is not very well approximated in this case by the long-range tail. In fact the tensor force contributes mainly, in this type of approximation, through a correction term known as the second Born correction. Kuo and Brown (1965) have shown that this correction term can be approximated quite well by a central potential. The significance of this last approximation, for this work, is that much of the effect of the tensor force

can be incorporated in a renormalization of the central part of the effective potential.

The effective potential will also depend on the density of the many-body system in which the interaction takes place. The physical reason for this density dependence can be seen by considering uniform nuclear matter, in which the density is related to the number of single-particle states (in this case plane-wave states) which are occupied. The Fermi momentum k_F of the ground state and the density ρ are related by

$$\rho = (2/3\pi^2)\ k_F^{\ 3}\ , \qquad (1)$$

and it is seen that the larger the density, the more states that are occupied. The exclusion principle does not allow the interaction to take place via intermediate states which are occupied, and the more states that are excluded in this way the weaker the G matrix becomes. Thus it is expected that the G matrix elements become smaller as the density increases, and this is found to be the case in detailed calculations (Bhargava and Sprung 67, Wong 67). If this density dependence is carried over to a finite nucleus, then interactions taking place in the central core of the nucleus are weaker than those occuring in the lower-density region. The effect of this in Hartree-Fock calculations will be seen later.

The approach adopted here is to use, for the effective

potential, some simple analytic force in which certain parameters are fixed by the requirement that the important features, expected of the effective potential, are reproduced. The important features that will be used here to determine the analytic force are:

1. that it produce the correct s-wave phase-shifts for free nucleon-nucleon scattering.
2. that it have roughly the same long-range behaviour as "realistic" potentials.
3. that it have the correct saturation properties in nuclear matter.
4. that it have small second-order corrections in nuclear matter.

Properties 1 and 2 follow from the work of Moszkowski and Scott previously mentioned, and our emphasis on the s-wave is simply due to the fact that this is the strongest component of the interaction. Condition 3 is a natural one if the systematic behaviour of a wide range of nuclei is to be considered. The importance of this condition has been shown quantitatively by the work of Bhaduri and Tomusiak (1966). The fourth condition arises because the Hartree-Fock approximation, using the reaction matrix, is essentially a first order approximation in the Brueckner-Goldstone theory. If this approximation is to be a good one it is necessary that the second and higher-order corrections be

small. It must also be pointed out that the variational methods described in the last chapter are only justified to the extent that these higher-order corrections are small.

In order to carry out the detailed calculations of later chapters, a further feature of the force is desirable;

5. Matrix elements of the analytic force used should be easy to calculate.

Because of this last condition the non-central parts of the effective potential will be ignored. As previously mentioned this is justified to some extent because the principal non-central component of v, the tensor force, contributes to G largely as a central term. One effect of the non-central terms which are being neglected is to create a spin-orbit force in the average Hartree-Fock potential. This spin-orbit force is needed to give the correct single-particle levels in spherical nuclei, though it does not normally have much effect in deformed light nuclei. Consequently we include a small one-body spin-orbit force

$$V_{SO} = -2 \underset{\sim}{\ell} \cdot \underset{\sim}{s}$$

in the Hartree-Fock potential. The magnitude of this force has been chosen to give the splitting of 5 MeV, between the $d_{5/2}$ and $d_{3/2}$ levels, which is observed in stripping reactions with ^{16}O. The criterion of easy evaluation

of matrix elements is well satisfied by the Volkov force:

$$v(r) = (w + mP_x + bP_\sigma + hP_\tau)(V_a \exp(-r^2/\lambda_a^2) + V_r \exp(-r^2/\lambda_r^2)) \quad (2)$$

The operators P_x, P_σ and P_τ exchange the space, spin and isospin co-ordinates respectively. The sum of two gaussians produces a radial shape which is very similar to the Moszkowski-Scott form, and yet much easier to handle. This form of force has been used extensively by Volkov (1965) in 1p shell calculations, and, for nuclei lighter than ^{16}O, is capable of giving reasonable agreement for nuclear binding energies, sizes and low energy spectra. Forces similar to this have also been studied by Brink and Boeker (1967). Unfortunately when such forces are used in Hartree-Fock calculations for nuclei heavier than ^{16}O they give binding energies which are too large and sizes which are too small. This overbinding and collapse becomes progressively worse as the number of nucleons is increased.

A force of the type given in equation (2) has been used for most of the Hartree-Fock calculations discussed in this work. This force is denoted as force 1 and the parameters which appear in (2) are given in Table 1. These parameters are such as to give fairly close agreement with the effective ranges and scattering lengths of s-wave scattering of free nucleons, the correct binding energy of ^{16}O, and the low energy spectra of 1p shell nuclei.

TABLE 1

FORCE PARAMETERS

$$v(r,R) = (1 - c_3 \rho^{2/3}(R))(w+mP_x+bP_\sigma+hP_\tau)(V_a \exp(-r^2/\lambda_a^2) + V_r \exp(-r^2/\lambda_r(k)^2))$$

where $\lambda_r(k) = \lambda_r^\circ [1 + C_1(k - c_2)^2]$

Force No.	V_a	V_r	λ_a	λ_r°	C_1	C_2	C_3	W	M	b	h
1	-78.03	82.8	1.50	0.80	0.0	0.0	0.0	0.29	0.71	0.20	-0.05
2	-78.03	82.8	1.50	0.76	0.496	0.70	0.0	0.29	0.71	0.20	-0.05
								(w + m)	ν^*		(b - h)
3	-150.0	155.0	1.50	1.09	0.26	0.81	0.922	1.00	-1.682		0.44
4	-250.0	255.0	1.50	1.247	0.15	0.836	1.180	1.00	-1.228		0.40

*Note $\nu = 10(w - m) + 8(b + h)$

The first attempt (Hughes, Sprung and Volkov) to alter this form of the force, so that it could give closer agreement with the s-wave scattering, was a simple one, and a slightly more general approach is used here. It has already been pointed out that the Moszkowski-Scott type of force has an attractive tail which depends on the relative energy of th e interacting particles and that this dependence is such that the correct scattering phase shifts are produced. In the force (2) the amount of attractive tail can be varied by varying λ_r, and for any given energy λ_r can be chosen so as to reproduce a particular phase shift. In this way λ_r can be chosen to be afunction of the relative energy, or the relative wave number k, in such a way that a given phase-shift is produced at every energy. Figure 2 shows λ_r as a function of k designed to fit either the singlet or triplet s-wave scattering phase-shifts. Because matrix elements will not be evaluated in the relative co-ordinate system, it is not convenient to use separate values of λ_r for singlet and triplet states. Instead a weighted average value is used, in which the triplet and singlet values of λ_r are weighted by their relative strengths $[1 + (b - h)]$ and $[1 - (b - h)]$ respectively. These average values of λ_r can be well represented by a parabola in k over the energy range of interest. In this way (2) becomes modified to:

$$v(r) = (w + m\,P_x + b\,P_\sigma + h\,P_\tau)(V_a \exp(-r^2/\lambda_a^2) + V_r \exp(-r^2/\lambda_r^2(k)) \quad (3)$$

where $\lambda_r(k) = \lambda_r^0 [1 + c_1 (k - c_2)^2]$

A variation of 0.1 fm. in λ_r produces a change in the phase-shifts of about 0.1 radians, so that this averaging procedure does not cause significant changes in the phase-shifts and fairly close agreement with the experimental values is maintained. The values of λ_r^0, c_1 and c_2 are given in table 1 and together with the remaining parameters of force 1 this defines force 2. It must be noticed that, in contrast to the usual type of Moszkowski-Scott force, this one can become repulsive for large k values, i.e. when $\lambda_r(k)$ becomes larger than λ_a. This feature does not appear in calculations with finite nuclei but it does mean that a saturation point is found in nuclear matter. The results of Hartree-Fock calculations in light nuclei using force 2 are discussed in chapter 7.

The binding energy per nucleon in nuclear matter, determined by first order perturbation theory, is shown, as a function of k_F, in figure 3 for forces 1 and 2. While force 1 clearly does not saturate at all, force 2 saturates at a large density and with a high value for the binding energy. This saturation point can be brought closer to the observed values by increasing the Majorana exchange

parameter, but this procedure seems arbitrary and possibly non-physical. Furthermore, nuclear deformation depends rather sensitively on the Majorana component (Volkov 65). An alternative way of bringing about the correct saturation of nuclear matter is to incorporate a density dependence into the form of the force. Bethe (1966) has suggested a factor of the form $(1 - \alpha k_F^2)$, which has the desired effect of decreasing the strength of the interaction as the density increases. When k_F is zero the density (1) is also zero and the density factor is one. This corresponds to free nucleon-nucleon scattering from which forces 1 and 2 have been derived, and so this extra factor should essentially multiply these forces. The parameter α and the exchange parameters of (3) can now be varied until the force produces the correct saturation values of k_F and binding energy, in nuclear matter. If this is done the value found for the Majorana exchange does not need to be increased and the value of α is around 0.17 fm^2. This causes a reduction of the strength of the interaction by about 30% at saturation in nuclear matter. However, this density factor cannot simply be tagged onto forces 1 and 2, because these forces, were also required to give the right binding energy for ^{16}O, and the inclusion of the density factor decreases this energy considerably. To account for this the strength of the free nucleon-nucleon scattering force must be increased.

To incorporate this density dependence in finite nuclei k_F is replaced by the density from (1), and this density is evaluated at the centre of mass of the interacting particles. This prescription is in the spirit of the local density approximation proposed by Breuckner and Wada (1956). The resulting force is written:

$$v(r_1, r_2) = (1 - c_3 \rho^{2/3}(R))(w + mP_x + bP_\sigma + hP_\tau)$$

$$(V_a \exp(-r^2/\lambda_a^2) + V_r \exp(-r^2/\lambda_r^2(k)) \quad \ldots (4)$$

where $\lambda_r(k) = \lambda_r^0 [1 + c_1 (k - c_2)^2]$

and $r = |\underset{\sim}{r}_1 - \underset{\sim}{r}_2|, \quad R = |\tfrac{1}{2}(\underset{\sim}{r}_1 + \underset{\sim}{r}_2)|$.

The choice of parameters to use in (4) is, in principle, straightforward.

λ_a is chosen to give a long-range behaviour compatible with "realistic" potentials.

$(V_a + V_r)$, the core height, is kept to some small fixed value in order to make the radial shape similar to a Moszkowski-Scott type of potential.

$\lambda_r(k)$ is chosen to give an average fit to singlet and triplet phase shifts.

(b - h) determines the ratio of singlet and triplet strengths of the potential. A best value can be chosen to minimize the discrepancy between the two curves which give the correct values of λ_r to use for singlet and triplet phase

shifts.

c_3 and $\nu = 10(w - m) + 8(b + h)$ are determined by fitting the saturation values of $k_F = 1.4$ fm.$^{-1}$ and binding energy of -16.0 MeV per nucleon in nuclear matter.

V_a is adjusted to fit the binding energy of ^{16}O. Apart from these conditions the exchange parameters are normalized so that

$$w + m = 1 \tag{5}$$

There is one remaining degree of freedom in the four exchange parameters. The energies of even-even nuclear configurations, and nuclear matter is such a configuration, depend to first order only on the exchange parameters ν and $(w + m)$. Because of this the remaining degree of freedom cannot be fixed in this work.

Forces 3 and 4 have been determined following this type of procedure and RHF calculations with these forces are described in chapter 7. It is seen from (4) that this type of force is not translationally invariant because of the density function which is fixed in space. Furthermore if the density of the system is not spherically symmetric the force is not rotationally invariant. However as long as the density is derived in a self-consistent way there is nothing unphysical about this. The condition that the second-order corrections in nuclear matter be small, has not been examined for these forces. It is hoped

that, because the forces used are reasonably smooth and have soft cores, these second order corrections will be small. Nevertheless the omission of condition 4 must be borne in mind.

Determination of Matrix Elements

The discussion of chapter 2 has shown that the matrix elements of the interaction taken between harmonic oscillator states are required in the RHF calculation. In order to calculate these matrix elements certain further approximations have to be made. The two-body state which is a product of two harmonic oscillator states, without being antisymmetrized, is written as $|il)$, and the matrix element $(il|v|jm)$ will be considered for the remainder of this chapter.

The spin-isospin factor in (4) can be treated immediately and an integral over the space co-ordinates r_1 and r_2 remains. It is necessary to interpret the meaning of the relative wave number k, in $\lambda_r(k)$, as it appears in this integral. In the special case that the two oscillator states $|i)$ and $|l)$ have the same oscillator parameters, the two-body state $|il)$ can be transformed quite simply into a finite sum of similar states in which the relative and centre of mass co-ordinates are separated (Brody and Moshinsky 60 When this is done the matrix element $(il|v|jm)$ can be written

as a sum over simpler matrix elements of the form $(nmn_z|v|n'm'n_z')$, in which the states $|nmn_z)$ are states of the relative co-ordinate $(r_1 - r_2)/\sqrt{2}$. Kallio (1965) has shown that the value of k to use in the matrix element $(nmn_z|v|nmn_z)$, for the case of spherical states is given by

$$k^2 = (2n + |m| + n_z + 3/2)\,\alpha \qquad (6)$$

This expression is simply the mean square value of $(k_1 - k_2)/\sqrt{2}$ for the state $|nmn_z)$. However starting from $(il|v|jm)$ an alternative, though not equivalent, mean square value for k is

$$k^2 = \tfrac{1}{4}(2n_i + 2n_\ell + 2n_j + 2n_m + |m_i| + |m_\ell| + |m_j| + |m_m| + n_{zm} + n_{zi} + n_{zj} + n_{z\ell} + 6)\alpha \qquad (7)$$

In the approximation defined by (6) it is necessary to use a different value of k in each of the simple matrix elements which occur in the sum for $(il|v|jm)$. In the approximation defined by (7) there is only one k value which defines $\lambda_r(k)$ uniquely for $(il|v|jm)$, and there is consequently no need to rely on the separation of the relative co-ordinate in order to evaluate the matrix element. The results obtained using these two approximations for a typical matrix element in the spherical case are shown in figure 4. The variation of the matrix element with the size of the oscillator parameter is shown and it is seen that the two approximations are

almost identical. The approximation (7) will be used from now on and it is extended to the most general type of matrix element as

$$k^2 = \tfrac{1}{4}\{(2n_i + |m_i| + 1)\alpha_i + (2n_\ell + |m_\ell| + 1)\alpha_\ell + (2n_j + |m_j| + 1)\alpha_j$$

$$+ (2n_m + |m_m| + 1)\alpha_m + (n_{zi} + \tfrac{1}{2})\beta_i + (n_{z\ell} + \tfrac{1}{2})\beta_\ell + (n_{zj} + \tfrac{1}{2})\beta_j$$

$$+ (n_{zm} + \tfrac{1}{2})\beta_m\}. \qquad (8)$$

It must be noted that the matrix elements obtained in this way satisfy the requirement of being hermitian, since k^2 is symmetric with respect to all the states in the matrix element.

In order to incorporate the density dependence of the force, the nuclear density will be approximated by a gaussian shape normalized to give the correct number of particles. A gaussian distribution for the density is similar to the shape found for light nuclei in experiments, and such an analytic form is very convenient because $\rho^{2/3}$ is then also a gaussian. A further important feature of this gaussian approximation is that the general matrix elements of the force (4) can be determined analytically in this case. This is shown in detail in appendix 3. In approximation I the gaussian density is determined so that it has the same mean square values for the cylindrical co-ordinates ρ and z, as the nuclear density determined from the nuclear

wave function. Except when the RHF wave function is asymmetric the RHF density distribution is very close to that of the pure configuration which was used as a starting point in the calculation. Therefore we make the further approximation of calculating the mean square values of ρ and z from the pure configuration. If these mean square values are ρ_0 and z_0 respectively, then this approximation to the density is

$$\rho_I(r) = 2^{-1/2}\ \pi^{-3/2}\ \rho_0^{-2}\ z_0^{-1}\ A\ \exp\{-\rho^2/\rho_0^{\,2} - z^2/2z_0^{\,2}\}. \qquad (9)$$

This approximation overestimates the central density when compared with the actual density distribution of the nuclear wave function. Sometimes this overestimation is very marked as can be seen in the case of ^{16}O in figure 5. The effect of this is to over-suppress the interactions and the binding energy of the 1s shell particles. As these particles usually make a considerable contribution to the total energy of the nucleus the total energy is also suppressed. A second approximation has therefore been designed to give the correct density for this core region. This gaussian approximation is arranged to have the same central density as the starting configuration. The shape of this second approximate density is the same as that of the density of the starting configuration, i.e. $\langle\rho^2\rangle/\langle z^2\rangle$ is the same

for the true and approximate densities. This gives

$$\rho_{II}(r) = D \exp\{-\rho^2/K\rho_0^2 - z^2/2Kz_0^2\} \qquad (10)$$

where D is the central density and K is given by

$$K = [2^{-1/2}\,\pi^{-3/2}\,A/D\,\rho_0^2\,z_0]^{2/3} \qquad (11)$$

This approximation is shown for ^{16}O in figure 5, and it is seen that the approximate density distribution in this case extends beyond the true density distribution. It is also seen that in the region where $r^2\rho(r)$ is a maximum this second approximate density is less than the true density. This means that for the bulk of the particles the interaction is not sufficiently suppressed by this approximation, and consequently the total binding energy is too large in this approximation. For the case of ^4He the density distribution of the dominant configuration is exactly gaussian and in this case the two approximations coincide. For the other nuclei considered the best situation lies between these two extremes. Unfortunately the extremes are quite widely separated for the other nuclei as will be seen in chapter 7, and while some of the features of the density dependent force can be distinguished here, an improved density approximation is clearly needed.

CHAPTER 4

COMPUTATIONAL ASPECTS OF THE RESTRICTED-HARTREE FOCK CALCULATION

In this chapter technical problems related to our choice of representation and form of interaction are considered. Most of the RHF calculations which we have performed used a representation based on the first three shells of harmonic oscillator states. This gives 10 different space states (which will be called orbitals) which, when combined with spin and isospin states, produce a representation of 40 single-particle states. The Hartree-Fock states to be found have definite isospin, i.e. they are occupied either by a proton or a neutron. This reduces the density matrix ρ to the direct sum of two 20 x 20 matrices, which are denoted by $\rho^{(n)}$ and $\rho^{(p)}$ for neutrons and protons respectively.

The interaction to be used has the form

$$V_{ij} = (w + mP_x + bP_\sigma + hP_\tau)\ v(r_{ij})$$

and the dependence on the spin and isospin co-ordinates is very simple. In fact if we define:

$\delta^{\sigma}_{ij} = 0$ if states $|i\rangle$ and $|j\rangle$ have opposite spins

$= 1$ if states $|i\rangle$ and $|j\rangle$ have the same spins

$\delta^{\tau}_{ij} = 0$ if states $|i\rangle$ and $|j\rangle$ have opposite isospins

$= 1$ if states $|i\rangle$ and $|j\rangle$ have the same isospins

$\delta^{\sigma}_{il;jm} = 0$ if states $|il\rangle$ and $|jm\rangle$ have different spins

$= 1$ if states $|il\rangle$ and $|jm\rangle$ have the same spins,

then the matrix element of the interaction can be written

$$(il|v|jm) = \delta^{\sigma}_{il;jm}\,\delta^{\tau}_{il;jm}\,[V_{iljm}(w\delta^{\sigma}_{ij}\,\delta^{\tau}_{ij} + b\,\delta^{\sigma}_{im}\,\delta^{\tau}_{ij} + h\delta^{\sigma}_{ij}\,\delta^{\tau}_{im}) + V_{ilmj}\,m\delta^{\sigma}_{ij}\,\delta^{\tau}_{ij}] \qquad (1)$$

In this expression V_{iljm} represents the configuration-space part of the matrix element. Using this and the relevant equation of (27) in chapter 2, it is a matter of simple algebra to show that the average potential Γ is diagonal in isospin and that for neutrons this potential is given by

$$\Gamma^{(n)}_{ij} = \Sigma^{(n)}_{l,m}\,\rho^{(n)}_{lm}\,\delta^{\sigma}_{il;jm}\{V_{iljm}[(w+h)\,\delta^{\sigma}_{ij} + (b-m)\,\delta^{\sigma}_{im}] - V_{ilmj}[(w+h)\,\delta^{\sigma}_{im} + (b-m)\,\delta^{\sigma}_{ij}]\}$$

$$+ \Sigma^{(p)}_{l,m}\,\rho^{(p)}_{lm}\,\delta^{\sigma}_{il;jm}\{V_{iljm}[w\delta^{\sigma}_{ij} + b\delta^{\sigma}_{im}] - V_{ilmj}[h\delta^{\sigma}_{im} - m\delta^{\sigma}_{ij}]\}\,. \qquad (2)$$

The summations $\Sigma^{(n)}$ and $\Sigma^{(p)}$ in this expression are to be carried out respectively over neutron and proton states l and m. The equivalent form for the proton potential is obtained

from (2) by interchanging $\rho^{(n)}$ and $\rho^{(p)}$.

It is also possible to define an average over the neutron and proton potentials as

$$\Gamma^{(av)}_{ij} = \tfrac{1}{2}(\Gamma^{(n)}_{ij} + \Gamma^{(p)}_{ij}) = \Sigma_{l,m} (\rho^{(n)}_{lm} + \rho^{(p)}_{lm}) \delta^{\sigma}_{iljm}$$

$$\{V_{iljm} [(w + \tfrac{1}{2}h) \delta^{\sigma}_{ij} + (b - \tfrac{1}{2}m) \delta^{\sigma}_{im}] - V_{ilmj}$$

$$[(\tfrac{1}{2}w + h) \delta^{\sigma}_{im} + (\tfrac{1}{2}b - m) \delta^{\sigma}_{ij}]\} . \qquad (3)$$

In the special case that neutrons and protons appear symmetrically and $\rho^{(n)}$ is equal to $\rho^{(p)}$, then

$$\Gamma^{(av)} = \Gamma^{(n)} = \Gamma^{(p)} .$$

This is true in particular for the low lying states of light even-even nuclei.

It must be noted that the calculations have been carried out with real density matrices, as opposed to complex ones. This constraint on the solutions is equivalent to requiring that the nuclear system has a symmetry plane. This can be seen as follows. The nuclear density is given by

$$\rho_N(r) = \Sigma_{\alpha} \langle r|\alpha\rangle \langle\alpha|r\rangle = \Sigma_{ij} \rho_{ij} \psi_i(r) \psi_j(r)^* ,$$

where

$$\psi_i(r) = \langle r|i\rangle ,$$

is the single-particle wave function for the i'th representation state. ρ is hermitian and if it is real also,

then we can write

$$\rho_N(r) = \tfrac{1}{2} \Sigma_{ij} \rho_{ij} (\psi_i(r) \psi_j(r)^* + \psi_i(r)^* \psi_j(r)) .$$

In the cylindrical representation this gives

$$\rho_N(r) = \tfrac{1}{2}\Sigma_{ij} \rho_{ij} F_{ij}(\rho,z) [e^{i(m_i - m_j)\phi} + e^{-i(m_i - m_j)\phi}]$$

$$= \Sigma_{ij} \rho_{ij} F_{ij}(\rho,z) \cos(m_i - m_j)\phi , \qquad (4)$$

where F_{ij} is a real valued function of the cylindrical co-ordinates ρ and z. The density $\rho_N(r)$ given by (4) has reflection symmetry across the x-z plane. It can also be seen from (4) that asymmetry across the y-z plane is produced by density matrix elements ρ_{ij} between states whose m values differ by an odd integer. In a similar way asymmetry across the x-y plane is induced by density matrix elements connecting states whose n_z values differ by an odd integer.

It was mentioned in the first chapter that simple configurations would be used as starting points for our RHF calculations. However the density matrix $\rho^{(0)}$ for such a simple configuration is diagonal and so the wave function has none of the assymmetries listed in the preceding paragraph. It has already been pointed out that the RHF calculation always retains any symmetry which exists at the start, and therefore it is necessary to allow for

asymmetries at the initial stage of the calculation. The method used to do this is quite arbitrary and consists in taking the eigenvectors of a matrix of random numbers as initial states. However, in order to keep close to the shell model type of states, the matrix to be diagonalized is weighted with diagonal elements an order of magnitude larger than the off-diagonal elements. In this way we start with initial single-particle states which are close to the states of the simple configuration (a typical overlap is 90%). Because the states are ordered according to their eigenvalues and occupied in this order, the initial configuration can be chosen by making the diagonal elements, corresponding to occupied states, smaller than those corresponding to unoccupied states. The amount of mixing in the initial states can be reduced by making the diagonal elements larger.

In order to have some measure of the difference between the density matrix ρ resulting from the RHF calculation and the density matrix $\rho^{(0)}$ for the corresponding configuration, we introduce the sum

$$\sigma = \Sigma_{ij} \, (\rho^{(0)}_{ij} - \rho_{ij})^2 \, .$$

This can be separated into partial sums over certain pairs of states, as follows:

$$\sigma_1 = \sum_{ij} (\rho^{(0)}_{ij} - \rho_{ij})^2 \text{ for } m_i = m_j, \; \Pi_i = \Pi_j$$

$$\sigma_2 = \sum_{ij} (\rho^{(0)}_{ij} - \rho_{ij})^2 \quad \text{for } m_i = m_j,\ \Pi_i \neq \Pi_j$$

$$\sigma_3 = \sum_{ij} (\rho^{(0)}_{ij} - \rho_{ij})^2 \quad \text{for } m_i \neq m_j,\ \Pi_i = \Pi_j$$

$$\sigma_4 = \sum_{ij} (\rho^{(0)}_{ij} - \rho_{ij})^2 \quad \text{for } m_i \neq m_j,\ \Pi_i \neq \Pi_j \quad .$$

Π_i denotes the parity of the representation state $|i\rangle$. As a matter of normalization we will use the root mean square values

$$\theta_i = [\sigma_i / \ell_i]^{1/2} \tag{5}$$

where ℓ_i is the number of terms in the sum for σ_i. These mixing parameters θ_i give an indication of how different the RHF solution is from the simple configuration with the diagonal density matrix $\rho^{(0)}$. Unfortunately it is found that the values of θ_2 and θ_4 though small, are extremely unstable, depending on the random starting point for the first iteration. It is concluded that the mixing between states of opposite parity is not necessarily convergent even when the energy is.

Separate computer programs are used for the RHF calculations in the 3 and 4 oscillator shell representations. A program HARFOK is based on the 3 shell representation and uses one 20 x 20 matrix, which is

$$\rho^{tot} = \rho^{(n)} + \rho^{(p)}$$

Equation (3) is used to construct the average potential Γ^{av},

and this program is used for even-even configurations in which neutrons and protons appear symmetrically. A program HARFO1, which has separate density matrices $\rho^{(n)}$ and $\rho^{(p)}$ for the neutron and proton systems, has also been used. Because of some difficulties with convergence, which will be explained below, no results for this program are shown here. The 4 shell program HARFO4, uses one density matrix, which is the sum of the neutron and proton density matrices. In this case though, there are 80 single-particle states in the representation and matrices that are 20 x 20 in HARFOK become 40 x 40 in HARFO4. Even in the 4 shell program there is no constraint on the single-particle states other than that imposed by the reality of the density matrix. This program is naturally more time consuming than HARFOK and has been used sparingly. An indication of the relative times taken by these programs will be given in appendix 4, where these programs are shown schematically.

One further technical point will be made here. Both RHF programs diagonalize the symmetric matrices representing $T + \Gamma$, by a Jacobi type of procedure, rather than by the faster Householder procedure. The reason for this is that the Householder procedure has a tendency to produce eigenvectors which are not exactly orthogonal. It is felt that this may cause errors in the density matrix to accumulate

over several iterations.

We come now to the question of convergence. Equations (27) in chapter 2 define our iteration procedure, and it has been said that iterations should continue until convergence is obtained. However, there is no proof that this or any similar procedure must converge, and in fact very often this procedure clearly does not. Still worse, there is no proof that successive approximations $E^{(p)}$ to the energy of a ground state improve, i.e. become smaller. Again there are cases where this does not occur. What has been found in the present series of calculations is that the approximations $E^{(p)}$ normally appear to converge fairly rapidly (e.g. in 4 to 8 iterations). But after this initial convergence, the values of $E^{(p)}$ may vary slowly by as much as 0.05 MeV per iteration. This effect is almost certainly larger than any rounding error which might occur in the diagonalization. Some examples are shown in figures 6, 7, 8 and 9.

Figure 6 is a rather extreme case of what may occur, showing at first an apparent convergence of the energy but later on a marked improvement. Part of the reason for this particularly poor convergence is that the representation states have what is obviously the wrong shape to describe the true Hartree-Fock system. This suggests that iterations will converge more rapidly when the best set of oscillator

parameters is used. Figure 7 shows the same configuration as Figure 6 but now in the spherical representation, which is the best one. However, the representation states are now a little larger than the best possible ones. In this case convergence is not obvious even after 58 iterations and the best energy encountered is that of the random starting point! This is in sharp contrast to Figure 8 which shows the same configuration but now with the best oscillator parameters as determined by GHA calculation. In this case the variations in $E^{(p)}$ after the 11'th iteration are of the order of 10^{-5} MeV, which is the same as the order of magnitude of errors in the eigenvalues $\varepsilon_\alpha^{(p)}$ resulting from the diagonalization procedure. Figure 9 shows a different nucleus but again in the best representation as determined by the corresponding GHA calculation. In this case the RHF calculation builds up an asymmetry in the density distribution which does not exist in the simple configuration. Because of this, convergence is slower than for the previous example but is nevertheless quite definitely achieved after 14 iterations. It is reasonable that convergence should be improved by starting as close as possible to the Hartree-Fock solution, and the results just discussed show that the choice of the correct representation parameters is important in this respect. In order to compare different calculations we use

the energy after 20 iterations, unless it is apparent that there is no convergence. Furthermore, the final energies $E^{(p)}$ are considered to have errors of ± 0.05 MeV.

The difficulties associated with convergence are worse for HARFO4 than for HARFOK, and are almost certainly dependent on the size of the matrices which are diagonalized in each iteration. Once again convergence seems to be faster when the values for the size parameters of the oscillator states, which give the lowest energy, are used.

In those cases where the approximations $E^{(p)}$ converge, the single particle energies $\varepsilon_{\alpha}^{(p)}$ converge more slowly, but they do converge. The eigenstates, which appear as columns of the matrix B in (1-27), converge even more slowly than the single-particle levels, and when there are degenerate single-particle levels they may not converge at all.

Quite apart from these problems of slow convergence, there are situations where there is clearly no convergence. To see how this can occur we consider a specific example. Suppose that the states chosen initially are just the states of the representation, and that the first 17 are occupied. In the first iteration the average potential, produced by these 17 occupied states, is computed and the corresponding eigenstates are found. Because of the restricted nature of the calculation most of these eigenstates are essentially

the same as the states with which we started. However when the new eigenstates are ordered according to increasing single-particle energy, they do not correspond to the old ones. In particular if the 17th state was originally a spin-up state, it will become a spin-down state. The spin-down state has a lower energy than the spin-up state, in the potential produced by the spin-up system. This is the crux of the matter, because it means that following our procedure the spin of the last state changes at each iteration. It also means that when the energies $E^{(p)}$ are calculated according to the formulae in chapter 2, they represent the energy of the spin-down system in the average potential produced by the spin-up system or vice versa. These energies are the same but neither is self consistent. This points out that unless the density matrix $\rho^{(p)}$ converges, or at least comes close to convergence, the results of the RHF program are meaningless. In general this problem does not occur for configurations with maximum space symmetry, but an exceptional case occurs in ^{8}Be and is discussed in chapter 6. This awkward "flip-flop" phenomenon can be avoided in various ways. One way might be to use a representation of states which had time-reversal symmetry, or were either symmetric or antisymmetric with respect to an interchange of spin. Alternatively one could change the

method, used in the iterations, to select the occupied states.

Before leaving the matter of convergence it must be pointed out that if 40 states are occupied in the 3-shell representation, then no matter how they are chosen the density matrix is just the 40 x 40 unit matrix. Because of this convergence is immediate. Quite generally the RHF calculation can only improve the energy of a state by mixing occupied and unoccupied states. The number of unoccupied states in the calculation is a measure of the number of degrees of freedom allowed. For the special case of no unoccupied states, just considered, there are no degrees of freedom and the result of the RHF calculation is a simple configuration.

The generalized Harmonic Approximation is carried out by the program MINDET. This is a very simple program consisting essentially of a minimization procedure and procedures to evaluate the energy of a configuration wave function for arbitrary oscillator parameters. The minimization procedure is due to Powell (1964), though some modifications have been made. This procedure works very well for a general n-dimensional quadratic function, and is explained further in appendix 5. It has been found that if the root mean square sizes of the orbitals are used as independent parameters, instead of the oscillator

constants, then the energy function is more symmetric about the minimum, and convergence of the minimization procedure is correspondingly faster. We have for $|nmn_z:\alpha\beta>$

$$<x^2>^{1/2} = <y^2>^{1/2} = [\tfrac{1}{2}(2n + |m| + 1) / \alpha]^{1/2}$$

$$<z^2>^{1/2} = [(n_z + \tfrac{1}{2}) / \beta]^{1/2}$$

In order to compare sizes of orbitals with different quantum numbers it is more convenient to use the parameters for the $|000:\alpha\beta>$ state.

Thus
$$a = (1/2\alpha)^{1/2} \qquad (6)$$
$$b = (1/2\beta)^{1/2}$$

Because the different space orbitals must be kept orthogonal, it is not sufficient to have independent a and b parameters for each state. The necessary constraints are considered in appendix 1, and it can be seen that the dimension of the parameter space for nuclei in the 2s-1d shell is of the order of 10 if the maximum number of parameters is used. In some cases the number of parameters can be reduced. For example the ground state configurations of ^{16}O and Ca^{40} are obviously spherical, so that the a's can be made equal to the corresponding b's. However, apart from these special cases the GHA results quoted here correspond to the most general set of parameters.

A very similar program, MINCAR, has been used to carry out this same calculation with configurations of cartesian states $|n_x n_y n_z : \alpha_x \alpha_y \alpha_z)$. In this case there are more parameters, and the constraints are imposed in an analogous way to those for the cylindrical states. The results obtained with MINCAR are equivalent to those obtained with MINDET, except when the equilibrium shape is not cylindrically symmetric.

The minimization routine normally evaluates $3N + 4$ points per pass when working in an N dimensional parameter space, and these passes continue until convergence is obtained. In practice about $\frac{1}{2}N$ passes are used and convergence is surprisingly fast. Even so it is necessary to calculate some 200 energies for nuclei towards the end of the 2s-1d shell, and this can become rather time consuming. The time to evaluate one point is roughly proportional to the square of the number of orbitals filled. For ^{40}Ca, in which there are ten filled orbitals, the time per point is about 6 seconds (an IBM 7040 computer was used).

CHAPTER 5

DEFORMATION IN LIGHT NUCLEI

The use of a representation of cylindrical harmonic oscillator states with two shape parameters each, as opposed to a representation of spherical states with one parameter each, can be justified to some extent by equation (28) of chapter 2. The larger the number of parameters which occur in the energy function in this equation, the closer the minimum value of the energy should come to the true Hartree-Fock value. However, it must be noted that some degrees of freedom lead to considerable improvement in the minimum value of E, while others lead to no improvement. Which degrees of freedom are the most important must, in general, be discovered by carrying out the relevant minimizations. However, some qualitative statements can be made by applying two intuitive rules to the minimization of the energy of a configuration wave function as in equation (30) of chapter 2.

1. The Hartree-Fock potential Γ has a shape which is close to that of the density of the system.
2. The best harmonic oscillator wave functions to use

should come from a harmonic well of about the same shape as the Hartree-Fock potential.

These two ideas were used by Mottelson (1958) to predict equilibrium shapes of configuration wave functions. In order to allow for the most general shapes at this stage we will use the cartesion representation of states $|n_x n_y n_z; \alpha_x \alpha_y \alpha_z\rangle$. To simplify our qualitative discussion the harmonic oscillator wave functions to be used in the configuration will be taken from the same asymmetric potential well. Thus the energy of the configuration can be written $E(\alpha_x, \alpha_y, \alpha_z)$. Mottelson's argument is that the shape of the configuration wave function is given by

$$\langle x^2\rangle : \langle y^2\rangle : \langle z^2\rangle = \frac{1}{\alpha_x} \Sigma_i (n_{xi} + \tfrac{1}{2}) : \frac{1}{\alpha_y} \Sigma_i (n_{yi} + \tfrac{1}{2}) :$$

$$\frac{1}{\alpha_z} \Sigma_i (n_{zi} + \tfrac{1}{2}) = N_x/\alpha_x : N_y/\alpha_y : N_z/\alpha_z,$$

and that the shape of the harmonic potential is given by

$$\langle x^2\rangle : \langle y^2\rangle : \langle z^2\rangle = \frac{1}{\alpha_x^2} : \frac{1}{\alpha_y^2} : \frac{1}{\alpha_z^2} .$$

If these shapes are to be the same then

$$\frac{1}{\alpha_x} : \frac{1}{\alpha_y} : \frac{1}{\alpha_z} = N_x : N_y : N_z \qquad (1)$$

This argument is not connected with a variational principle,

but Ripka (1966) has shown how (1) can be derived from such a principle. In fact if the harmonic potential is used instead of the Hartree-Fock potential, the energy of the configuration can be written

$$E = \hbar^2/m \, (N_x \alpha_x + N_y \alpha_y + N_z \alpha_z) \, . \qquad (2)$$

If the α are varied arbitrarily to make E a minimum the system simply expands to infinity and the particles become free. However, the fact that the potential must arise in a self-consistent way from the particles themselves, can be regarded as a constraint on the volume of the system, thus

$$\alpha_x \alpha_y \alpha_z = \text{Const.} \qquad (3)$$

If the minimization of (2) is now carried out subject to (3), equation (1) results.

This result can be immediately generalized because in the harmonic well the kinetic and potential energies are equal. Thus the minimum for the total energy occurs at the same shape as the minimum for the kinetic and potential energies. It follows that condition (1) will hold whenever the total potential energy of the configuration wave function has its minimum at the same shape as the kinetic energy. This general result includes the special case that the potential energy is independent

of the deformation. In this case the SU(3) symmetry group can be used at zero deformation to classify the potential energies of simple configurations. Ripka has used this technique to predict the ordering of configurations for 2s-1d shell nuclei. He also shows that the ordering obtained by minimizing the kinetic energy is the same as the ordering obtained with an SU(3) model.

Though the Mottelson rule depends on the behaviour of the potential, there is a weaker result which is independent of the interaction. If the configuration to be minimized is transformed by interchanging the x and y axes, then all the orbitals are transformed according to

$$[n_x\ n_y\ n_z] \rightarrow [n_y\ n_x\ n_z],$$

and the oscillator parameters $(\alpha_x, \alpha_y, \alpha_z)$ are transformed to $(\alpha_y, \alpha_x, \alpha_z)$. In general a new configuration results with the same shape and energy. However, if the configuration itself is unchanged in this transformation, that is if the orbitals $[n_x\ n_y\ n_z]$ are merely permuted by the transformation

$$[n_x\ n_y\ n_z] \rightarrow [n_y\ n_x\ n_z] \quad ,$$

then it follows that the energy of the configuration wave function is symmetric about the $\alpha_x = \alpha_y$ plane. Furthermore if the potential is such that there is a unique minimum then this minimum must lie in the $\alpha_x = \alpha_y$ plane. This

general symmetry argument applies equally well to y-z and z-x symmetries. An alternative statement of the result is that any spatial symmetry which exists in the configuration wave function at a point where $\alpha_x = \alpha_y = \alpha_z$, also exists in the configuration wave function which gives the lowest energy. Unfortunately this result does not hold when different orbitals are allowed to have different oscillator constants.

Table 2 shows the ratio of axes for the equilibrium shapes of some simple configurations as predicted by (1). It should be noticed that the great majority of these configurations have cylindrical symmetry at equilibrium, and such configurations can be described by the less general cylindrical representation. Because of the higher symmetry of the cylindrical oscillator states, they are generally more convenient to use. This is why most of our calculations use this representation. It will be shown later, when dealing with asymmetric nuclei, that the RHF calculation in a cylindrical representation can be as good as the GHA calculation in a cartesian representation.

The extra degrees of freedom obtained by allowing different spatial orbitals to have different size parameters, i.e. to come from oscillator potentials of different sizes, are not considered in the Mottleson rule. If the i'th orbital has oscillator constants

TABLE 2

MOTTELSON RULE EQUILIBRIUM SHAPES FOR SOME CARTESIAN CONFIGURATIONS

NUCLEUS	CONFIGURATION	x^2 : y^2 : z^2	Q/R^2
^{4}He	1S	1.00 1.00 1.00	0.00
^{8}Be	1S, $[001]^4$	1.00 1.00 4.00	1.00
	1S, $[002]^4$	1.00 1.00 9.00	1.45
^{12}C	1S, $[100]^4$, $[010]^4$	2.78 2.78 1.00	-0.54
	1S, $[001]^4$, $[002]^4$	1.00 1.00 9.00	1.45
^{16}O	1S, 1P	1.00 1.00 1.00	0.00
	1S, $[001]^4$, $[010]^4$, $[002]^4$	1.00 2.25 6.25	0.97
	1S, $[001]^4$, $[002]^4$, $[003]^4$	1.00 1.00 16.00	1.67
^{20}Ne	1S, 1P, $[002]^4$	1.00 1.00 2.47	0.66
	1S, 1P, $[110]^4$	1.70 1.70 1.00	-0.32
	1S, 1P, $[003]^4$	1.00 1.00 3.45	0.90
^{24}Mg	1S, 1P, $[002]^4$, $[011]^4$	1.00 1.56 3.06	0.63
	1S, 1P, $[020]^4$, $[200]^4$	2.25 2.25 1.00	-0.45
	1S, 1P, $[002]^4$, $[003]^4$	1.00 1.00 5.06	1.15

TABLE 2

MOTTELSON RULE EQUILIBRIUM SHAPES FOR SOME CARTESIAN CONFIGURATIONS (cont'd)

NUCLEUS	CONFIGURATION	x^2 :	y^2 :	z^2	Q/R^2
^{28}Si	1S, 1P, $[200]^4$, $[020]^4$, $[110]^4$	2.78	2.78	1.00	-0.54
	1S, 1P, $[002]^4$, $[011]^4$, $[101]^4$	1.00	1.00	2.39	0.63
	1S, 1P, $[002]^4$, $[011]^4$, $[003]^4$	1.00	1.49	5.08	1.01
^{32}S	1S, 1P, $[002]^4$, $[020]^4$, $[011]^4$, $[101]^4$	1.00	1.78	2.25	0.34
	1S, 1P, $[002]^4$, $[011]^4$, $[101]^4$, $[110]^4$	1.00	1.00	1.65	0.36
	1S, 1P, $[200]^4$, $[020]^4$, $[002]^4$, $[110]^4$	1.31	1.31	1.00	-0.17
	1S, 1P, $[200]^4$, $[020]^4$, $[101]^4$, $[011]^4$	1.31	1.31	1.00	-0.17
	1S, 1P, $[002]^4$, $[101]^4$, $[011]^4$, $[003]^4$	1.00	1.00	4.00	1.00
^{36}A	1S, 1P, $[200]^4$, $[020]^4$, $[011]^4$, $[101]^4$, $[110]^4$	1.27	1.27	1.00	-0.15
	1S, 1P, $[002]^4$, $[020]^4$, $[200]^4$, $[011]^4$, $[101]^4$	1.00	1.00	1.78	0.41
	1S, 1P, $[002]^4$, $[020]^4$, $[011]^4$, $[101]^4$, $[003]^4$	1.00	1.72	3.69	0.73
^{40}Ca	1S, 1P, 2S-1D	1.00	1.00	1.00	0.00
	1S, 1P, $[002]^4$, $[020]^4$, $[200]^4$, $[011]^4$, $[101]^4$, $[003]^4$	1.00	1.00	2.08	0.53
	1S, 1P, $[002]^4$, $[020]^4$, $[011]^4$, $[101]^4$, $[110]^4$, $[003]^4$	1.00	1.56	1.64	0.17

$$\alpha_{xi} = k_i \, \alpha_x$$

$$\alpha_{yi} = k_i \, \alpha_y$$

$$\alpha_{zi} = k_i \, \alpha_z$$

so that all the orbitals have the same shape, but their sizes are determined by the k_i, then the shapes of the nucleus and the harmonic well are consistent if

$$\frac{1}{\alpha_x} : \frac{1}{\alpha_y} : \frac{1}{\alpha_z} = \Sigma_i \frac{(n_{xi} + \tfrac{1}{2})}{k_i} : \Sigma_i \frac{(n_{yi} + \tfrac{1}{2})}{k_i} : \Sigma_i \frac{(n_{zi} + \tfrac{1}{2})}{k_i} \tag{4}$$

On the other hand the minimum value of the kinetic energy, subject to the constraint (3) is given by

$$\frac{1}{\alpha_x} : \frac{1}{\alpha_y} : \frac{1}{\alpha_z} = \sum_i k_i (n_{xi} + \tfrac{1}{2}) : \sum_i k_i (n_{yi} + \tfrac{1}{2}) : \sum_i k_i (n_{zi} + \tfrac{1}{2}) \tag{5}$$

which is not the same as (4). When detailed minimizations are performed, it is found that there is a slight tendency for different orbitals to have different sizes, particularly in some excited states and some very light nuclei. There is a more noticeable tendency for the deformations to differ, and therefore equations (4) and (5) will not be considered further.

Nuclear configurations will be specified by writing the orbitals and the number of particles occupying them in

an obvious way. Thus

$$(000)^4,\ (001)^4,\ (010)^4,\ (0\text{-}10)^4$$

denotes the ground state configuration of ^{16}O in which the 1s and 1p shells are filled. Cylindrical states are denoted as $(n\ m\ n_z)$, and cartesian states as $[n_x\ n_y\ n_z]$. The configuration above can be written in the cartesian representation as

$$[000]^4,\ [001]^4,\ [010]^4,\ [100]^4.$$

It is convenient to denote filled shells by an abbreviated notation. Thus the above configuration can be expressed more simply as 1S, 1P.

The deformation of cylindrically symmetric nuclear densities will be defined by the parameter

$$Q/R^2 = (2\langle z^2\rangle - \langle x^2\rangle - \langle y^2\rangle)/(\langle x^2\rangle + \langle y^2\rangle + \langle z^2\rangle), \qquad (6)$$

the value of this parameter is given for the equilibrium shapes in table 2. We will now make some quantitative statements about some typical configurations, considering in particular the effect of allowing the representation states to deform. All the calculations considered in this chapter have been carried out with force 1 (of Table 1).

Consider first the lowest energy configuration of ^{20}Ne,

$$1S,\ 1P,\ (002)^4,$$

for which table 2 gives an equilibrium shape which is

cylindrically symmetric. Figure 10 shows the energy obtained from RHF calculations in three and four shell representations and the energy of the simple configuration, as a function of the deformation of the representation states. The deformation parameter d is simply the value of Q/R^2 for the (000) orbital (this is the same as the deformation of the ^{16}O core). The volume has been chosen to give the best energy for the simple configuration at zero deformation. It is seen that the RHF calculations always give a lower energy than the configuration, as is to be expected. The energy gained in doing the three shell RHF calculation is almost independent of the deformation, and is considerably smaller than that gained by allowing the representation to deform from the spherical situation. Another important point is that the best deformation to use for this three shell RHF calculation is very close to the deformation which gives the minimum energy for the pure configuration. This minimum occurs when the axes of the nuclear density have roughly the ratio

$$\langle x^2 \rangle : \langle y^2 \rangle : \langle z^2 \rangle = 1:1:2.24 \qquad (7)$$

which is very close to the shape predicted by the Mottelson rule. For the shape (7), $Q/R^2 = 0.61$.

If the shape of the RHF calculation was independent of the representation then it could be expected that the energy would also be independent. The fact that the energy

gained in the three shell RHF calculation is practically indpendent of the deformation d, suggests that the difference between the RHF solution and the configuration is not their shape but some slight polarization of the orbitals which does not vary appreciably with the shape. This is borne out by figure 11, which shows the variation of the parameter Q/R^2 for the configuration and for the three shell RHF solution. Figure 12 shows the previously defined mixing parameters θ_1 and θ_3, again for the three shell representation. It can be seen that θ_1 goes through a shallow minimum in the region where the energy is a minimum and θ_3 decreases slowly with deformation. This seems to support the idea of a slight polarization at all deformations. The GHA result obtained by minimizing with respect to all the available oscillator constants and the RHF result obtained using the oscillator constants resulting from the GHA calculation, are shown for comparison in figure 10. The degrees of freedom involved in allowing different sizes and deformations for the different orbitals make a slight improvement and the energy gained by the RHF calculation is unchanged. The value of Q/R^2 for the best three shell RHF solution is 0.593 which is still close to the value in Table 2. In order to understand the success of the Mottelson rule we consider the variation of the total kinetic and potential energy for the configuration

wave function. This is shown in figure 13. The minimum for the kinetic energy occurs at the shape predicted by (1) and the potential energy reaches a minimum at a somewhat smaller but positive deformation. It is obvious that the minimum energy for the configuration occurs somewhere in between. The reason that the Mottelson rule holds so well is that the potential energy change is small and has its minimum value close to where the kinetic energy is a minimum. It must be pointed out here that there is no tendency towards asymmetry in the RHF calculation, even though this is allowed.

The results of the four shell calculation, shown in figure 10, are less dependent on the shape of the representation than those of the three shell one. The reason for this is that in the four shell calculation there is a complete shell of unoccupied states, the 2p-1f shell, and the occupied 1p states can change their shape by mixing with the unoccupied states of the same parity. The lowest energy obtained in the four shell calculations, shown in figure 10, is a little lower than the energy from the three shell calculation using the best oscillator parameters of the GHA calculation. This suggests that the extra degrees of freedom in the four shell calculation are used to build up orbitals with different oscillator constants. The four shell calculation is able to build up

more of the tail region of the true single-particle wave functions, because the representation now contains states which are extended over a larger region. The single-particle tails will be considered in detail below.

We next consider similar calculations for the ^{8}Be configuration $(000)^4$, $(001)^4$. Table 2 shows an equilibrium shape which again is cylindrically symmetric with $Q/R^2 = 1.0$. Figure 14 shows the variation of energy with deformation for the pure configuration and for the three and four shell RHF solutions. Once again the size of the representation states has been chosen to minimize the energy of the pure configuration at zero deformation. There is a striking difference between this and figure 10, which arises because in the case of ^{8}Be there are one and two complete shells of unoccupied oscillator states in the two representations. These extra degrees of freedom, available in the RHF calculations for ^{8}Be, can be seen very clearly in the dependence of the energy on the deformation of the representation. Near the spherical situation the energies of the RHF solutions are flatter than that of the pure configuration and the minima for the three curves are separated. The GHA result obtained by allowing the two occupied orbitals to have independent sizes and deformations is close to the best RHF energy. Furthermore the three shell RHF solution obtained using the GHA representation

has almost the same energy as the pure configuration. This means that the RHF calculations are able to construct orbitals of different size and shape, even when the representation states are constrained to have the same size and shape. It is largely this feature which causes the RHF solutions to be so much lower than the pure configuration.

There is an additional feature in ^{8}Be which is characteristic of light nuclei. Because the average Hartree-Fock potential goes to zero at large distances from the centre of the nucleus, the eigenstates of this potential have larger tails than the harmonic oscillator states (which come from a potential which becomes strongly repulsive at large distances). The tails for single-particle states which are strongly bound, i.e. have low single-particle energies, are smaller than those for states which are only just bound. The weakly bound states for which the tail region is important are just those which spatially are in or near the surface of the nucleus. Because of this, in a nucleus like ^{8}Be which is almost all surface, the inclusion of higher shells increases the tails of all the particles and has a significant effect on the energy of the system. In the case of ^{20}Ne there is a smaller proportion of surface particles and they do not make much contribution to the total binding energy. Thus the

inclusion of the higher shells does not have so much effect on the total energy of heavier nuclei. These points are evident in figures 10 and 14.

The mixing parameters θ_1 and θ_3 for the three shell RHF calculation are shown in figure 16, and they demonstrate that the solution becomes closer to the pure configuration as the deformation is increased. The minimum energies of the pure configuration and the three shell RHF solution occur for Q/R^2 values of 0.965 and 0.975 respectively both of which are very close to the value given by the Mottelson rule. The Q/R^2 value for the three shell RHF solution in the GHA representation is a little less, being 0.954 . Figure 17 shows the variation of the kinetic and potential energies for the pure configuration. These have minimum values fairly close to one another and as explained above this is the reason for the success of the Mottelson rule. It should be noted that in this case the variation of kinetic energy is about four times that of the total potential energy.

Figures 18, 19 and 20 show the variation of the total energy, shape, and kinetic and potential energies with deformation, for the doubly closed shell configuration of ^{16}O. As expected the minima for the energies occur at zero deformation. There is no tendency for the potential to deform the system and so the Mottelson rule holds

exactly. The four shell RHF calculation at the spherical point is 0.07 MeV below the three shell calculation. This justifies the assertion that except in very light nuclei the tails of the single-particle states are not significant in terms of total energy. However, as will be seen in the next chapter, the single-particle levels for ^{16}O are all deeply bound and this may be part of the reason why there is such a small change in total energy here.

We now consider the asymmetric or triaxial nucleus ^{24}Mg for which our cylindrical representation is not so well suited. The ^{24}Mg configuration of cartesian states

$$1S,\ 1P\ [002]^4,\ [011]^4$$

which has the lowest energy, has an asymmetric shape as predicted in table 2. The closest configuration of cylindrical states is

$$1S,\ 1P\ (002)^4,\ (011)^4\ .$$

Figure 21 shows the energy obtained for this cylindrical configuration, and from three and four shell RHF calculations based on this configuration as a function of the deformation of the representation. Also shown for comparison are the results of the GHA calculation for the cylindrical configuration, the three shell RHF calculation using the oscillator parameters found in this GHA calculation, and the cartesian GHA calculation for the cartesian configuration

mentioned above. The three shell RHF calculation is definitely better than the pure configuraton of cylindrical states, even when full use is made of varying all the oscillator parameters. This indicates that the ability of the RHF calculation to change the occupied (011) orbital into a cartesian type orbital by mixing it with the unoccupied (0-11) orbital, is important in terms of the total energy. Furthermore the fact that the configuration of cartesian states can have a lower energy, indicates that the ability of the ^{16}0-like core to become asymmetric is also important. The four shell RHF result is slightly lower than the cartesian configuration. This shows that the four shell calculation is able to deform the core.

The shape parameter Q/R^2 is shown in figure 22. The asymmetry parameter for the RHF solution is defined as

$$\chi = |\langle x^2 - y^2 \rangle / \langle x^2 + y^2 \rangle| ,$$

and is also shown in figure 22. It can be seen that this is constant as the deformation varies, with a value of 0.227 . The corresponding value for the configuration of cartesian states is 0.195 . The axes of the nuclear density for this configuration have the ratio

$$\langle x^2 \rangle : \langle y^2 \rangle : \langle z^2 \rangle = 1:1.50:2.72$$

which is close to the ratio predicted by the Mottelson rule.

From the results discussed above we can draw the following conclusions.

1. The Hartree-Fock states resemble harmonic oscillator states which have the same spatial symmetry as the nuclear density. That is, when a nucleus has an equilibrium shape which is asymmetric, cylindrically symmetric or spherically symmetric, the harmonic oscillator wave functions should be taken from a harmonic well of the same type.

2. For the force considered here the Mottelson rule for equilibrium shapes works well, this being a reflection of the fact that the shapes corresponding to minimum potential energy and minimum kinetic energy are close to one another. The effect of the interaction is to make the equilibrium shape slightly less deformed than that predicted by the Mottelson rule (i.e. the shape which gives minimum kinetic energy). It has been shown by Volkov (1967) that the exchange parameters of the force play a large part in determining the minimum potential energy shape.

3. The GHA and RHF calculations give very similar results when the right type of oscillator states (e.g. cylindrical or asymmetric) are used. However, the RHF calculation is definitely better for very light nuclei like ^{8}Be. On the other hand RHF calculations which are

restricted to the spherical representation will only be as good as the general GHA calculation if there are at least two shells of unoccupied states in the representation. This last statement does not, of course, apply for spherical nuclei.

4. Except for very light nuclei, the best oscillator parameters to use in an RHF calculation, as defined by the minimization of equation (28) in chapter 1, are very close to those obtained by the relevant GHA calculation, together with suitable average values for representation states which are not occupied in the GHA calculation.

5. As the representation becomes more deformed the RHF solution comes closer to a pure configuration.

6. The equilibrium deformations obtained do not depend significantly on the type of calculation (though the representation parameter d may do) as can be seen clearly in figures 14 and 15 for ^{8}Be. This gives much support to the physical reality of the deformation.

The Hartree-Fock states which arise in our RHF calculations show very little parity mixing unless the size parameters for the representation states are significantly different from the best such parameters. There is some mixing of states with different m and spin values, which is caused by the one-body spin-orbit force. When the

Hartree-Fock potential becomes deformed, this effect of the spin-orbit force is lessened because the deformed cylindrically symmetric potential favours states of good m. In the case of asymmetric nuclei there is a very definite mixing of states with m values of opposite sign in order to simulate cartesian states. This effect is practically independent of deformation.

An oscillator state with given parameters can be expanded as an infinite sum of oscillator states with different parameters, but only states of the same m and parity occur in such a sum. This suggests that the mixing between states of the same m and parity, which occurs in the RHF calculation, is an attempt to change the size and deformation of the corresponding orbitals. However, it has been seen that this mixing does not vanish even when the best oscillator parameters are used, and this indicates that there is a further polarization of the orbitals. One effect of this residual polarization is to build up a tail on the single-particle wave functions. This tail is most significant in single-particle states that have single-particle energies near zero, and consequently affects the total energy of light nuclei. For nuclei heavier than ^{16}O these tails are probably not significant in terms of total energy.

The effect of mixing parity in the single-particle

wave functions is to create states whose centre of mass is not at the origin. In this way the particles can polarize to one side of the nucleus. In general this increases the kinetic energy. However, if the size parameters used in the representation states differ significantly from their best values, then the particles may polarize in this way to gain or lose potential energy.

CHAPTER 6

A SURVEY OF RESTRICTED HARTREE-FOCK SOLUTIONS WITH MAXIMUM SPACE SYMMETRY

The purpose of this chapter is to examine the nature of some of the GHA and RHF solutions with maximum space symmetry, for all the even-even nuclei up to ^{40}Ca. This survey will be carried out using force 1. However, before this is done it must be remarked that the approximate many-body states found in these calculations cannot be compared directly with experimentally observed states. The reason for this is that the true eigenstates of the nuclear Hamiltonian have well defined quantum numbers for angular momentum, parity and total linear momentum, whereas the Hartree-Fock states do not. Approximate eigenstates, like Hartree-Fock states, which have less symmetry than the true eigenstates, are called intrinsic states. They can generally be improved by being projected onto subspaces of states of the proper symmetry. In the present case the deformed intrinsic states which result from Hartree-Fock calculations should be projected onto the subspaces of states with well defined angular momentum, linear momentum and parity. When this is done an intrinsic state gives rise to a possibly

infinite number of states which have the same symmetry properties as true eigenstates and can be compared with them.

Because the centre-of-mass energy has been explicitly subtracted in the Hamiltonian used here it is not felt that projection onto a subspace of zero total linear momentum will change the energy by very much. Furthermore most of the RHF solutions discussed here have very small uncertainties in the parity quantum number, so the projection onto states of good parity will be ignored. Unfortunately the uncertainty in the angular momentum of the Hartree-Fock states cannot be dismissed. It has been shown by Ripka(1966) that, for 2s-1d shell nuclei, each intrinsic Hartree-Fock state gives rise to 4 or 5 states with good angular momentum and these projected states bear a strong resemblance to the rotational bands predicted by the adiabatic approximation. When the intrinsic RHF states are calculated in a spherical representation, Ripka has found that the lowest energy of these projected states lies about 2 to 3 MeV below the energy of the intrinsic state. This energy difference is related to the moment of inertia in an adiabatic approximation and therefore might be expected to change when a deformed representation is used and the intrinsic state becomes more

deformed*.

This small gain in energy is not very significant if one is only interested in the systematic behaviour of binding energies over a wide range of nuclei, but is significant if a comparison is to be made with the low energy spectrum of a particular nucleus. In fact, in order to obtain a sequence of states with different J values, to be compared with an experimental spectrum, it is necessary to use this projection technique or some form of the adiabatic approximation.

It will be seen in this chapter that for many nuclei there are often a number of RHF states within 10 or 20 MeV of the lowest one, which arise when different configurations are used as starting points. If a spectrum of states with different J values is projected out of each of these intrinsic states, and if two of these spectra are identical, then the two corresponding intrinsic states can be regarded as different approximations to the same true state. That is if $\Psi(\gamma)$ is an intrinsic state, γ labelling the configuration from which it was derived, and if P^J_M is the projection operator which gives rise to states.

---

*Note:

Recently Lamme and Boeker (1967) have shown that the gain in energy, obtained by projection, is 6.5 MeV for the ^{8}Be ground state and 5.1 MeV for the ^{12}C ground state. This is in accord with the idea that the energy gained increases with deformation.

$$\Psi_M^J(\gamma) = P_M^J \Psi(\gamma)$$

with definite angular momentum, then the intrinsic states $\Psi(\gamma)$, $\Psi(\gamma')$ are essentially the same if

$$\langle \Psi_M^J(\gamma) | H | \Psi_M^J(\gamma) \rangle = \langle \Psi_M^J(\gamma') | H | \Psi_M^J(\gamma') \rangle \quad .$$

An obvious example of such a pair of states is the pair of ^{20}Ne configurations

$$1S, 1P, [002]^4$$

$$1S, 1P, [020]^4 \quad ,$$

which have the same prolate shape but with the longest axis directed along the z or y directions. It is not clear that all intrinsic states which are approximations to the same partial spectrum must be so obviously related, particularly when the occupied single-particle states have no obvious symmetry. However, because Ripka has found that the energy of the lowest projected state is close to the energy of the intrinsic state, it may be assumed that two intrinsic states with significantly different energies are in fact distinct intrinsic states. It will be assumed in this work that two intrinsic states which have significantly different sizes or shapes or single-particle levels are in fact distinct. This assumption is based on the idea that the sizes, shapes and single particle levels are physically meaningful quantities which can be calculated in the Hartree-Fock approximation.

Another awkward feature of these intrinsic states is that they are not necessarily orthogonal. However, it is felt that this is not significant unless detailed comparisons with low energy spectra are to be made.

The first even-even nucleus is ^{4}He. Because of the small number of particles in this case, it is not clear that any approximation using an average potential should give a good approximation to the ground state. The results obtained for the $(000)^4$ configuration will be given in the next chapter when the systematic behaviour of binding energies and sizes is discussed, but this is mainly in the interest of completeness.

Beryllium 8

The ground state configuration

$$1S,\ (001)^4$$

has been discussed in chapter 4, in detail. The values of the a and b parameters (defined in equation (6) of chapter 4) for the oscillator states, that result from the minimization of the energy of the configuration wave function, are shown in table 3. It can be seen that the (000) orbital becomes more deformed than the (001) orbital. It must be pointed out here that the (001) orbital has a deformation even when the oscillator parameters are equal, but this natural deformation which is

due to the quantum numbers is being ignored. In fact, for the values of a and b quoted in table 3, the density disbribution of the (001) orbital is more deformed than that of the (000) orbital. However the harmonic well for which the (001) orbital is an eigenstate is less deformed than that for which the (000) orbital is an eigenstate, and it is more meaningful to compare the deformations of the corresponding potentials. This will be done from now on.

In this case the average potential felt by a (000) particle, is produced by 3 particles in the (000) orbital and by 4 in the (001) orbital which have a more deformed density distribution. It is quite natural that this potential should be more deformed than the average potential felt by a (001) particle and coming mainly from the (000) orbital. As was mentioned in chapter 4, the RHF* solution with a three shell representation does not make a significant improvement on the GHA result. The energies and shapes of the two solutions are given in table 3b.

In the cartesian representation the configurations

---

*Note:

In this chapter an RHF calculation will mean a three shell calculation.

$$1S,\ [001]^4$$

$$1S,\ [010]^4$$

$$1S,\ [100]^4$$

are obviously not distinct and are all equivalent to configuration A in the cylindrical representation. However in the cylindrical representation there is an alternative configuration with maximum space symmetry, namely

$$1S,\ (010)^4\ , \qquad (B)$$

This is an oblate shaped configuration as opposed to the prolate one considered above. The a and b parameters are shown in table 3a for the corresponding GHA wave function and table 3b shows that in this case the RHF solution is a considerable improvement. The reason for this is that in the RHF calculation the occupied (010) orbital mixes with the unoccupied (0-10) orbital to produce an orbital of the cartesian type [010]. The asymmetry parameter $\chi = \langle x^2 - y^2 \rangle / \langle x^2 + y^2 \rangle$ and the deformation parameter Q/R^2 can be used to determine the ratio $x^2 : y^2 : z^2$. This ratio is shown for the two intrinsic states that have been considered, in table 3c, and it is clear from these values that the two solutions have very much the same shape. The discrepancy between these shapes is a result of the difficulty in representing

single-particle states which are symmetric about the y axis, in terms of single-particle states which are symmetric about the z axis. If the representation used in the RHF calculation increased, this discrepancy would diminish. The difference between the energies of the two solutions is caused by the same difficulty. It should be noted that the oscillator parameters used in the two RHF calculations are not the same, each set being obtained from separate GHA calculations.

If any further evidence that these RHF solutions are not distinct, is needed, it is supplied by the single-particle levels. These are shown in figure 24 for the configuration wave functions obtained in the GHA calculation and for the RHF solutions which use these configurations as starting points. For configuration B the RHF calculation makes a significant change to the single-particle spectrum and the result is close to the spectrum obtained for configuration A.

The fact that these intrinsic states are not distinct shows that the GHA calculation by itself gives spurious solutions, that is solutions which do not satisfy the Hartree-Fock requirement of self-consistency, and which are not even good approximations to such states. However, self-consistent intrinsic states can be well approximated by some of the GHA solutions.

TABLE 3a

BERYLLIUM 8 a AND b PARAMETERS DETERMINED BY GHA CALCULATION

CONFIGURATION	ORBITAL	(000)	(001)	(0±10)	(002)	(0±11)	(0±20)	(100)	(003)
A	a	0.856	0.905	-	-	-	-	-	-
	b	1.365	1.145	-	-	-	-	-	-
B	a	1.070	-	1.044	-	-	-	-	-
	b	0.865	-	0.944	-	-	-	-	-
C	a	1.037	-	-	1.218	-	-	-	-
	b	1.828*	-	-	1.828*	-	-	-	-

*These parameters are affected by the orthogonality constraints.

TABLE 3b

BERYLLIUM 8 ENERGIES, SIZES AND DEFORMATIONS FROM GHA AND RHF CALCULATIONS

	GHA			RHF			
CONFIGURATION	ENERGY	RADIUS	Q/R^2	ENERGY	RADIUS	Q/R^2	χ
A	-47.05	2.11	0.954	-47.36	2.11	0.956	0.
B	-31.49	2.04	-0.407	-45.11	2.09	-0.436	-0.462
C	- 3.03	3.55	1.390	·····See chapter 5·····			

TABLE 3c

BERYLLIUM 8 RATIOS $X^2:Y^2:Z^2$ FOR SOLUTIONS

CONFIGURATION	CALCULATION	X^2 :	Y^2 :	Z^2
A	RHF	1.00	1.00	3.75
B	RHF	1.17	3.18	1.00
C	GHA	1.00	1.00	7.84

The last configuration to be considered is

$$1S,\ (002)^4 \qquad (C)$$

and the GHA results are shown in tables 3a and 3b and in figure 24. The RHF calculation produced considerable parity mixing in this case and did not converge. It is concluded that there is no intrinsic state satisfying the Hartree-Fock conditions and directly related to configuration C.

Carbon 12

For this nucleus there are, once again, three equivalent cartesian configurations which have maximum space symmetry. These are:

$$1S,\ [100]^4,\ [010]^4$$

$$1S,\ [010]^4,\ [001]^4$$

$$1S,\ [001]^4,\ [100]^4$$

For each of these configurations the equilibrium shape given by the Mottelson rule is cylindrically symmetric, and so there is no loss of generality in using the cylindrical representation. The above configuration, which is oblate in shape, is written as

$$1S,\ (010)^4,\ (0\text{-}10)^4 \qquad (A)$$

The results of the GHA and RHF calculations for configuration A are shown in table 4. As in the case of ^{8}Be the innermost orbital is more deformed than the outer pair. If the

GHA minimization is carried out treating the oscillator parameters for the orbitals (010) and (0-10) independently they are found to be very nearly equal when the minimization procedure has almost converged. In the GHA calculation quoted in table 4a the parameters for these orbitals were constrained to be equal as were the b parameters. It is seen that there is only a very small difference between the GHA and RHF solutions. This is shown by the energies and shapes in table 4b and 4c and by the single-particle levels in figure 25.

In an attempt to find a different intrinsic state one could start with the configuration

$$1S,\ (001)^4\ (010)^4 \qquad (B)$$

The results are shown in table 4 and, as might be expected from the discussion of ^{8}Be, the cylindrical orbital (010) breaks down into a cartesian type of orbital, by mixing with the unoccupied (0-10) orbital. In this way an oblate state results from the RHF calculation with the smaller axis in the y direction and this is indicated by the asymmetry parameter. The ratio $x^2:y^2:z^2$ is shown for the various configurations in table 4c and the single-particle energies in figure 25. It is quite clear from these results that configurations A and B give rise to the same intrinsic state.

A separate prolate intrinsic state with maximum

TABLE 4a

CARBON 12 a AND b PARAMETERS DETERMINED BY GHA CALCULATION

CONFIGURATION	ORBITAL	(000)	(001)	(0±10)	(002)	(0±11)	(0±20)	(100)	(003)
A	a	1.142	-	1.046	-	-	-	-	-
	b	0.817	-	0.886	-	-	-	-	-
B	a	0.950	0.950	0.978	-	-	-	-	-
	b	1.160	1.046	1.076	-	-	-	-	-
C	a	0.855	0.897	-	0.935	-	-	-	-
	b	1.408*	1.598	-	1.408*	-	-	-	-

*These parameters are affected by the orthogonality constraints.

TABLE 4b

CARBON 12 ENERGIES, SIZES AND DEFORMATIONS FROM GHA AND RHF CALCULATIONS

	GHA			RHF			
CONFIGURATION	ENERGY	RADIUS	Q/R^2	ENERGY	RADIUS	Q/R^2	χ
A	-76.63	2.13	-0.506	-76.96	2.13	-0.504	0.0
B	-64.63	2.10	0.312	-74.44	2.11	0.296	0.321
C	-62.29	2.85	1.407	-63.17	2.85	1.406	0.0

TABLE 4c

CARBON 12 RATIOS $X^2:Y^2:Z^2$ FOR SOLUTIONS

CONFIGURATION	CALCULATION	X^2 :	Y^2 :	Z^2
A	RHF	2.50	2.50	1.00
B	RHF	1.00	1.95	2.24
C	RHF	1.00	1.00	8.10

space symmetry can be constructed by starting with 4 particles in the 2s-1d shell, thus:

$$1S,\ (001)^4,\ (002)^4 \qquad (C)$$

The results obtained with configuration C are given in table 4 and figure 25 and it is clear that this gives a distinctly different intrinsic state about 14 MeV above the lower one.

Oxygen 16

The ground state of two closed shells is

$$1S,\ 1P \qquad (A)$$

and has been discussed in chapter 4 briefly. It is expected to be spherical. The a and b parameters for the lowest energy of this configuration and the results of the RHF and GHA calculations are shown in table 5. In the minimization, the parameters of the (001) and (0±10) orbitals were allowed to vary independently of one another and to give a truly spherical density they should finally be equal. The small discrepancy between them is spurious and gives an an indication of the accuracy of the minimization procedure. If one of these parameters is changed by 0.005 the resulting change in the energy of the configuration is about 0.004 MeV. Generally the a and b parameters quoted from the MINDET program are accurate to within 0.002, in the sense that if the minimization were

repeated using a different starting point the new final values would agree to this accuracy with the values quoted.

The single-particle levels for the GHA and RHF solutions are shown in figure 26 and it is to be noted that the RHF calculation produces the conventional $p_{3/2}$ and $p_{1/2}$ levels in the spherical average potential. The splitting of these levels is 3.00 MeV, and the unoccupied $d_{5/2}$, $s_{1/2}$ and $d_{3/2}$ levels occur at +3.08, +7.33 and +8.08 MeV respectively.

The low lying 0+ excited state of ^{16}O is generally believed to be based on an intrinsic state which is a 4-particle 4-hole excitation of the ground state. This configuration is, in the cartesian representation,

$$1S,\ [001]^4,\ [010]^4,\ [002]^4$$

which as seen in table 2 has an asymmetric equilibrium shape. The cylindrical configuration

$$1S,\ (001)^4,\ (010)^4,\ (002)^4 \qquad (B)$$

can be used as a starting point to obtain the corresponding intrinsic state and the results are given in table 5 and figure 26. The RHF calculation produces the asymmetric shape and this is accompanied by a gain in binding energy of 11 MeV. The result of a GHA calculation in the cartesian representation is also shown in table 5 and agrees very well with the RHF result. The slightly lower

TABLE 5a

OXYGEN 16 a AND b PARAMETERS DETERMINED BY GHA CALCULATION

CONFIGURATION		ORBITAL (000)	(001)	(0±10)	(002)	(0±11)	(0±20)	(100)	(003)
A	a	1.007	0.959	0.962	-	-	-	-	-
	b	1.007	0.959	0.962	-	-	-	-	-
B	a	0.922	0.911	0.973	0.955				
	b	1.290*	1.374	1.166	1.290*				
C	a	0.857	0.882	-	0.924	-	-	-	0.955
	b	1.804*	1.635*	-	1.804*	-	-	-	1.635*

*These parameters are affected by the orthogonality constraints.

TABLE 5b

OXYGEN 16 ENERGIES, SIZES AND DEFORMATIONS FROM GHA AND RHF CALCULATIONS

	GHA			RHF			
CONFIGURATION	ENERGY	RADIUS	Q/R^2	ENERGY	RADIUS	Q/R^2	χ
A	-129.19	2.05	0.0	-129.19	2.05	0.0	0.0
B	- 85.74	2.24	0.964	- 96.12	2.55	0.947	0.258
C	- 77.84	3.63	1.628	-	-	-	-

TABLE 5c

OXYGEN 16 RATIOS $X^2:Y^2:Z^2$ FOR SOLUTIONS

CONFIGURATION	CALCULATION	X^2 :	Y^2 :	Z^2
A	RHF	1.00	1.00	1.00
B	RHF	1.00	1.70	4.99
C	GHA	1.00	1.00	14.10

energy in the cartesian GHA calculation comes from the ability, in this case, of the individual orbitals to take up an asymmetric shape.

The 8-particle-8-hole excitation derived from the configuration

$$1S,\ (001)^4,\ (002)^4,\ (003)^4 \qquad (C)$$

is considered next. The fact that this configuration, with 4 particles in each of 4 different shells, can have an equilibrium energy in the same region as the other configurations considered, shows very dramatically the ability of the orbitals of the (00n) type to lose kinetic energy when they are allowed to deform. The Hartree-Fock calculation for this configuration has not been carried out, but as the equilibrium shape is cylindrical it is not expected that this would decrease the energy significantly. In particular the order of the 4 and 8-particle-hole excitations would not be changed. The results for these excited states are similar to those obtained by Abragall, Caurier and Monsonego (1967).

Neon 20

For this nucleus there are two distinct configurations in the cartesian representation, which have maximum space symmetry and reasonably low energies. They are:

$$1S,\ 1P,\ [002]^4$$

$$1S,\ 1P,\ [011]^4,$$

and are prolate and oblate respectively. As may be expected from the remarks made earlier about the [00n] type of orbital, the prolate state has the lower energy. In the cylindrical representation there are four similar configurations which will be considered. They are:

$$1S,\ 1P,\ (002)^4 \qquad (A)$$

$$1S,\ 1P,\ (020)^4 \qquad (B)$$

$$1S,\ 1P,\ (011)^4 \qquad (C)$$

$$1S,\ 1P,\ (100)^4 \qquad (D)$$

The results are shown in the usual way in table 6 and in figure 27. As expected the prolate configuration A lies the lowest in energy, and it is not changed very much by the RHF calculation. The oblate configuration B gives rise to an intrinsic state at -142.39 MeV which is fairly well separated from the prolate one. It should be noticed in this case that the one single-particle orbital in the 2s-1d shell, after the RHF calculation, is a mixture of the form

$$(|020\rangle \pm |0\text{-}20\rangle)/\sqrt{2}$$

The variation in the density of such a state around the z axis is given by $\cos^2 2\varphi$ which is shown in figure 23. While this is not strictly cylindrically symmetric it gives an

equal contribution to the density in the x and y directions. This is why the asymmetry parameter is zero. This oblate state is the analogue, in the cylindrical representation, of the oblate cartesian configuration considered above.

The next two ^{20}Ne configurations become asymmetric in the RHF calculation. At this point it becomes misleading to judge the shape of the Hartree-Fock states by the Q/R^2 parameter alone. This is because this parameter and the asymmetry one are connected to a fixed co-ordinate system, whereas the RHF state is not. The shapes of these first four ^{20}Ne solutions are given more explicitly by the ratios $x^2:y^2:z^2$ which are shown in table 6c. It now becomes clear that both the second and third configurations produce intrinsic states with essentially the same oblate shape. When the single-particle levels from the GHA and RHF calculations for configurations B and C are compared in figure 27, it is clear that the RHF calculation acts to make the two single-particle spectra very similar. Finally the total binding energies and the radii are the same for the two cases and it must be concluded that the second and third intrinsic states are not distinct.

When the first and fourth solutions are compared in the same way as the second and third have been, it can be seen that these two solutions are not distinct

TABLE 6a

NEON 20 a AND b PARAMETERS DETERMINED BY GHA CALCULATION

CONFIGURATION	ORBITAL	(000)	(001)	(0±10)	(002)	(0±11)	(0±20)	(100)	(003)
A	a	0.964	0.905	0.938	0.940	-	-	-	-
	b	1.134*	1.211	1.002	1.134*	-	-	-	-
B	a	1.082	1.004	1.021	-	-	1.049	-	-
	b	0.965	0.945	0.918	-	-	0.955	-	-
C	a	1.022	1.029	0.961	-	1.017	-	-	-
	b	1.083	0.981	1.079	-	1.064	-	-	-
D	a	1.092*	0.954	1.058	-	-	-	1.092*	-
	b	0.971	0.942	0.942	-	-	-	1.035	-
E	a	1.027	1.007	0.985	-	-	-	-	1.110
	b	1.076	1.462*	1.023	-	-	-	-	1.462*

*These parameters are affected by the orthogonality constraints.

TABLE 6b

NEON 20 ENERGIES, SIZES AND DEFORMATIONS FROM GHA AND RHF CALCULATIONS

CONFIGURATION	GHA			RHF			
	ENERGY	RADIUS	Q/R^2	ENERGY	RADIUS	Q/R^2	χ
A	-156.46	2.30	0.603	-157.82	2.30	0.593	0.0
B	-139.90	2.26	-0.270	-142.39	2.26	-0.268	0.0
C	-136.87	2.26	0.150	-142.33	2.26	0.149	0.139
D	-135.18	2.31	-0.277	-146.80	2.28	-0.247	0.214
E	- 99.10	2.79	0.895	-	-	-	-

TABLE 6c

NEON 20 RATIOS $X^2:Y^2:Z^2$ FOR SOLUTIONS

CONFIGURATION	CALCULATION	X^2 :	Y^2 :	Z^2
A	RHF	1.00	1.00	2.26
B	RHF	1.54	1.54	1.00
C	RHF	1.32	1.00	1.44
D	RHF	1.81	1.17	1.00
E	GHA	1.00	1.00	3.43

either. In this case the RHF calculation has mixed the (100) orbital with the unoccupied 2s-1d shell orbitals to produce an orbital closely related to the cartesian [200]. The representation states determined by the GHA calculation for the configuration D are not at all suited to the description of a state with cylindrical symmetry about the x axis and this is the reason for the large discrepancy in size and in binding energy between the two solutions A and D.

The last configuration which is considered for ^{20}Ne is

$$1S,\ 1P,\ (003)^4. \qquad (E)$$

This is prolate and symmetric with the last 4 particles in the 2p-1f shell rather than the 2s-1d shell. The results for this configuration are shown in table 6 and figure 27. It can be seen that this intrinsic state occurs at a very much higher energy than the ones previously considered.

Magnesium 24

In the cartesian representation there are two distinct low-lying configurations within the 2s-1d shell which have maximum space symmetry. These are

$$1S,\ 1P,\ [002]^4,\ [011]^4 \qquad (W)$$

$$1S,\ 1P,\ [002]^4,\ [020]^4 \qquad (X)$$

Their equilibrium shapes are shown in table 2. The configurations, in the cylindrical representation, that are examined here are

$$1S,\ 1P,\ (002)^4,\ (011)^4 \qquad (A)$$

$$1S,\ 1P,\ (020)^4,\ (100)^4 \qquad (B)$$

$$1S,\ 1P,\ (020)^4,\ (0\text{-}20)^4 \qquad (C)$$

$$1S,\ 1P,\ (011)^4,\ (0\text{-}11)^4. \qquad (D)$$

The results of the GHA and RHF calculations are shown in table 7 and figure 28. The ratios $x^2:y^2:z^2$ in table 7c indicate that all the intrinsic states found have the same general shape. The single-particle levels in figure 28 show that the four intrinsic states have a structure very similar to the cartesian configuration W for which the cartesian GHA calculation has been carried out. The single-particle levels, for the configuration X, determined by a GHA calculation are shown on the left of figure 28 and it is clear that this is a very different spectrum. We draw the conclusion that the configurations B, C and D are not approximations to different intrinsic Hartree-Fock states. Furthermore we have considered here oblate states B and C which are similar to the cartesian configuration X, and these states did not give rise to intrinsic states similar to X. In fact the oblate states B and C changed quite drastically into intrinsic states very similar to configuration W. This implies that

the cartesian configuration X is itself not an approximation to a self-consistent Hartree-Fock state. It must be pointed out here that while other authors, in particular Ripka (1966) and Muthukrishnan (1967), have considered configuration X and have found related RHF states, their calculations were restricted in such a way as to prevent configuration X from being turned into configuration W. This shows that RHF calculations which are too restricted can lead to misleading results, i.e. spurious states.

A different intrinsic state with maximum space symmetry can be constructed by putting 4 particles into the 2p-1f shell and starting with the configuration

$$1S,\ 1P,\ (002)^4,\ (003)^4 \qquad (E)$$

The results for this configuration are given in table 7. In this case the equilibrium shape is cylindrically symmetric and the size and deformation are quite different from those of the previous configurations. It is felt that this configuration gives rise to a distinct intrinsic state, and it can be seen that this is about 13 MeV higher than the asymmetric state. This energy difference is very much less than that between the lowest intrinsic state found for ^{20}Ne, and the ^{20}Ne configuration which had 4 particles in the 2p-1f shell. This indicates that the presence of an occupied (002)

TABLE 7a

MAGNESIUM 24 a AND b PARAMETERS DETERMINED BY GHA CALCULATION

CONFIGURATION		ORBITAL (000)	(001)	(0±10)	(002)	(0±11)	(0±20)	(100)	(003)
A	a	0.965	0.955	0.925	0.955	0.964	-	-	-
	b	1.102*	1.170	1.145	1.102*	1.153	-	-	-
B	a	1.057*	0.967	1.084	-	-	1.071	1.057*	-
	b	0.922	0.909	0.887	-	-	0.909	0.943	-
C	a	1.164	1.046	1.070	-	-	1.066	-	-
	b	0.929	0.930	0.880	-	-	0.927	-	-
D	a	1.029	1.063	0.947	-	1.006	-	-	-
	b	1.168	0.989	1.171	-	1.057	-	-	-
E	a	0.943	0.887	0.937	0.914	-	-	-	0.963
	b	1.351*	1.382*	1.044	1.351*	-	-	-	1.382*

*These parameters are affected by the orthogonality constraints.

TABLE 7b

MAGNESIUM 24 ENERGIES, SIZES AND DEFORMATIONS FROM GHA AND RHF CALCULATIONS

	GHA			RHF			
CONFIGURATION	ENERGY	RADIUS	Q/R^2	ENERGY	RADIUS	Q/R^2	χ
A	-185.67	2.38	0.584	-190.89	2.38	0.579	0.119
B	-178.77	2.37	-0.412	-187.50	2.37	-0.404	0.161
C	-173.91	2.40	-0.414	-184.31	2.41	-0.421	0.170
D	-173.66	2.36	0.235	-181.17	2.37	0.323	0.044
E	-172.56	2.77	1.096	-	-	-	-

TABLE 7c

MAGNESIUM 24 RATIOS $X^2:Y^2:Z^2$ FOR SOLUTIONS

CONFIGURATION	CALCULATION	X^2 :	Y^2 :	Z^2
A	RHF	1.27	1.00	2.52
B	RHF	2.32	1.68	1.00
C	RHF	2.44	1.73	1.00
D	RHF	1.09	1.00	1.65
E	GHA	1.00	1.00	4.65

level makes a considerable difference to the single particle energy of the (003) level. The reason for this is that the interaction between orbitals of the same shape is greater than that between ones of different shape.

Silicon 28

There are two distinct low lying cartesian configurations for this nucleus. They are:

$$1S,\ 1P,\ [002]^4,\ [011]^4,\ [020]^4$$

$$1S,\ 1P,\ [002]^4,\ [011]^4,\ [101]^4,$$

and are oblate and prolate respectively. The corresponding configurations of cylindrically symmetric states are

$$1S,\ 1P,\ (100)^4,\ (020)^4,\ (0\text{-}20)^4 \qquad (A)$$

$$1S,\ 1P,\ (002)^4,\ (011)^4,\ (0\text{-}11)^4 \qquad (B)$$

The usual results are given in table 8 and in figure 29. In common with many other authors (e.g. Ripka 66, Muthukrishnan 67, Bernier and Harvey 67, Das Gupta and Harvey 67), we find that the two configurations have very similar energies. It should be noted that the shapes and single-particle spectra are distinctly different and that these are two distinct intrinsic states. The effective degeneracy of these intrinsic states is unsatisfactory, since there is good experimental evidence for two distinct rotational bands. The 0+ states for these bands

are separated by about 6 MeV, and consequently one expects to find two intrinsic Hartree-Fock states about 6 MeV apart. The relative energy of these two intrinsic states is by no means independent of the force parameters or of the method of calculation. An unnaturally large negative spin-orbit force will depress the oblate state. It has also been found that if the minimimization of the configuration wave function, to determine the oscillator parameters, is carried out with the sizes and deformations of all the orbitals equal, then the oblate solution is favoured by about 2.5 MeV. However, when the minimization is carried out over the most general set of parameters the pathological degeneracy shown in table 8 occurs. The question of these two ^{28}Si states is taken up again in chapter 7 when various forces are considered, but a reasonable decision as to which of these states lies lower cannot be made so far.

The configuration

$$1S,\ 1P,\ (002)^4,\ (011)^4,\ (003)^4 \qquad (C)$$

should lead to a distinct intrinsic state but only the GHA calculation is shown. This configuration is related to the cartesian state

$$1S,\ 1P,\ [002]^4,\ [011]^4,\ [003]^4$$

which is asymmetric. It is expected that an RHF calculation would change the (011) orbital of C into a car-

TABLE 8a

SILICON 28 a AND b PARAMETERS DETERMINED BY GHA CALCULATION

CONFIGURATION	ORBITAL	(000)	(001)	(0±10)	(002)	(0±11)	(0±20)	(100)	(003)
A	a	1.037*	0.977	1.099	-	-	1.066	1.037*	-
	b	0.886	0.883	0.846	-	-	0.879	0.886	-
B	a	0.960	0.984	0.908	0.963	0.952	-	-	-
	b	1.067*	1.129	1.240	1.067*	1.124	-	-	-
C	a	0.944	0.925	0.917	0.918	0.947	-	-	0.943
	b	1.328*	1.257*	1.206	1.328*	1.224	-	-	1.257*

*These parameters are affected by the orthogonality constraints.

TABLE 8b

SILICON 28 ENERGIES, SIZES AND DEFORMATIONS FROM GHA AND RHF CALCULATIONS

	GHA			RHF			
CONFIGURATION	ENERGY	RADIUS	Q/R^2	ENERGY	RADIUS	Q/R^2	χ
A	-234.79	2.41	-0.493	-245.97	2.41	-0.485	0.00
B	-244.13	2.41	0.568	-245.59	2.41	0.566	0.00
C	-213.06	2.70	0.985	-	-	-	-

TABLE 8c

SILICON 28 RATIOS $X^2:Y^2:Z^2$ FOR SOLUTIONS

CONFIGURATION	CALCULATION	X^2 :	Y^2 :	Z^2
A	RHF	2.44	2.44	1.00
B	RHF	1.00	1.00	2.18
C	GHA	1.00	1.00	3.91

tesian type of orbital similar to [011]. This change would cause a significant decrease in energy. Because of this we can only say that the related intrinsic state is less than 32 MeV above the lowest intrinsic state.

Sulphur 32

The low energy cartesian configurations with maximum space symmetry for this nucleus are

$1S, 1P, [002]^4, [020]^4, [011]^4, [101]^4$ (W)

$1S, 1P, [002]^4, [011]^4, [101]^4, [110]^4$ (X)

$1S, 1P, [002]^4, [020]^4, [200]^4, [011]^4$ (Y)

$1S, 1P, [002]^4, [020]^4, [101]^4, [110]^4$ (Z)

These configurations are asymmetric, prolate, oblate and oblate respectively and the equilibrium shapes predicted by the Mottelson rule are given in table 2. The cylindrical configurations restricted to the 2s-1d shell which will be considered are

$1S, 1P, (011)^4, (020)^4, (0\text{-}20)^4, (100)^4$ (A)

$1S, 1P, (002)^4, (011)^4, (0\text{-}11)^4, (020)^4$ (B)

$1S, 1P, (002)^4, (020)^4, (0\text{-}20)^4, (100)^4$ (C)

$1S, 1P, (002)^4, (011)^4, (0\text{-}11)^4, (100)^4$ (D)

The results are shown in the usual way in table 9 and figure 30. Configuration A produces an asymmetric state by mixing orbitals (011) and (0-11) and this is related to the asymmetric cartesian configuration W. It must be

remembered that the representation used, in the RHF calculations which are being quoted, is limited to ten orbitals. Because of this there are only two unoccupied orbitals in the ^{32}S calculations and the correspondingly small number of degrees of freedom allowed inhibits any significant change in shape. Configuration B has a zero asymmetry parameter in the RHF calculation but the (020) orbital has mixed with the (0-20) orbital to produce single-particle states whose density varies as $\cos^2 2\varphi$ (cf. figure 23). The intrinsic state resulting from configuration B is closely related to the prolate cartesian configuration listed above. The shape of the intrinsic state given in table 9c is quite close to that given by the Mottelson rule for the cartesian configuration. Configuration C gives an oblate intrinsic state which is not very different from the pure configuration. However configuration D does not remain cylindrically symmetric in the RHF calculation and there is in this case a definite change in the single-particle spectrum for the 1p shell and for the highest occupied state. The total binding energy in this case is greatly reduced and drops below that of either the prolate or oblate solutions. It is concluded that this configuration is collapsing to the asymmetric state found from configuration A.

The last configuration to be discussed is

TABLE 9a

SULPHUR 32 a AND b PARAMETERS DETERMINED BY GHA CALCULATION

CONFIGURATION		ORBITAL (000)	(001)	(0±10)	(002)	(0±11)	(0±20)	(100)	(003)
A	a	0.997*	1.023	1.051	-	1.026	1.021	0.997*	-
	b	0.915	0.872	0.899	-	0.926	0.911	0.897	-
B	a	0.994	0.991	0.925	0.961	0.952	0.953	-	-
	b	1.019*	1.067	1.117	1.019*	1.050	1.079	-	-
C	a	0.997*	0.888	1.046	0.918	-	1.021	0.997*	-
	b	0.976*	1.039	0.850	0.976*	-	0.885	0.976*	-
D	a	0.971*	0.965	0.946	0.945	0.958	-	0.971*	-
	b	1.027*	1.069	1.144	1.027*	1.060	-	1.027*	-
E	a	0.939	0.948	0.895	0.916	0.929	-	-	0.935
	b	1.254*	1.192*	1.316	1.254*	1.184	-	-	1.192*

*These parameters are affected by the orthogonality constraints.

TABLE 9b

SULPHUR 32 ENERGIES, SIZES AND DEFORMATIONS FROM GHA AND RHF CALCULATIONS

	GHA			RHF			
CONFIGURATION	ENERGY	RADIUS	Q/R^2	ENERGY	RADIUS	Q/R^2	χ
A	-291.48	2.38	-0.354	-297.21	2.38	-0.351	-0.059
B	-288.13	2.38	0.320	-290.95	2.38	0.317	0.0
C	-283.36	2.38	-0.147	-286.74	2.38	-0.155	0.003
D	-278.01	2.39	0.320	-294.23	2.39	0.322	0.139
E	-283.02	2.64	0.910	-	-	-	-

TABLE 9c

SULPHUR 32 RATIOS $X^2:Y^2:Z^2$ FOR SOLUTIONS

CONFIGURATION	CALCULATION	X^2 :	Y^2 :	Z^2
A	RHF	1.71	1.93	1.00
B	RHF	1.00	1.00	1.57
C	RHF	1.29	1.28	1.00
D	RHF	1.32	1.00	1.84
E	GHA	1.00	1.00	3.50

$1S, 1P, (002)^4, (011)^4, (0\text{-}11)^4, (003)^4$ (E)

which is a prolate state. The results for this configuration given in table 9 show that this state has an energy comparable with that of the oblate intrinsic state discussed above. The shape and single-particle spectrum for configuration E show that this is likely to give rise to a further distinct intrinsic state.

Argon 36

There are two cartesian configurations which are natural candidates for the lowest in energy. These are:

$1S, 1P, [002]^4, [020]^4, [011]^4, [101]^4, [100]^4$ (X)

$1S, 1P, [002]^4, [020]^4, [200]^4, [011]^4, [101]^4$ (Y)

and are oblate and prolate respectively. The configurations of cylindrical states, which will be considered initially, are:

$1S, 1P, (011)^4, (0\text{-}11)^4, (020)^4, (0\text{-}20)^4, (100)^4$ (A)

$1S, 1P, (002)^4, (011)^4, (0\text{-}11)^4, (020)^4, (0\text{-}20)^4$ (B)

$1S, 1P, (002)^4, (011)^4, (020)^4, (0\text{-}20)^4, (100)^4$ (C)

The results are given in table 10 and figure 31. It is seen that the prolate configuration A remains cylindrically symmetric whereas the other two become slightly asymmetric. The single-particle energies for solutions B and C are rearranged by the RHF calculation to appear more like those of solution A. This is particularly noticeable in

the 1p shell. Finally the shapes given in table 10c indicate that the three solutions A, B and C are all of more or less the same oblate shape. It is concluded that there is only one self-consistent intrinsic state here and that it is close to the oblate configuration A. Because the cylindrically symmetric prolate configuration B has reverted to the oblate intrinsic state it seems reasonable to assume that the prolate cartesian state Y would also be unstable. The prolate state has been reported by Muthukrishnan (1967) but this state has only been found in calculations where the collapse to the oblate state was prohibited.

The prolate configuration

$$1S,\ 1P,\ (002)^4,\ (011)^4,\ (0\text{-}11)^4,\ (020)^4,\ (003)^4 \qquad (D)$$

has also been considered and the results of the GHA solution are shown. This configuration is closely related to the asymmetric cartesian one

$$1S,\ 1P,\ [002]^4,\ [011]^4,\ [101]^4,\ [110]^4,\ [003]^4 \qquad (Z)$$

and it is expected that configuration D would become asymmetric in an RHF calculation. It has been remarked before that the onset of asymmetry in an RHF calculation is always accompanied by a significant decrease in the energy. Thus the figure of -326.88 MeV given in table 10b must be regarded as a rather poor upper bound to the energy of the related intrinsic state.

TABLE 10a

ARGON 36 a AND b PARAMETERS DETERMINED BY GHA CALCULATION

CONFIGURATION		ORBITAL (000)	(001)	(0±10)	(002)	(0±11)	(0±20)	(100)	(003)
A	a	0.957*	1.041	1.004	-	0.995	0.978	0.957*	-
	b	0.936	0.857	0.944	-	0.904	0.936	0.904	-
B	a	1.032	0.982	0.939	0.953	0.949	0.944	-	-
	b	0.974*	1.011	1.022	0.974*	0.990	1.010	-	-
C	a	0.943*	0.931	0.995	0.943*	0.957	0.971	0.943*	-
	b	0.959*	0.988	0.901	0.959*	0.963	0.906	0.889	-
D	a	0.975	0.951	0.908	0.910	0.926	0.941	-	0.929
	b	1.166*	1.132*	1.196	1.166*	1.093	1.118	-	1.132*

*These parameters are affected by the orthogonality constraints.

TABLE 10b

ARGON 36 ENERGIES, SIZES AND DEFORMATIONS FROM GHA AND RHF CALCULATIONS

	GHA			RHF			
CONFIGURATION	ENERGY	RADIUS	Q/R^2	ENERGY	RADIUS	Q/R^2	χ
A	-373.24	2.34	-0.249	-375.06	2.34	-0.246	0.0
B	-356.86	2.35	0.135	-365.72	2.36	0.121	0.118
C	-356.93	2.33	-0.060	-365.27	2.33	-0.078	0.044
D	-326.88	2.54	0.665	-	-	-	-

TABLE 10c

ARGON 36 RATIOS $X^2:Y^2:Z^2$ FOR SOLUTIONS

CONFIGURATION	CALCULATION	X^2 :	Y^2 :	Z^2
A	RHF	1.49	1.49	1.00
B	RHF	1.27	1.00	1.34
C	RHF	1.17	1.08	1.00
D	GHA	1.00	1.00	2.49

Actually the asymmetric cartesian configuration

1S, 1P, $[002]^4$, $[020]^4$, $[011]^4$, $[101]^4$, $[003]^4$

almost certainly has an equilibrium energy close to and possibly lower than that of the cartesian configuration Z. This new cartesian configuration is related to the cylindrical one

1S, 1P, $(002)^4$, $(011)^4$, $(0\text{-}11)^4$, $(100)^4$, $(003)^4$

which has not been considered.

Calcium 40

It has been pointed out in chapter 4 that the three shell RHF calculation for ^{40}Ca gives a density matrix which is always the 20 x 20 unit matrix. A result of this is that the many-body state which results from the RHF calculation is the same as the pure configuration

1S, 1P, 2S-1D (A)

However the RHF calculation does produce single-particle states which are not simply the representation states. In fact the single-particle states produced are the $1s_{1/2}$, $1p_{3/2}$, $1p_{1/2}$, $1d_{5/2}$, $2s_{1/2}$, $1d_{3/2}$, states which arise in the spherically symmetric average potential. These levels are shown in figure 32 and should be compared with the numbers given earlier for ^{16}O. The $2s_{1/2}$ level has sunk relative to the d levels. In the harmonic potential the s and d levels are degenerate, though the d level is

split by the spin-orbit force. In the Woods-Saxon well, which is squarer than the harmonic one, the d level falls below the s level. Insofar as the Hartree-Fock potential has a shape, it is closely related to the shape of the density, and thus in $^{16}0$ which has a fairly square shape the average of the d levels is found below the s level. In this last ^{40}Ca calculation, the nuclear density has a central peak far higher than is reasonable from experimental considerations. This large central density will make the Hartree-Fock potential very strongly attractive near the centre, and its overall shape is not at all square. In figure 32 it is seen that the d levels are above the s level which suggests that the Hartree-Fock potential becomes sharper than a harmonic well. This depression of the s level is not physical because the true ^{40}Ca density is not like the density found here. A better effective interaction, such as the ones described in the next chapter, would give a squarer density and not give this depression. The a and b parameters for the GHA calculation are given in table 11a, the energies and size parameters in table 11b and the $x^2:y^2:z^2$ ratios in table 11c. The GHA calculation has been carried out for the 4-particle-4-hole excitation

$$1S,\ 1P,\ (002)^4,\ (011)^4,\ (0\text{-}11)^4,\ (020)^4,\ (0\text{-}20)^4,\ (003)^4, \tag{B}$$

TABLE 11a

CALCIUM 40 a AND b PARAMETERS DETERMINED BY GHA CALCULATION

CONFIGURATION	ORBITAL (000)	(001)	(0±10)	(002)	(0±11)	(0±20)	(100)	(003)
A	0.913*	0.945	0.945	0.913*	0.930	0.930	0.913	-
	0.913*	0.945	0.945	0.913*	0.930	0.930	0.913*	-
B	0.994	0.951	0.916	0.903	0.922	0.927	-	0.918
	1.123*	1.081*	1.050	1.123*	1.018	1.031	-	1.081*

*These parameters are affected by the orthogonality constraints.

TABLE 11b

CALCIUM 40 ENERGIES, SIZES AND DEFORMATIONS FROM GHA CALCULATIONS

	GHA		
CONFIGURATION	ENERGY	RADIUS	Q/R^2
A	-465.52	2.28	0.0
B	-397.22	2.46	0.473

and the results are shown in table 11 and figure 32. This configuration will give rise to a cylindrically symmetric prolate intrinsic state, which is the analogue of the configuration believed to be responsible for the first 0+ excited state in ^{16}O.

Conclusions

It is of course possible to extend the number of configurations with maximum space symmetry, without limit. However, the restricted number considered here include the most interesting ones, and at the same time could be considered in some detail in a reasonable amount of time. Apart from the states of maximum space symmetry, there are many interesting configurations which have this symmetry broken in one orbital. These configurations can often provide further intrinsic states in the same energy range as those considered above. By way of example three important cases are listed here.

1. ^{8}Be: 1S, $(010)^2$, $(0\text{-}10)^2$
   this configuration gives rise to an oblate intrinsic state in ^{8}Be.
2. ^{16}O: 1S, $[001]^4$, $[010]^4$, $[100]^4$, $[002]^4$
   this configuration is a 2-particle-2-hole excitation of the ^{16}O ground state and is comparable in energy with the 4-particle-4-hole state previously considered.

3. ^{24}Mg: 1S, 1P, $[002]^4$, $[011]^2$, $[101]^2$

this configuration gives a cylindrically symmetric prolate intrinsic state for ^{24}Mg which is comparable in energy with the states of maximum space symmetry considered above.

A review of the solutions that have been discussed shows that the intrinsic states found seldom differ from simple configurations. In fact in many cases the differences between an intrinsic RHF state and the related configuration arise directly from the one-body spin-orbit force. It can be argued that because of the limited representation used the single-particle states are not free to become anything other than harmonic oscillator states. Nevertheless, it is significant that, whenever a configuration becomes asymmetric in an RHF calculation, the asymmetry is produced largely by a cartesian type of harmonic oscillator orbital which is constructed out of the cylindrical orbitals. Thus whenever large mixings do occur they occur to produce an intrinsic state close to a cartesian configuration rather than a cylindrical one. The types of cartesian states which are produced from the cylindrical states follow the general rule

$$(0 \pm 11) \rightarrow [101] \text{ or } [011]$$

$$(0 \pm 20) \rightarrow [110]$$

$$(100) \rightarrow [200] \text{ or } [020]$$

This pattern is closely related to the structure of the cylindrical states in the cartesian representation, as shown in appendix 1. In fact it can be seen that the cylindrical states tend to produce the cartesian states with which they have the largest overlap.

Another feature of the solutions is that whenever an orbital (n m n_z) is occupied and the time-reversed orbital (n-m n_z) is not, then an RHF single-particle state is produced which contains these two orbitals in roughly equal amounts. This effect can be regarded as the occurrence of asymmetry in the RHF solution. However it can also be regarded as the occurrence of time-reversal symmetry in the single-particle states. This indicates that time-reversal symmetry is preferred over cylindrical symmetry in the Hartree-Fock states.

CHAPTER 7

THE SYSTEMATIC BEHAVIOUR OF BINDING ENERGIES AND SIZES OF LIGHT NUCLEI FOR DIFFERENT EFFECTIVE FORCES

The results for the ground states of the even-even nuclei discussed in the last chapter are summarized in table 12. The results for ^{4}He and ^{80}Zr have been included at this stage. It will be remarked once more, that the GHA results are very similar to the RHF ones when the intrinsic state has cylindrical symmetry. The four-particle-four-hole excited states of ^{16}O and ^{40}Ca will be denoted by $^{16}O^{*}$ and $^{40}Ca^{*}$ throughout this chapter. In the special cases of $^{16}O^{*}$, ^{24}Mg and ^{32}S, where the intrinsic state is asymmetric, there is a marked difference in the RHF and GHA energies.

The nuclear binding energy E, predicted by a simple liquid drop model, depends on the mass number A as

$$E = k_V A + k_S A^{2/3}, \qquad (1)$$

in which case the binding energy per nucleon satisfies

$$E/A = k_V + k_S A^{-1/3} . \qquad (2)$$

When the experimentally observed binding energies are corrected for the Coulomb repulsion, and the consequent

TABLE 12

SUMMARY OF BINDING ENERGIES, SHAPES AND SIZES FOR EVEN-EVEN NUCLEI USING FORCE 1

NUCLEUS	BINDING ENERGY		RMS RADIUS		Q/R^2	
	GHA	RHF	GHA	RHF	GHA	RHF
^{4}He	- 32.72	- 32.72	1.44	1.44	0.00	0.00
^{8}Be	- 47.05	- 47.36	2.11	2.11	0.954	0.956
^{12}C	- 76.63	- 76.96	2.13	2.13	-0.506	-0.504
^{16}O	-129.19	-129.19	2.05	2.05	0.00	0.00
$^{16}O^{*}$	- 85.74	- 96.12	2.24	2.55	0.964	0.947
^{20}Ne	-156.46	-157.82	2.30	2.30	0.603	0.593
^{24}Mg	-185.67	-190.89	2.38	2.38	0.584	0.579
$^{28}Si(O)^{\dagger}$	-243.79	-245.97	2.41	2.41	-0.493	-0.485
$^{28}Si(P)^{\dagger}$	-244.13	-245.59	2.41	2.41	0.568	0.566
^{32}S	-291.48	-297.21	2.38	2.38	-0.354	-0.359
^{36}A	-373.24	-375.06	2.34	2.34	-0.249	-0.246
^{40}Ca	-465.52	-	2.28	-	0.00	-
$^{40}Ca^{*}$	-397.22	-	2.46	-	0.473	-
^{80}Zr	-1448.36	-	2.14	-	0.00	-

* NOTE $^{16}O^{*}$ and $^{40}Ca^{*}$ denote the four-particle-four-hole excited states.

† NOTE $^{28}Si(0)$ and $^{28}Si(P)$ denote the oblate and prolate configurations for ^{28}Si.

binding energy per nucleon is plotted against $A^{-1/3}$, it is found that the points for A greater than 16 lie very close to a straight line, as predicted by (2). The constant k_V is negative (about -16.0 MeV) and represents the average energy per nucleon in uniform nuclear matter. k_S is positive and expresses the fact that in a finite nucleus the nucleons near the surface are less strongly bound than those in the central core. It should be noticed that a larger value of k_S implies a larger difference in the binding energies of core and surface particles. This means that for larger k_S (i.e. for larger slopes in the plot of E/A vs $A^{-1/3}$) the surface is less bound relative to the core. Figure 33 shows both the experimental values of E/A and the values obtained with force 1. It is clear that beyond ^{40}Ca there is no agreement with the experimental line. Below ^{40}Ca there is some correspondence between the theoretical and experimental values, but the erratic slope of the curve joining the theoretical points indicates that with this force there is nothing corresponding to a well defined surface energy for these light nuclei. The dotted lines in figure 33 connect the doubly closed shell nuclei ^{4}He, ^{16}O and ^{40}Ca. Because the intermediate points all lie above these dotted lines there is a definite shell structure reflected in this model

calculation. It has been mentioned in chapter 5 that because ^{8}Be is nearly all surface the restricted type of Hartree-Fock calculation carried out here is not very good. If the tail regions of the single-particle states were properly allowed for, there would be a reduction in energy. This same argument applies equally well to ^{4}He, to a lesser extent to ^{12}C, and to a much lesser extent to ^{16}O and beyond. Because of these corrections it is not unreasonable that some shell structure should appear below ^{16}O in the theoretical curve. However the fact that the ^{4}He point is below the experimental one, whereas the ^{16}O one is above, indicates that, from the point of view of surface energy force 1 is not adequate in this region.

Another reason why shell structure appears in Hartree-Fock calculations, is that the deformed intrinsic states, for nuclei which are not of the doubly closed shell type, do not have good angular momentum. As has been mentioned before, the result of projecting out states of good angular momentum is to give slightly increased binding energies. The binding energies increase in this procedure because the directional constraints, which are necessarily imposed in obtaining a deformed solution, are removed. These constraints of orientation are related to the uncertainty in angular momentum

(i.e. to $\langle (J-\langle J \rangle)^2 \rangle$). This is probably the dominant reason for the shell structure in the 2s-1d shell, though there are other reasons such as non-central forces. Despite all these excuses, the forces to be considered further in this chapter have less shell structure and are to be preferred because of this.

The experimentally observed r.m.s. radii of nuclei exhibit an A dependence very close to

$$r = r_0 A^{1/3} \qquad (3)$$

The observed radii and the equilibrium radii found using force 1 are shown plotted against $A^{1/3}$ in figure 34. The pronounced collapse for nuclei above ^{40}Ca is very evident here. ^{80}Zr is actually smaller in size than ^{40}Ca. Once again the dotted lines connect the doubly closed shell nuclei and there is a definite shell structure evident between these. There is very poor general agreement between theory and experiment in these sizes, and this clearly reflects the inability of force 1 to saturate.

Further features of the calculations carried out with force 1 are the excitation energies of the four-particle-four-hole states in ^{16}O and ^{40}Ca. These values are 33.0 and 68.3 MeV respectively. Both these numbers are very much higher than the values of 6.1 and 3.35 MeV which are observed for the first 0+ excited state in these nuclei. As rotational spectra are observed based

on these 0+ states, one reasonably expects to find deformed Hartree-Fock intrinsic states at low energies in both nuclei. The very high energies found for the intrinsic states here, indicate a further inadequacy in the effective interaction.

The derivation of force 2, and its motivation have been explained in chapter 3. To recapitulate, the repulsive range parameter λ_r becomes dependent on the relative wave number of the interacting particles as shown in figure 2. The force parameters are given in table 1 and the Hartree-Fock calculation of nuclear matter saturates at a high density and energy as seen in figure 3. The standard procedure of using a GHA calculation to determine a best set of oscillator constants and then using these oscillator constants in an RHF calculation, has been used with force 2. The results are given in table 13. Once again, with the exception of the asymmetric states, the GHA and RHF results are very close. The binding energy per nucleon is plotted against $A^{-1/3}$ in figure 35, and r.m.s. radii against $A^{1/3}$ in figure 36. Compared to figure 33, figure 35 shows a drastic change in the binding energy of ^{80}Zr, and this is certainly a reflection of the saturation property in nuclear matter. There is still considerable shell structure with this force, though for the 2s-1d shell the area

TABLE 13

SUMMARY OF BINDING ENERGIES, SHAPES AND SIZES FOR EVEN-EVEN NUCLEI USING FORCE 2

NUCLEUS	BINDING ENERGY		RMS RADIUS		Q/R^2	
	GHA	RHF	GHA	RHF	GHA	RHF
^{4}He	- 33.42	- 33.59	1.55	1.50	0.00	0.00
^{8}Be	- 49.75	- 50.14	2.23	2.22	0.961	0.963
^{12}C	- 79.54	- 80.02	2.29	2.28	-0.512	-0.511
^{16}O	-128.72	-128.85	2.26	2.25	0.00	0.00
$^{16}O^{*}$	- 89.89	- 99.88	2.73	2.73	0.963	0.950
^{20}Ne	-154.38	-155.88	2.56	2.55	0.606	0.600
^{24}Mg	-180.60	-186.28	2.69	2.69	0.608	0.605
$^{28}Si(O)$ †	-231.67	-233.93	2.76	2.76	-0.508	-0.503
$^{28}Si(P)$ †	-224.84	-230.13	2.73	2.71	0.489	0.497
^{32}S	-268.74	-274.82	2.79	2.79	-0.371	-0.368
^{36}A	-332.40	-334.09	2.80	2.80	-0.262	-0.261
^{40}Ca	-400.07	-	2.80	-	0.00	-
$^{40}Ca^{*}$	-350.67	-	2.97	-	0.496	-
^{80}Zr	-939.28	-	3.30	-	0.00	-

* NOTE $^{16}O^{*}$ and $^{40}Ca^{*}$ denote the four-particle-four-hole excited states.

† NOTE $^{28}Si(O)$ and $^{28}Si(P)$ denote the oblate and prolate configurations for ^{28}Si.

above the dotted line has been reduced slightly. The energy behaviour for nuclei lighter than ^{16}O is certainly no better for force 2 than for force 1 and there is no well-defined surface energy. However for A greater than 16 the situation is improved, and the three points for ^{16}O, ^{40}Ca and ^{80}Zr are almost collinear. The overall slope of the E/A curve for force 2 is greater than the slope of the experimental points. As stated above this means that the surface is less bound, relative to the core, than it should be. The density dependence to be introduced in forces 3 and 4 has the effect of increasing the relative binding of the surface nucleons.

The radii shown in figure 36 are a definite improvement over those in figure 34. Once again there is a drastic change in the ^{80}Zr point, which is a reflection of the saturation property in nuclear matter. The four doubly closed shell nuclei fall close to a straight line that has a slope slightly less than the slope of the experimental line. The shell structure between ^{16}O and ^{40}Ca is considerably reduced in these radii.

Returning to table 13 it can be seen that the excitation energies of $^{16}O^{*}$ and $^{40}Ca^{*}$ are 29.0 and 49.4 MeV. Both these numbers, but particularly the latter one, are less than the comparable numbers for force 1. However they are still a long way from the sort of values indicated

by experiment. The reduction of the $^{40}Ca^{*}$ excitation energy relative to the $^{16}O^{*}$ excitation energy is partially a consequence of the improved slope of the E/A curve for force 2. However, the reduction of the $^{16}O^{*}$ value is caused by the increased equilibrium size of the nuclei. To see how this occurs, consider two different interactions v and v', which give rise to the same total binding energy but different equilibrium sizes. If the single particle levels are ε_α and ε_α' and the kinetic energies of these levels are T_α and T_α', then from chapter 2 the binding energies are

$$\tfrac{1}{2} \sum_\alpha (T_\alpha + \varepsilon_\alpha) = \tfrac{1}{2} \sum_\alpha (T_\alpha' + \varepsilon_\alpha')$$

If v' gives a larger size then the kinetic energy of the orbitals is reduced (i.e. T_α' is less than T_α). It follows that ε_α' is greater than ε_α. The single particle levels ε_α are negative; the ε_α' are less negative. The excitation energy of the four-particle-four-hole state is related to the gap between the single-particle levels of the occupied and unoccupied levels. When this gap is reduced by increasing the size of the nucleus then the excitation energy of $^{16}O^{*}$ is also reduced.

Another feature of this force is that it gives a 3.8 MeV splitting for the oblate and prolate ^{28}Si configurations. As remarked in the last chapter these configurations give degenerate results with force 1, and

are found to be degenerate by many other authors. The 3.8 MeV difference found here is small compared to the total energies involved, but is believed to be significant. This result at least shows that in a fully self-consistent calculation the two configurations can be split without resorting to an unnaturally large spin-orbit force. Comparing forces 1 and 2 it is seen that the relative position of the oblate and prolate states is dependent on the details of the force.

Forces 3 and 4 have been completely rederived using the criteria set down in chapter 3. Unfortunately the binding energy of finite nuclei is not easy to fit in this scheme. As V_a is decreased (i.e. made more negative) in the free nucleon-nucleon scattering part of the force, c_3 must be increased to give the proper saturation in nuclear matter. In finite nuclei the increased density dependence suppresses the effect of decreasing V_a, and the consequent change in binding energy is small. By way of example, when V_a is decreased from -153 MeV to -250 MeV, and the other parameters are determined by fitting the scattering data and by saturating nuclear matter, then the binding energy of ^{16}O changes from -104 MeV to -120 MeV. These figures are for density approximation I. It has further been found that if the value of k_F used for the saturation density in nuclear matter is increased

from 1.4 fm^{-1} to 1.5 fm^{-1} the value of c_3 decreases by about 30%.

Because of the uncertainty in the density approximation, which was mentioned in chapter 3, and which will be discussed more fully below, there is no point in a rigourous attempt to fit the binding energy of ^{16}O. Instead we have used two slightly different forces which give approximately the right binding energies. The first of these, force 3, has V_a = -150 MeV and is fitted to a saturation k_F of 1.5 fm^{-1} in nuclear matter. Force 4 is stronger in the free scattering limit, having a value of -250 MeV for V_a, and is fitted to a lower saturation density in nuclear matter given by k_F = 1.4 fm^{-1}. Despite these differences the two forces produce very similar results in finite nuclei. This suggests that the nuclear matter and scattering properties of the force determine to a large extent the properties of finite nuclei. Before the results can be discussed it is necessary to consider the two density approximations that were defined in chapter 3.

The first approximation, seen for ^{16}O in figure 5, gives the correct density in the surface region and a definite overestimate of the density in the central region. As already explained this gives an underestimate of the binding energy. In the GHA minimization the density is

treated self-consistently, and in minimizing the total binding energy there is a tendency to reduce the density because this increases the strength of the force. Decreasing the density should mean increasing the size. The approximate density I is essentially determined by the size, because it is fitted to the $\langle \rho^2 \rangle$ and $\langle z^2 \rangle$ values. Thus when this approximate density is decreased the size must be increased. The second approximate density is fitted to the central density and to the ratio $\langle \rho^2 \rangle / \langle z^2 \rangle$. As can be seen for ^{16}O in figure 5, this approximate density is generally too small and the binding energy is overestimated. However, there is a very dangerous weakness inherent in this approximation. The magnitude of the approximate density is determined by the central density and this in turn is determined by the sizes of a few of the even parity states. In the spherical representation it is just the s states which determine this central density, in the three shell cylindrical representation it is the (000) (002) and (100) states. Because of this feature, there is an unphysical tendency to increase the size of the (000), (002) and (100) orbitals. Increasing the size of these orbitals decreases the central density and increases the density in the surface region. Thus, while in our approximation the density is reduced and the strength of the interaction is increased, the overall effect is really that the density approximation

becomes a very poor one. This second density approximation actually gives a lower energy for $^{40}Ca^{*}$ than for ^{40}Ca, but this anomaly can be related to a very poor density approximation arising in the manner described above. In the following discussion of results, density approximation II must be treated with caution and serves mainly as a lower bound for the energies and radii. The results given for forces 3 and 4 are all from GHA calculations and because of this the asymmetric nuclei ^{24}Mg and ^{32}S are omitted. The excited state $^{16}O^{*}$ has been included because its behaviour is very interesting, but it must be remembered in this case that the RHF calculation will produce an asymmetric state and a consequent gain in binding energy of about 10 MeV. The $^{40}Ca^{*}$ results with density approximation II are omitted for the reason mentioned above. The ^{36}A result with force 4 and density approximation II has not been computed. With these exceptions the results for force 3 are shown in table 14 and figures 37 and 38, the results for force 4 in table 15 and figures 39 and 40.

It can be seen at once from tables 14 and 15 that the two forces give very similar results, though force 4 gives larger binding energies and radii. Figures 37 and 39 show a general improvement in the overall slope of the E/A curve, when compared with figure 35. The radii in

TABLE 14

SUMMARY OF BINDING ENERGIES, SHAPES AND SIZES FOR EVEN-EVEN NUCLEI USING FORCE 3

NUCLEUS	BINDING ENERGY		RMS RADIUS		Q/R^2	
	GHA(I)	GHA(II)	GHA(I)	GHA(II)	GHA(I)	GHA(II)
^{4}He	- 25.16	- 25.16	1.91	1.91	0.00	0.00
^{8}Be	- 42.93	- 48.80	2.67	2.58	0.948	0.965
^{12}C	- 71.19	- 88.02	2.72	2.55	-0.497	-0.502
^{16}O	-113.82	- 151.58	2.72	2.48	0.00	0.00
^{16}O*	- 85.88	- 94.55	3.22	3.10	0.940	0.936
^{20}Ne	-139.16	- 167.10	3.05	2.90	0.590	0.589
^{28}Si(O) †	-209.11	- 252.08	3.32	3.21	-0.495	-0.495
^{28}Si(P) †	-213.61	- 269.20	3.31	3.06	0.588	0.544
^{36}A	-300.49	- 394.38	3.38	3.29	-0.259	-0.336
^{40}Ca	-352.34	- 421.08	3.41	3.31	0.00	0.00
^{40}Ca*	-323.87	-	3.58	-	0.485	-
^{80}Zr	-804.96	-1003.13	4.11	3.83	0.00	0.00

GHA(I) and (II) denote density approximations I and II.

NOTE ^{16}O and ^{40}Ca* denote the four-particle-four-hole excited states.

†NOTE ^{28}Si(O) and ^{28}Si(P) denote the oblate and prolate configurations for ^{28}Si.

TABLE 15

SUMMARY OF BINDING ENERGIES, SHAPES AND SIZES FOR EVEN-EVEN NUCLEI USING FORCE 4

NUCLEUS	BINDING ENERGY		RMS RADIUS		Q/R^2	
	GHA(I)	GHA(II)	GHA(I)	GHA(II)	GHA(I)	GHA(II)
^{4}He	- 24.95	- 24.95	2.01	2.01	0.00	0.00
^{8}Be	- 44.85	- 52.26	2.75	2.66	0.928	0.954
^{12}C	- 75.65	- 97.91	2.82	2.61	-0.487	-0.491
^{16}O	-120.62	- 172.13	2.82	2.51	0.00	0.00
$^{16}O^{*}$	- 93.57	- 105.89	3.31	3.16	0.915	0.910
^{20}Ne	-148.71	- 187.10	3.17	2.97	0.577	0.577
$^{28}Si(O)^{\dagger}$	-223.04	- 292.84	3.43	3.35	-0.456	-0.487
$^{28}Si(P)^{\dagger}$	-230.41	- 309.74	3.43	3.10	0.581	0.521
^{36}A	-322.31	-	3.52	-	-0.230	-
^{40}Ca	-377.23	- 489.90	3.55	3.52	0.00	0.00
$^{40}Ca^{*}$	-351.24	-	3.70	-	0.468	-
^{80}Zr	-862.83	-1114.11	4.28	3.94	0.00	0.00

GHA(I) and (II) denote density approximations I and II.

*NOTE $^{16}O^{*}$ and $^{40}Ca^{*}$ denote the four-particle-four-hole excited states.

†NOTE $^{28}Si(O)$ and $^{28}Si(P)$ denote the oblate and prolate configurations for ^{28}Si.

figure 38 and 40 also show an improved overall slope, and the general agreement with experiment is considerably improved.

The larger binding energies with force 4 arise because this force is essentially stronger than force 3, particularly in the low density limit. The larger radii with force 4 can be ascribed to the fact that the density dependence is stronger, and so there is a stronger tendency to reduce the nuclear density. The curves for forces 3 and 4 are a little ambiguous because the points have been replaced by lines connecting the results for the two density approximations. The separation of the two approximations is larger for force 4 because the density dependence is stronger. The one point which is not ambiguous is the ^{4}He point. The fact that the ^{4}He value lies above the possible range of ^{16}O values indicates a very definite improvement over the first two forces. Apart from the ^{4}He point it is not possible to make a detailed comparison of forces 3 and 4 with force 2. However, it does seem that the overall slope is improved and that the shell structure is reduced. The underbound results, with density approximation I, are certainly very much better than the previous ones. The overall slopes of the E/A curves for forces 3 and 4 are still larger than that of the experimental line. This implies

that the surface nucleons are still not sufficiently bound. The slope of the force 3 curve is a little better than that of the force 4 curve, which suggests that the saturation density of nuclear matter plays a role here.

The general agreement with the experimental results in figures 38 and 40 is surprisingly good. Once again though, the overall slopes of the curves could be improved. It is worth noting that in this case force 4 seems to give a slightly better slope than force 3. It is not possible to be specific about the excitation energies of $^{16}O^{*}$ and $^{40}Ca^{*}$, but if one assumes that the first density approximation is close to the truth, then these excitation energies are less than those obtained in GHA calculations for forces 1 and 2. In these excited states four particles are taken out of one shell and put into a higher one. Thus these particles move to a lower density region and their interaction is increased. Unfortunately the size of this effect cannot be judged until a better approximation to the nuclear density is used.

One of the most surprising features of the results summarized in tables 12, 13, 14 and 15, is the lack of variation in the Q/R^2 values. It is seen that for any given nucleus the Q/R^2 value at equilibrium is changed only slightly when considerable changes are made

to the properties and form of the force. This is a very strong point in support of the argument that the equilibrium deformations are determined very largely by the kinetic energy, as explained in chapter 5.

These density dependent forces have another point in common and this is that they give a splitting of the ^{28}Si states which favours the prolate state. The splitting is small, particularly in comparison to the uncertainty produced by the density approximation, but is almost certainly meaningful. The fact that there is a reversal of the order of the prolate and oblate states, produced by the density dependence, indicates that the detailed nature of the interaction plays a critical role in determining the relative energy of these states. Furthermore the splitting is increased in going from force 3 to force 4. It is conjectured that this is a result of the increased density dependence in force 4, and that the interactions in the oblate state take place in a higher average density than those in the prolate state.

In concluding it is noted that a simple density dependent factor in the effective interaction gives a better systematic behaviour for the energies and sizes of light nuclei. Furthermore the saturation of nuclear matter and the s-wave scattering determine to a very

large extent the properties of finite nuclei. The shell structure in the systematic behaviour is almost certainly reduced by the density dependence.

CHAPTER 8

CONCLUSIONS

The last three chapters, chapters 5, 6 and 7, have each been concerned with slightly different aspects of the results of the RHF calculations. In fact these three aspects, the mechanics of deformation, the nature of RHF solutions for even-even nuclei up to ^{40}Ca, and the role played by various features of the effective interaction, have been presented here more or less in the chronological order in which they were considered. This explains for example, why the calculations of chapter 6 did not use one of the better forces developed in chapter 7.

In chapter 6 it was shown clearly that the deformation of light even-even nuclei was a very important degree of freedom in RHF calculations. Furthermore it was shown, using ^{8}Be and ^{20}Ne as examples, that the deformation of these light nuclei could be produced in an RHF calculation either by using a deformed representation, or by using a representation that was large enough for there to be many unoccupied states, for the nuclei considered. In fact it appeared from these examples that a spherical representation could be used

with confidence as long as there were two shells of unoccupied states included in the representation. The next most important degree of freedom in the RHF solutions, appeared to be asymmetry. However this feature only appeared in a few specific intrinsic states, and could be predicted from symmetry arguments about the related cartesian configurations. The cartesian configurations were in fact a good guide to the possible RHF intrinsic states, and the Mottelson rule was able to predict quite well the equilibrium shapes of these states. This Mottelson rule was, in turn, related to the rather slow variation of the potential energy, as compared to changes in the kinetic energy.

In chapter 6 a survey of the intrinsic states for various nuclei was undertaken. Here it was shown that not all of the cartesian configurations gave rise to related self-consistent states. Many of the cylindrical configurations collapsed, in the RHF calculation, to finally appear as states related to a different configuration. This points out the danger of imposing restrictive symmetries on the single-particle states. Other authors have imposed such restrictions and found intrinsic states which appear to be spurious in the more general calculations carried out here. As a result we

report fewer distinct intrinsic states than these authors. Another point brought out in chapter 6 was that it does not cost very much energy to promote four particles from the 2s-1d shell to the 2p-1f shell. This is a result of the ability of the (003) orbital to lose much of its kinetic energy by becoming highly deformed.

In chapter 7 we investigated the effect of some different features of the force. This was prompted largely by the marked collapse of nuclei above ^{28}Si, which occurred with force 1. Force 2 was an immediate improvement over force 1 as regards this collapse in finite nuclei. This improvement can only be ascribed to the ability of this force to saturate nuclear matter, even though the saturation point was not close to the experimentally predicted one. This shows the importance of the requirement of saturation, and the distinct separation that exists between saturating and non-saturating interactions.

Force 2 still gave nuclei which were too small, and the general behaviour of the energies left something to be desired. The density dependent forces, forces 3 and 4, were designed to give the correct saturation of nuclear matter, and made a definite improvement in the sizes. As was explained in chapter 7, increasing the size of nuclei in this way causes the single-particle levels to be less bound. The levels found with force 1

were considerably more bound than those found in (p,2p) and (e,e'p) knockout reactions. The levels, obtained with forces 3 and 4, have not been compared with experiment here, but it is felt that forces which give the correct size must give approximately the right single-particle levels. The two density approximations used caused a certain amount of ambiguity in the results for the last two forces, and as a result not much can be said about the systematic behaviour of the energies. Despite this ambiguity though, it is clear that these density dependent forces represented an improvement over the earlier ones.

The fact that two fairly different density dependent forces were used, and that they gave very similar results, indicates that the criteria used in determining the forces are physically meaningful. However it may also mean that the analytic form of the force may have to be further modified, in order to make more improvements in the results for finite nuclei.

It seems quite feasible, in the light of the work done to date, to extend the RHF calculation to five shells. In order to do this, in a practicable way, it may be necessary to make some restrictions on the representation. In particular it may be necessary to use oscillator states with the same oscillator parameters.

It also seems advantageous to use the cartesian representation rather than the cylindrical one, in order to better accommodate asymmetric intrinsic states. With a five shell program of this type it would be possible to carry out detailed and fully self-consistent analyses of nuclei beyond ^{40}Ca. However, to relate results obtained above ^{40}Ca to experimental ones will require the inclusion, in a self-consistent way, of the effect of the Coulomb interaction.

A very obvious improvement is needed in the density approximation used when calculating matrix elements. Rather than the approximations I and II, a sum of two or more gaussians can be used to fit the true nuclear density. Actually the sum of gaussians must be fitted to the true density taken to the 2/3 power. Such an approximation will make it possible to calculate matrix elements analytically, and at the same time to fit the nuclear density very well.

With an improved density approximation it is hoped that the systematic behaviour of light nuclei will be well reproduced. In particular it is hoped that the shell structure, which results from an improved calculation, will be small enough to be explained by the uncertainties in the angular momentum for the intrinsic states.

APPENDIX 1

HARMONIC OSCILLATOR WAVE FUNCTIONS WITH CYLINDRICAL SYMMETRY

1. THE WAVE FUNCTIONS IN CONFIGURATION SPACE

The Wave Functions are

$$\Psi_{nmn_z} = N_{nmn_z}\, e^{im\phi}\, (\alpha^{\frac{1}{2}}\rho)^{|m|}\, L_n^{|m|}(\alpha\rho^2)\, e^{-\frac{1}{2}\alpha\rho^2}\, H_{n_z}(\beta^{\frac{1}{2}}z)\, e^{-\frac{1}{2}\beta z^2}$$

where $N_{nmn_z} = \frac{1}{\sqrt{2\pi}} \sqrt{\frac{2\alpha n!}{(n+|m|)!}} \left(\frac{\beta}{\pi}\right)^{\frac{1}{4}} \sqrt{\frac{1}{2^{n_z}\, n_z!}}$

and are eigenfunctions of:

$$\left[-\frac{\hbar^2}{2m}\nabla^2 + \frac{mw_\rho^2}{2}\rho^2 + \frac{mw_z^2}{2}z^2 \right] \Psi_{nmn_z} = E_{nmn_z}\, \Psi_{nmn_z}$$

where

$$E_{nmn_z} = (2n + |m| + 1)\,\hbar w_\rho + (n_z + \tfrac{1}{2})\hbar w_z$$

and

$$\alpha = \frac{mw_\rho}{\hbar} \qquad \beta = \frac{mw_z}{\hbar}.$$

α, β have dimensions of $(\text{length})^{-2}$ or $(\text{wave number})^2$.

Examples are

$$\Psi_{000} = \alpha^{\frac{1}{2}} \beta^{\frac{1}{4}} \pi^{-3/4} e^{-\frac{1}{2}\alpha\rho^2} e^{-\frac{1}{2}\beta z^2}$$

$$\Psi_{0\pm10} = \alpha\beta^{\frac{1}{4}} \pi^{-3/4} \rho e^{\pm i\phi} e^{-\frac{1}{2}\alpha\rho^2} e^{-\frac{1}{2}\beta z^2}$$

$$\Psi_{001} = 2^{\frac{1}{2}} \alpha^{\frac{1}{2}} \beta^{3/4} \pi^{-3/4} z e^{-\frac{1}{2}\alpha\rho^2} e^{-\frac{1}{2}\beta z^2}$$

The mean square dimensions for the state Ψ_{nmn_z} are

$$\overline{\rho^2} = (2n + |m| + 1)/\alpha, \quad \overline{z^2} = (n_z + \tfrac{1}{2})/\beta$$

The volume of the ellipsoid of revolution passing through the points $(\langle x^2\rangle^{\frac{1}{2}}, 0, 0)$, $(0, \langle y^2\rangle^{\frac{1}{2}}, 0)$, $(0, 0, \langle z^2\rangle^{\frac{1}{2}})$ is given by

$$V = (4\pi/3)\ (n + \tfrac{1}{2}|m| + \tfrac{1}{2})\ (n_z + \tfrac{1}{2})^{\frac{1}{2}}/\alpha\beta^{\frac{1}{2}} .$$

Note that $\langle x^2\rangle = \langle y^2\rangle = \tfrac{1}{2}\langle\rho^2\rangle$.

In the special case that $\alpha = \beta$, these wave functions are simply related to the spherical oscillator states $|n,l,m)$, however the phase convention used here for time-reversed states with opposite m values is not that of Condon and Shortley.

The state Ψ_{n,m,n_z} is prolate, spherical, or oblate as

$$(2n_z + 1)\alpha - (2n + m + 1)\beta \gtrless 0.$$

It is convenient in the following to write:

$$\psi_{n_i,m_i,n_{z_i}}(r) = (2\pi)^{-\frac{1}{2}} e^{im_i\phi} \psi^r_i(\rho) \psi^a_i(z),$$

where i labels a set of states and,

$$\psi^r(\rho) = (2\alpha n!/(n + |m|)!)^{\frac{1}{2}} (\alpha^{\frac{1}{2}}\rho)^{|m|} L_n^{|m|}(\alpha\rho^2) e^{-\frac{1}{2}\alpha\rho^2},$$

$$\psi^a(z) = (\beta^{\frac{1}{2}}/\pi^{\frac{1}{2}} 2^{n_z} n_z!)^{\frac{1}{2}} H_{n_z}(\beta^{\frac{1}{2}}z) e^{-\frac{1}{2}\beta z^2} .$$

When carrying out searches for the best oscillator parameters it is found to be more efficient if the size parameters

$$a = (1 / 2\alpha)^{\frac{1}{2}}, \qquad b = (1 / 2\beta)^{\frac{1}{2}} ,$$

are used instead of α and β. These new parameters are the r.m.s. values of x and z for the $|000)$ state with oscillator constants α and β. The deformation of the state will be measured by

$$d = \frac{2b^2 - 2a^2}{b^2 + 2a^2} = \frac{2\alpha - 2\beta}{\alpha + 2} , \text{ or } \frac{b^2}{a^2} = 2\frac{(1+d)}{2-d}$$

and d is proportional to the quadrupole moment of the $|000)$ state divided by its radius squared. Thus the $|000)$ state is prolate, spherical, or oblate as

$$d \lessgtr 0 .$$

Note that $-1 < d < +2$.

The volume V is proportional to a^2b and this is used as a volume parameter.

The part of $\Psi_{n\ m\ n_z}$ which depends on z, together with the appropriate normalization factor, is a one-dimensional harmonic oscillator wave function. The product of three wave functions of this type, for the x,y and z co-ordinates, gives a cartesian oscillator wave function $\Psi_{n_x n_y n_z}$. This wave function is associated with the $[n_x n_y n_z]$ orbital, and is used in the cartesian GHA calculations. The interrelations between the various types of oscillator wave functions are summarized in a recent paper by Chasman and Wahlborn (1967).

The two-dimensional states $|nm\rangle$, which are obtained from the $|n\ m\ n_z\rangle$ states by removing the z-dependent part, are related to products of pairs of one-dimensional states $|n_x\rangle|n_y\rangle$ as follows:

$$|00\rangle = |0\rangle\ |0\rangle$$

$$|0\pm1\rangle = \sqrt{\tfrac{1}{2}}\ |1\rangle\ |0\rangle \pm i\sqrt{\tfrac{1}{2}}\ |0\rangle\ |1\rangle$$

$$|0\pm2\rangle = \tfrac{1}{2}\ |2\rangle\ |0\rangle \pm i\sqrt{\tfrac{1}{2}}\ |1\rangle\ |1\rangle - \tfrac{1}{2}\ |0\rangle\ |2\rangle$$

$$|1\ 0\rangle = -\sqrt{\tfrac{1}{2}}\ |2\rangle\ |0\rangle - \sqrt{\tfrac{1}{2}}\ |0\rangle\ |2\rangle .$$

The oscillator constants are all the same in these formulae. These equations can be used directly to express the cylindrical states in terms of the cartesian states $|n_z n_y n_z\rangle$.

ORTHONORMALITY CONSTRAINTS

The pair of states $|n,m,n_z;\alpha,\beta)$, $|n',m',n'_z;\alpha',\beta')$ are automatically orthogonal if they are of opposite parity or have different m values. When this is not the case, then either

$$(n,m) \neq (n',m') \text{ and } \alpha = \alpha',$$

or

$$n_z \neq n'_z \quad \text{and } \beta = \beta',$$

must hold for the states to be orthogonal.

A suitable, but not unique, set of a and b parameters for the first twenty states is given below, however for a smaller set of these states some of these constraints can be removed. As an example the most general parameters for the GHA for the Ne^{20} ground state are given separately. An additional constraint of timereversal symmetry has also been incorporated below, so that states of the form $|n,m,n_z)$ and $|n,-m,n_z)$ have the same oscillator constants. This makes very little difference in the GHA calculations carried out in this work and makes no difference in the RHF calculations, however it enables the matrix elements for the RHF programme to be calculated more quickly.

Parameters for Neon 20 minimization.

n	m	n_z	Oscillator Parameters	
0	0	0	a_1	b_1
0	0	1	a_2	b_2
0	+1	0	a_3	b_3
0	-1	0	a_3	b_3
0	0	2	a_4	b_1

Quantum numbers and constraints for the first four shells of states.

Shell	n	m	n_z	parity	Oscillator Parameters	
1S	0	0	0	+1	a_1	b_1
1P	0	0	1	-1	a_2	b_2
	0	+1	0	-1	a_3	b_3
	0	-1	0	-1	a_3	b_3
2S,1D	0	0	2	+1	a_1	b_1
	0	+1	1	+1	a_4	b_4
	0	-1	1	+1	a_4	b_4
	0	+2	0	+1	a_5	b_5
	0	-2	0	+1	a_5	b_5
	1	0	0	+1	a_1	b_6
2P,1F	0	0	3	-1	a_2	b_2
	0	+1	2	-1	a_3	b_3
	0	-1	2	-1	a_3	b_3
	0	+2	1	-1	a_6	b_7
	0	-2	1	-1	a_6	b_7
	1	0	1	-1	a_2	b_8

Quantum numbers and constraints for the first four shells of states. (cont'd)

Shell	n	m	n_z	parity	Oscillator Parameters	
	0	+3	0	-1	a_7	b_9
	0	-3	0	-1	a_7	b_9
	1	+1	0	-1	a_3	b_{10}
	1	-1	0	-1	a_3	b_{10}

These constraints must be used in all RHF calculations regardless of which configuration is being considered, because in this calculation all states are used and must be orthogonal.

---

2. THE WAVE FUNCTIONS IN MOMENTUM SPACE

Denoting the general point in k-space as (k_ρ, θ, k_z), the transformed function is

$$\Phi_{nmn_z}(k_\rho,\theta,k_z) = N_{nmn_z}(2\pi)^{-3/2}\int e^{i\underline{k}\cdot\underline{r}}\,\Psi_{nmn_z}(\rho,\phi,z)\,\rho d\rho d\phi dz.$$

This integral can be evaluated to give

$$\Phi_{n,m,n_z} = N'_{nmn_z}\, e^{im\theta}\, i^{2n+|m|}(\alpha^{-\frac{1}{2}}k_\rho)^{|m|}L_n^{|m|}(\alpha^{-1}k_\rho^2)\, e^{-\frac{1}{2}\alpha^{-1}k_\rho^2}$$

$$\times\; i^{n_z} H_{n_z}(\beta^{-\frac{1}{2}}k_z)\, e^{-\frac{1}{2}\beta k_z^2}\,.$$

and

$$N'_{nmn_z} = \beta^{-\frac{1}{2}} \alpha^{-1} N_{nmn_z}$$

NOTE

N'_{nmn_z} can be obtained from N_{nmn_z} by replacing α, β everywhere with their inverse. And thus apart from the phase factor $i^{2n+|m|+n_z}$, Φ is obtained by replacing α, β with their inverses. This is very useful when calculating matrix elements.

Further Notation

Again put

$$\Phi_{n_i m_i m_{z_i}} = (2\pi)^{-\frac{1}{2}} e^{im_i\theta} i^{2n_i+|m_i|} \Phi_i^r (k_\rho) i^{n_{z_i}} \Phi_i^a (k_z)$$

So:

$$\Phi^r(k_\rho) = (2\alpha^{-1} n!/(n+|m|)!)^{\frac{1}{2}} (\alpha^{-\frac{1}{2}} k_\rho)^{|m|} L_n^{|m|} (\alpha^{-1} k_\rho^2) e^{-\frac{1}{2}\alpha^{-1} k_\rho^2}$$

$$\Phi^a(k_z) = (\beta^{-\frac{1}{2}}/\Pi^{\frac{1}{2}} 2^{n_z} n_z!)^{\frac{1}{2}} H_{n_z}(\beta^{-\frac{1}{2}} k_z) e^{-\frac{1}{2}\beta^{-1} k_z^2}.$$

3. MOSHINSKY TRANSFORMATION BRACKETS IN ONE AND TWO DIMENSIONS

The one dimensional harmonic oscillator states can

be expressed in terms of a creation operator a^+ (Messiah 65) as

$$|n) = (n!)^{-\frac{1}{2}} (a^+)^n |0), \quad n = 0, 1, 2 \ldots$$

and the product of two such states forms a two body wave function,

$$|n_1;n_2) = (n_1!n_2!)^{-\frac{1}{2}} (a_1^+)^{n_1} (a_2^+)^{n_2} |0).$$

If the relative and centre of mass co-ordinates for the two particles are defined as

$$x = (x_1 - x_2)/\sqrt{2}$$

$$X = (x_1 + x_2)/\sqrt{2}$$

Then the creation operators for harmonic oscillator states in these co-ordinates are

$$a_r^+ = (a_1^+ - a_2^+)/\sqrt{2}$$

and

$$a_c^+ = (a_1^+ + a_2^+)/\sqrt{2}$$

respectively. It should be noticed that it is at this stage that the assumption of equal oscillator constants for $|n_1)$ and $|n_2)$ is made. Now the overlap we require is

$$(n_1;n_2|n;N) = (0|a_1^{n_1} a_2^{n_2} (a_1^+ - a_2^+)^n (a_1^+ + a_2^+)^N |0) (n_1!n_2!n!N!2^n\ 2^N)^{-\frac{1}{2}}$$

and after expanding the operators on the right hand side using the binomial theorem it is found that:

$$(n_1;n_2|n;N) = (n_1!n_2!n!N!)^{\frac{1}{2}}\, 2^{\frac{-n+N}{2}} \sum_r (-1)^r \frac{1}{(n_1-n+r)!(n_2-r)!(n-r)!r!}$$

if $n_1 + n_2 = n + N$ and,

$$(n_1;n_2|n;N) = 0$$

otherwise.

This formula was first derived by Brink and can be extended to the two dimensional case immediately. It is shown by Messiah (65) that the two dimensional states can be obtained by using two independent creation operators a_+^+ and a_-^+. Thus

$$|n_+,n_-) = (n_+!n_-!)^{-\frac{1}{2}}\, (a_+^+)^{n_+}(a_-^+)^{n_-}\, |0)$$

and in terms of our usual notation,

$$|n,m) = |n_+,\, n_-)$$

if
$$m = n_+ - n_-$$
$$2n + |m| = n_+ + n_- \quad .$$

Now it follows that:

$$(n_{1+},n_1;n_{2+},n_{2-}|\, n_+,n_-;N_+,N_-) = (n_{1+},n_{2+}|\, n_+,N_+)\,(n_{1-},n_{2-}|\, n_-,N_-)$$

In this way the two-dimensional transformation bracket is simply a product of two one-dimensional brackets.

APPENDIX 2

MATRIX ELEMENTS OF ONE-BODY OPERATORS AND THE CENTRE OF MASS CORRECTION

1. SOME BASIC INTEGRALS

We define:

$$R_{ij}^{(n)} = \int_0^\infty \Psi_i^r(\rho)\ \rho^n\ \Psi_j^r(\rho)\ \rho d\rho \qquad n = 0, 1 \ldots.$$

$$R_{ij}^{(-n)} = \int_0^\infty \Phi\ {}_i^r(k_\rho)\ k_\rho^n\ \Phi_j^r(k_\rho)\ k_\rho dk_\rho \qquad n = 1, 2 \ldots.$$

$$Z_{ij}^{(n)} = \int_{-\infty}^{\infty} \Psi_i^a(z)\ z^n\ \Psi_j^a(z)\ dz \qquad n = 0, 1 \ldots.$$

$$Z_{ij}^{(-n)} = \int_{-\infty}^{\infty} \Phi_i^a(k_z)\ k_z^n\ \Phi_j^a(k_z)\ dk_z \qquad n = 1, 2 \ldots.$$

where again i,j label some set of states and the various Ψ and Φ functions are defined above.

The R's and Z's have the form of overlaps between radial or azimuthal parts respectively. Many more complex matrix elements of one-body operators, and of separable two-body operators can be reduced to products of these basic integrals as we will now show in some detail.

FORTRAN function subprograms GROLAP and GZOLAP have

written to evaluate $R_{ij}^{(n)}$ and $Z_{ij}^{(n)}$ for n = -2,-1,0,1,2.

2. REDUCTION OF THE ONE-BODY SPIN-ORBIT FORCE

We write

$$\underset{\sim}{\ell}.\underset{\sim}{s} = \tfrac{1}{2}(\ell_+ s_- + \ell_- s_+) + \ell_z s_z$$

where ℓ_+, ℓ_-, s_+, s_- are the usual operators, $(\ell_x + i\ell_y)$ etc.

Using $\underset{\sim}{\ell} = \underset{\sim}{r} \times \underset{\sim}{k}$ we find quite easily

$$\ell_+ = -i\rho e^{i\phi} k_z + iz\, e^{i\theta} k_\rho$$

$$\ell_- = i\rho e^{-i\phi} k_z - iz\, e^{-i\theta} k_\rho$$

Thus

$$\langle i|\underset{\sim}{\ell}.\underset{\sim}{s}|j\rangle = \tfrac{1}{2}\langle i|\ell_+ s_-|j\rangle + \tfrac{1}{2}\langle i|\ell_- s_+|j\rangle + \langle i|\ell_z s_z|j\rangle$$

The spin and angular variables can be integrated out quite easily giving factors of the form* $\delta(m_i - m_j)$, $\delta(m_i - m_j \pm 1)$ etc. The integrations over ρ and z are now of the basic types given in section 1 of this appendix, and we obtain:

$$\langle i|\underset{\sim}{\ell}.\underset{\sim}{s}|j\rangle = \delta(m_i - m_j)\ \delta(s_i - s_j)\ m_i s_i\ R_{ij}^{(0)}\ Z_{ij}^{(0)} + \tfrac{1}{2}\,\delta(m_i - m_j + 1)$$

$$\delta(s_i - s_j - 1)\ \{i^{(n_{zj} - n_{zi} + 1)} R_{ij}^{(1)} Z_{ij}^{(-1)} + i^{(2n_j + |m_j| - 2n_i - |m_i| - 1)}$$

$$R_{ij}^{(-1)} Z_{ij}^{(1)}\} + \tfrac{1}{2}\,\delta(m_i - m_j - 1)\ \delta(s_i - s_j + 1)\ \{i^{(n_{zj} - n_{zi} - 1)} R_{ij}^{(1)} Z_{ij}^{(-1)}$$

---

*NOTE

$$\delta(m) = 1 \text{ if } m = 0$$
$$= 0 \text{ if } m \neq 0$$

$$+ i^{(2n_j+|m_j|-2n_i-|m_i|+1)} R_{ij}^{(-1)} Z_{ij}^{(1)} \} \quad .$$

The selection rules for this matrix element are $|m_i - m_j| \leq 1$ and conservation of total $j_z = m + s$, and parity. When these conditions are satisfied the complex factors reduce to ± 1.

3. FURTHER REDUCTION FORMULAE

We have immediately that

$$\langle i|\rho^2|j\rangle = \delta(m_i - m_j)\ R_{ij}^{(2)} Z_{ij}^{(0)}$$

$$\langle i|z^2|j\rangle = \delta(m_i - m_j)\ R_{ij}^{(0)} Z_{ij}^{(2)}$$

whence:

$$\langle i|r^2|j\rangle = \delta(m_i - m_j)\ \{R_{ij}^{(2)} Z_{ij}^{(0)} + R_{ij}^{(0)} Z_{ij}^{(2)}\} \quad .$$

And similarly in momentum space:

$$\langle i|k^2|j\rangle = \delta(m_i - m_j)\ \{R_{ij}^{(-2)} Z_{ij}^{(0)} + R_{ij}^{(0)} Z_{ij}^{(-2)}\} \quad .$$

4. REDUCTION OF THE TWO-BODY CENTRE OF MASS CORRECTION

The centre of mass correction term is:

$$-\frac{P^2}{2mA} = -\frac{h^2}{2mA} \sum_i k_i^2 - \frac{h^2}{mA} \sum_{i<j} \underset{\sim}{k}_i \cdot \underset{\sim}{k}_j$$

where A is the number of nucleons and m the average mass of the nucleons. The first term on the right hand side of the equation above is incorporated as a renormalization of the usual kinetic energy. Thus:

$$T \rightarrow (1 - {}^{1}/_{A})\, T$$

The second term has the form of a separable two-body operator and contributes to the average Hartree-Fock potential Γ.

The general matrix element which we want to evaluate is:

$$(i\ell|\underset{\sim}{k}_1 . \underset{\sim}{k}_2|jm) = (i\ell|k_\rho^{(1)} k_\rho^{(2)} \cos(\theta_1-\theta_2)|jm) + (i\ell|k_z^{(1)} k_z^{(2)}|jm)$$

The integrations over θ_1 and θ_2 are simple in each term and give factors of $\frac{1}{2}\delta(m_i-m_j\pm 1)\ \delta(m_\ell-m_m\pm 1)$ and $\delta(m_i-m_j)\ \delta(m_\ell-m_m)$ respectively.

Apart from the usual symmetry rules of conserved m and parity we have for this matrix element in addition, $|m_i-m_j| \leq 1$, and the parities of i and j must be opposite.

The remaining integrals over ρ_1, ρ_2, z_1, and z_2 all separate into the basic types given above. Remembering the phase factors which come from transformation to k-space we get:

$$\langle i\ell|\underline{k}_1 . \underline{k}_2|jm\rangle = \tfrac{1}{2}\delta(m_i-m_j\pm 1)\ \delta(m_\ell-m_m\pm 1)\ i^{(2n_j+2n_m-2n_i-2n_\ell+|m_j|}$$

$$+|m_m|-|m_i|-|m_\ell|)} \times R_{ij}^{(-1)} R_{\ell m}^{(-1)} Z_{ij}^{(0)} Z_{\ell m}^{(0)} + \tfrac{1}{2}\delta(m_i-m_j)$$

$$\delta(m_{\ell}-m_{m})\; i^{(n_{zi}+n_{zm}-n_{zi}-n_{z\ell})} \times R_{ij}^{(0)}\; R_{\ell m}^{(0)} Z_{ij}^{(-1)} Z_{\ell m}^{(-1)}$$

Whenever the selection rules are satisfied the complex factors reduce to ±1.

APPENDIX 3

MATRIX ELEMENTS FOR THE TWO-BODY INTERACTION

As explained in the text the most general form of interaction we are interested in has the following form in configuration space:

$$\rho^{2/3}\left(\frac{r_1+r_2}{2}\right)\ v(r_1-r_2)=ce^{-2/3\left(\frac{\rho_c^2}{\rho_o^2}+\frac{1}{2}\frac{z_c^2}{z_c^2}\right)}$$

$$\left(V_a e^{-(r_1-r_2)^2/\lambda a^2}+V_r e^{-(r_1-r_2)^2/\lambda r^2}\right)$$

where we are using (ρ_c, φ_c, z_c) for the cylindrical co-ordinates of the centre of mass variable $(\frac{r_1+r_2}{2})$, and ρ_o and z_o as the r.m.s. values of ρ and z for the density distribution. Now the general matrix element

$$(i\ell \mid \rho^{2/3}\ (R)\ v(r) \mid jm)$$

can be reduced to sums and products of terms of the form

$$I^r(i,\ell,j,m,k,K)=\frac{1}{4\pi^2}\int \Psi_i^r(\rho_1)^*\Psi_\ell^r(\rho_2)^* e^{-im_i\phi_i-im_\ell\phi_2}$$

$$\times\ e^{-\frac{1}{2}k(\rho_1^2-2\rho_1\rho_2\cos\phi_{12}+\rho_2^2)}e^{-\frac{1}{2}K(\rho_1^2+2\rho_1\rho_2\cos\phi_{12}+\rho_2^2)}$$

$$\times\ \Psi_j^r(\rho_1)\ \Psi_m^r(\rho_2)\ e^{im_j\phi_1+im_m\phi_2}\rho_1\rho_2 d\rho_1 d\rho_2 d\phi_1 d\phi_2 .$$

and

$$I^z(n_1,n_2,n_3,n_4)=\int \psi^z_{n_1}(z_1)^* \psi^z_{n_2}(z_2)^* e^{-\frac{1}{2}k(z_1-z_2)^2} e^{-\frac{1}{2}K(z_1+z_2)^2}$$

$$\times \quad \psi^z_{n_3}(z_1)\ \psi^z_{n_4}(z_2)\ dz_1dz_2$$

As the states may all have different oscillator constants it is not possible to carry out the usual form of transformation into relative and centre of mass co-ordinates for the two-body wave functions, and so we have to evaluate these integrals explicitly as they stand.

I^r:

We write the product of the normalization constants as N so:

$$N = \frac{1}{4\pi^2}\left[\frac{2\alpha_1.2\alpha_2\ .2\alpha_3\ .2\alpha_4\ .n_1!.n_2!.n_3!.n_4!}{(n_1+|m_1|)!(n_2+|m_2|)!(n_3+|m_3|)!(n_4+|m_4|)!}\right]^{1/2}$$

then:

$$I = N\int e^{i(m_3-m_1)\phi_1} e^{i(m_2-m_4)\phi_2} (\alpha_1^{\frac{1}{2}}\rho_1)^{|m_1|} (\alpha_2^{\frac{1}{2}}\rho_2)^{|m_2|}$$

$$\times \quad (\alpha_3^{\frac{1}{2}}\rho_1)^{|m_3|} (\alpha_4^{\frac{1}{2}}\rho_2)^{|m_4|}\ L^{|m_1|}_{n_1}(\alpha_1\rho_1^2)\ L^{|m_2|}_{n_2}(\alpha_2\rho_2^2)$$

$$\times \quad L^{|m_3|}_{n_3}(\alpha_3\rho_1^2)\ L^{|m_4|}_{n_4}(\alpha_4\rho_2^2)\ e^{-\frac{1}{2}(\alpha_1+\alpha_3)\rho_1^2} e^{-\frac{1}{2}(\alpha_2+\alpha_4)\rho_2^2}$$

$$\times \quad e^{-\frac{1}{2}k(\rho_1^2-2\rho_1\rho_2\cos\phi_{12}+\rho_2^2)} e^{-\frac{1}{2}K(\rho_1^2+2\rho_1\rho_2\cos\phi_{12}+\rho_2^2)}\ \rho_1\rho_2 d\rho_1 d\rho_2 d\phi_1 d\phi;$$

The angular integration can be carried out immediately, using

$$e^{iz\,\mathrm{Cos}\phi} = \sum_{n=-\infty}^{\infty} i^n\, e^{in\phi}\, J_n(z)$$

Thus

$$\int e^{(k-K)\rho_1\rho_2\mathrm{Cos}\phi_{12}} e^{i(m_3-m_1)\phi_{12}} e^{iM(\phi_1+\phi_2)}\, d\phi_1\, d\phi_2$$

$$= 4\pi^2 J_{m_1-m_3}\,[-i(k-K)\rho_1\rho_2]\; i^{m_1-m_3}$$

Now from

$$J_\nu(-z) = (-1)^\nu J_\nu(z)$$

and

$$i^{-m} J_m(z) = i^m J_{-m}(z)$$

this can be written

$$4\pi^2\, J_{|m_3-m_1|}\,[i(k-K)\rho_1\rho_2]\; i^{-|m_1-m_3|}$$

As the required matrix element is unchanged by a change of numbering from 1,2,3,4, to 3,4,1,2, we will assume from here on that $m_3 \geq m_1$

So:

$$I = N\int 4\pi^2\; i^{m_1-m_3}\; (\alpha_1{}^{\frac{1}{2}}\rho_1)^{|m_1|}\,(\alpha_2{}^{\frac{1}{2}}\rho_2)^{|m_2|}\,(\alpha_3{}^{\frac{1}{2}}\rho_1)^{|m_3|}\,(\alpha_4{}^{\frac{1}{2}}\rho_2)^{|m_4|}$$

$$\times\; L_{n_1}^{|m_1|}(\alpha_1\rho_1^2)\; L_{n_2}^{|m_2|}(\alpha_2\rho_2^2)\; L_{n_3}^{|m_3|}(\alpha_3\rho_1^2)\; L_{n_4}^{|m_4|}(\alpha_4\rho_2^2)$$

$$\times\ e^{-\frac{1}{2}A\rho_1^2}\ e^{-\frac{1}{2}B\rho_2^2}\ J_{m_3-m_1}[i(k-K)\rho_1\rho_2]\ \rho_1\rho_2 d\rho_1 d\rho_2$$

where $A = \alpha_1 + \alpha_3 + k + K$

$B = \alpha_2 + \alpha_4 + k + K$

At this point we can simplify matters somewhat by noticing that in the first four shells of harmonic oscillator states the quantum number n is always 0 or 1 and

$$L_0^{\nu}(x) = 1$$

$$L_1^{\nu}(x) = 1 + \nu - x$$

Hence we write

$$L_n^{|m|}(x) = 1 + n|m| - nx \qquad n = 0 \text{ or } 1.$$

if we further put

$$t_1 = \tfrac{1}{2}\rho_1^2 \quad , \qquad t_2 = \tfrac{1}{2}\rho_2^2$$

and constants

$$C_0 = (1 + n_1|m_1|)(1 + n_3|m_3|)$$

$$C_1 = -2\alpha_1 n_1 (1 + n_3|m_3|) - 2\alpha_3 n_3 (1 + n_1|m_1|)$$

$$C_2 = 4\alpha_1\alpha_3 n_1 n_3$$

$$D_0 = (1 + n_2|m_2|)(1 + n_4|m_4|)$$

$$D = -2\alpha_2 n_2 (1 + n_4|m_4|) - 2\alpha_4 n_4 (1 + n_2|m_2|)$$

$$D = 4\alpha_2\alpha_4 n_2 n_4$$

Then the integral required is

$$I = 4\pi^2 N\, i^{m_1-m_3}\, (2\alpha_1)^{\frac{|m_1|}{2}} (2\alpha_2)^{\frac{|m_2|}{2}} (2\alpha_3)^{\frac{|m_3|}{2}} (2\alpha_4)^{\frac{|m_4|}{2}}$$

$$\times \sum_{r=0}^{2} \sum_{s=0}^{2} C_r D_s \int_0^\infty dt_2\, t_2^{\frac{1}{2}(|m_2|+|m_4|)+s}\, e^{-Bt_2} \int_0^\infty dt_1$$

$$\times t_1^{\frac{1}{2}(|m_1|+|m_3|)+r}\, e^{-At_1}\, J_{m_3-m_1}[2i(k-K)t_1^{\frac{1}{2}} t_2^{\frac{1}{2}}] \quad .$$

From Erdelyi (1954) we find the standard integral

$$\int_0^\infty t^{\frac{1}{2}\nu+n}\, J_\nu(2\alpha^{\frac{1}{2}}t^{\frac{1}{2}})\, e^{-At}\, dt = n!\alpha^{\nu/2} A^{-(n+\nu+1)}\, e^{-\alpha/A}\, L_n^{\nu}(\alpha/A).$$

which gives the integral over t_1. Defining further

$$\ell = \tfrac{1}{2}(|m_1| + |m_3| + m_1 - m_3)$$

$$j = \tfrac{1}{2}(|m_2| + |m_4| - m_1 + m_3)$$

we have

$$I = 4\pi^2 N\, i^{m_1-m_3} (2\alpha_1)^{\frac{|m_1|}{2}} (2\alpha_2)^{\frac{|m_2|}{2}} (2\alpha_3)^{\frac{|m_3|}{2}} (2\alpha_4)^{\frac{|m_4|}{2}}$$

$$\times [i(k-K)]^{m_3-m_1} \sum_{r,s} C_r D_s (\ell+r)!\, A^{-(\ell+r+m_3-m_1+1)} \int_0^\infty dt_2\, t_2^{j+s}$$

$$\times e^{-\chi^2/A.t_2}\, L_{\ell+s}^{m_3-m_1}\left[-\frac{(k-K)^2}{A}\, t_2\right] .$$

where $\chi^2 = AB - (k-K)^2$

The remaining integral can also be found in Erdelyi as:

$$\int_0^\infty e^{-pt}\, t^{\beta}\, L_n^{\alpha}(\gamma t)\, dt = \frac{\Gamma(\beta+n+1)}{n!}\,\frac{\gamma^n}{p^{\beta+n+1}}\; {}_2F_1\left[-n,-n-\alpha\,;-n-\beta;\frac{p}{\gamma}\right]$$

and hence:

$$I = 4\pi^2 N\,(2\alpha_1)^{\frac{|m_1|}{2}}(2\alpha_2)^{\frac{|m_2|}{2}}(2\alpha_3)^{\frac{|m_3|}{2}}(2\alpha_4)^{\frac{|m_4|}{2}}\,[(k-K)/A]^{m_3-m_1}$$

$$\times \sum_{rs} C_r D_s\,(j+\ell+r+s)!\,\left[-\frac{(k-K)^2}{\chi^2}\right]^{\ell+r} A^{j+s-\ell-r+1}\,\chi^{-2(j+r+1)}$$

$$\times {}_2F_1\left(-\ell-r,-\ell-r-m_3-m_1\,;-\ell-j-r-s\,;-\frac{\chi^2}{(k-K)^2}\right)$$

A FORTRAN function subprogram VDRFP has been written to evaluate this formula.

$I^Z(n_1,n_2,n_3,n_4)$

Denoting the relevant normalization constant by N again, so

$$N = (\beta_1\beta_2\beta_3\beta_4)^{-\frac{1}{4}}\,\pi^{-1}\,2^{-(n_1+n_2+n_3+n_4)/2}\,[n_1!n_2!n_3!n_4!]^{-\frac{1}{2}}$$

we have:

$$I^Z = N\int H_{n_1}(\beta_1^{\frac{1}{2}}x)\,H_{n_2}(\beta_2^{\frac{1}{2}}y)\,H_{n_3}(\beta_3^{\frac{1}{2}}x)\,H_{n_4}(\beta_4^{\frac{1}{2}}y)\,e^{-\frac{1}{2}(\beta_1+\beta_3)x^2}$$

$$\times e^{-\frac{1}{2}(\beta_2+\beta_4)y^2}\,e^{-\frac{1}{2}k(x-y)^2}\,e^{-\frac{1}{2}K(x+y)^2}\,dx\,dy$$

Rather than attack this integral directly we use the generating function for the Hermite polynomials

$$e^{2xz-z^2} = \sum_{n=0}^{\infty} \frac{z^n}{n!} H(x)$$

Thus:

$$\mathcal{S} = \int \exp[2\beta_1^{\frac{1}{2}} x z_1 - z_1^2 + 2\beta_2^{\frac{1}{2}} y z_2 - z_2^2 + 2\beta_3^{\frac{1}{2}} x z_3 - z_3^2 + 2\beta_4^{\frac{1}{2}} y z_4 - z_4^2 - \tfrac{1}{2}(\beta_1+\beta_3)x^2$$

$$-\tfrac{1}{2}(\beta_2+\beta_4)y^2 - \tfrac{1}{2}k(x-y)^2 - \tfrac{1}{2}K(x+y)^2]\,dx\,dy$$

can be expanded as an infinite multinomial in z_1, z_2, z_3, and z_4, thus:

$$\mathcal{S} = \sum_{n_1 n_2 n_3 n_4} \frac{z_1^{n_1} z_2^{n_2} z_3^{n_3} z_4^{n_4}}{n_1!\, n_2!\, n_3!\, n_4!} I^z(n_1 n_2 n_3 n_4)/N(n_1 n_2 n_3 n_4)$$

The evaluation of $\mathcal{S}$ is straightforward.

$$\mathcal{S} = e^{-(z_1^2+z_2^2+z_3^2+z_4^2)} \int_{-\infty}^{+\infty} dy\; e^{-\frac{1}{2}By^2 + 2(\beta_2^{\frac{1}{2}} z_2 + \beta_4^{\frac{1}{2}} z_4)y} \int_{-\infty}^{+\infty} dx$$

$$\times\; e^{-\frac{1}{2}Ax^2 + 2(\beta_1^{\frac{1}{2}} z_1 + \beta_3^{\frac{1}{2}} z_3)x + (k-K)yx}$$

where we have written

$$A = \beta_1 + \beta_3 + k + K$$

$$B = \beta_2 + \beta_4 + k + K$$

The subsequent evaluation using the standard integral

$$\int_{-\infty}^{\infty} e^{-ax^2+bx}\,dx = \Pi^{\frac{1}{2}}\, a^{-\frac{1}{2}}\, e^{b^2/4a}$$

is simply a matter of algebra, and gives

$$J = \left(\frac{2\Pi}{\chi}\right) \exp\left(\frac{2}{\chi^2} \cdot X\right)$$

where

$$X = \left(B-\frac{\chi^2}{2\beta_1}\right)u_1^2 + \left(A-\frac{\chi^2}{2\beta_2}\right)u_2^2 + \left(B-\frac{\chi^2}{2\beta_3}\right)u_3^2 + \left(A-\frac{\chi^2}{2\beta_4}\right)u_4^2 + 2Bu_1u_3$$

$$+2Au_2u_4 + 2(k-K)\,[u_1u_2+u_1u_4+u_2u_3+u_3u_4]$$

and $u_i = \beta_i^{\frac{1}{2}} z_i \qquad i = 1, 2, 3, 4$

$$\chi^2 = AB - (k-K)^2$$

Now the required integral $I(n_1,n_2,n_3,n_4,)$ appears in the coefficient of $u_1^{n_1}u_2^{n_2}u_3^{n_3}u_4^{n_4}$ in the expansion of the exponential. In fact we have explicitly

$$I(n_1,n_2,n_3,n_4) = N(n_1,n_2,n_3,n_4)\cdot n_1!n_2!n_3!n_4!\left(\frac{2\Pi}{\chi}\right)\left(\frac{2}{\chi^2}\right)^m \frac{1}{m!}$$

$$\times\,[\beta_1^{n_1}\beta_2^{n_2}\beta_3^{n_3}\beta_4^{n_4}]^{\frac{1}{2}} \times \text{Coeff of } u_1^{n_1}u_2^{n_2}u_3^{n_3}u_4^{n_4}$$

in exp [X] .

where $m = \frac{1}{2}(n_1+n_2+n_3+n_4)$

The various relevant coefficients which occur for the first four shells of oscillator wave functions have all been evaluated by hand and a FORTRAN function sub-program VDZFP incorporating them has been written.

APPENDIX 4

STRUCTURE OF THE RHF PROGRAMS AND STORAGE OF MATRIX ELEMENTS

A SIMPLIFIED STRUCTURE OF PROGRAMS HARFOK AND HARFO4

1. Read in: quantum numbers force parameters, representation size and shape parameters, nucleus and configuration parameters, and miscellaneous constants.
2. Store matrix elements of one-body part of Hamiltonian.
3. Calculate parameters for gaussian approximation to density of dominant configuration.
4. Store matrix elements of two-body part of Hamiltonian.
5. Fill HF matrix with random numbers and biased diagonal elements.
6. Diagonalize HF and order the eigenvectors according to their eigenvalues.
7. Form density matrix RHF from occupied states.
8. Put one-body matrix elements into HF and calculate average Hartree-Fock potential Γ, adding to HF.

9. Return to step 6 for prescribed number of iterations.

10. Calculate mixing parameters θ_1, θ_2, θ_3, and θ_4.

11. Output density matrix RHO.

The time for the calculation of all the matrix elements is about 20 seconds for the three shell program and about 2½ minutes for the four shell program. One iteration loop, consisting of steps 6 to 9, takes about 20 seconds for the three shell program, and approximately 12 seconds of this time is spent in diagonalizing the 20 x 20 HF matrix. For the four shell program the iteration loop takes about 3 minutes and about 1 minute of this is used to diagonalize the 40 x 40 HF matrix.

B STORAGE OF TWO-BODY MATRIX ELEMENTS FOR HARFOK

The two-body matrix elements between space states are stored in an array V. The matrix elements

$$(IL|V|JM) \quad I, L, J, M = 1, 2, \ldots 10$$

satisfy the relation

$$(IL|V|JM) = (LI|V|MJ)$$

and so it is necessary to store those for which $I \leq L$. Furthermore, for given I and L values, the values of J and M which satisfy the conservation rules, for total z

component of angular momentum and parity, are considerably restricted. In fact the largest number of (J,M) pairs that can be taken with any (I,L) pair is 16. As there are 55 (I,L) pairs we store the matrix elements in a 16 x 55 array. The columns of this array are numbered according to I and L by the index $\frac{1}{2}L\,(L-1) + I$, and the non-zero matrix elements which may occur for the (I,L) pair are stored starting at the head of the column. In order to remember the corresponding J and M values for the matrix elements, we use arrays JV(16,55) and MV(16,55). Now to locate a particular matrix element $(IL|V|JM)$, the indices are arranged so that $I \leq L$ and from the I and L values a column is picked. Then we must scan down this column in the JV and MV matrices until the JV and MV values coincide with the required J and M. Finally, when a row is located as containing the correct J and M, the matrix element is found in that row of V. It will be shown below that such a search procedure is not needed to construct the average potential, and is only considered here for clarity. The two-body centre-of-mass matrix elements are stored in an exactly similar way in an array COM(16,55) and the JV and MV arrays apply to COM as well as to V. Because there are not 16 (J,M) pairs for each (I,L) pair there are many zeroes in the V, JV and MV arrays, and, because of the more stringent selection rules

for the centre of mass elements, there are more zeroes in the COM array. In fact the storage efficiency of this method is about 50%.

The matrix element $(IL|V|JM)$ actually has more symmetries than the one mentioned above. In particular

$$\begin{aligned}(IL|V|JM) &= (LI|V|MJ) \\ &= (JM|V|IL) \\ &= (MJ|V|LI).\end{aligned}$$

If orbitals which differ only in the sign of m have the same oscillator constants and are denoted $|I)$ and $|\bar{I})$ then:

$$\begin{aligned}(IL|V|JM) &= (\bar{I}\bar{L}|V|\bar{J}\bar{M}) \\ &= (\bar{J}\bar{M}|V|\bar{I}\bar{L}) \\ &= (\bar{L}\bar{I}|V|\bar{M}\bar{J}) \\ &= (\bar{M}\bar{J}|V|\bar{L}\bar{I}).\end{aligned}$$

It must be pointed out that not all these eight forms are necessarily distinct and they may be all equivalent (if $I = L = J = M = \bar{I}$). However on average there are two other distinct matrix elements which are identical to $(IL|V|JM)$. Full use of this symmetry is made when storing matrix elements and so the time taken in evaluating them is reduced by a factor of 3.

The spin and isospin part of the interaction is not stored explicitly but is calculated from the exchange parameters as necessary.

RECOVERY OF TWO-BODY MATRIX ELEMENTS

The form of the matrix for the average potential is given in chapter 4 in the form

$$\Gamma_{ij} = \sum_{\ell m} \rho_{\ell m} \left(S^{+}_{i\ell jm} V_{i\ell jm} - S^{-}_{i\ell jm} V_{i\ell mj} \right)$$

where the $S^{\pm}_{i\ell jm}$ are spin-isospin factors and

$$V_{i\ell jm} = (IL|V|JM).$$

We are denoting the space state corresponding to $|i)$ by $|I)$. It would be possible to construct the matrix elements of Γ one by one using the equation above. However this would mean that a search would have to be carried out for all the non-zero elements $V_{i\ell jm}$, which contributed to a particular Γ_{ij}. Such a search procedure is rather time consuming. It takes much less time to consider the elements $V_{i\ell jm}$ one at a time and search for the various Γ_{ij} to which they contribute. In this way the V array is scanned once and once only, but each element may effect up to eight different positions in the Γ matrix. The number eight arises because $V_{i\ell jm}$ affects Γ_{ij} as a direct matrix element and Γ_{im} as an exchange matrix element and because there are four possible spin choices for the pairs (i,j) and (i,m).

C

A GENERAL PROCEDURE FOR STORING TWO-BODY MATRIX ELEMENTS FOR USE IN HARTREE-FOCK PROGRAMS

Because of the large number of matrix elements in the four shell program HARFO4, their storage and recovery are more critical. By way of example, if the the same procedure was used in HARFO4 as in HARFOK, to store the matrix elements, then we would require 27,720 storage words. This does not include the centre of mass correction terms.

A more efficient general procedure for storing matrix elements can be constructed as follows. A matrix element can be regarded as a number associated with a quadruple (i, l, j, m) of single-particle state indices. Quadruples can be regarded as equivalent if they give rise to equal matrix elements, and they can be grouped accordingly. In each group there will occur the distinct quadruples among

(i,l,j,m), (l,i,m,j), (j,m,i,l) and (m,j,l,i),

together with any others which are equivalent because of symmetries pertaining to the single-particle states. Many of these groups of quadruples can now be ignored, because the corresponding matrix elements are zero and so do not affect the problem. At this stage the symmetry of the interaction is used, for example conservation of parity.

If some symmetry is to be imposed on the single-particle states in the RHF calculation, so that the density matrix has some symmetry, then matrix elements which do not have a related symmetry do not occur in the formation of the average potential Γ. For example, if the Hartree-Fock states were constrained to have definite parity, the density matrix ρ would have zero matrix elements between states of opposite parity. Thus in forming Γ by

$$\Gamma_{ij} = \Sigma_{\ell m} \rho_{\ell m} \langle i\ell|V|jm\rangle$$

the matrix elements $\langle i\ell|V|jm\rangle$ in which ℓ and m have opposite parity, do not occur. Such matrix elements which do not occur may be regarded as zero and the corresponding gorups of quadruples may be ignored.

It now remains to list the remaining quadruple groups in some convenient order, and then the corresponding matrix elements can be stored in the same order. This can be done immediately if there is an ordering of the original set of quadruples, because any group of quadruples has a lowest quadruple in the original ordering, and the groups are naturally ordered by the order of their lowest quadruples. A program to use these ideas can be represented schematically as:

1. Consider all possible quadruples in some order.
2. If the symmetry rules, such as parity, etc., are not satisfied ignore this quadruple (i.e. the

corresponding matrix element is zero or is not required in the calculation).

3. If this is not the lowest quadruple in its group of equivalent quadruples ignore it.

4. Otherwise calculate the corresponding matrix element and store it.

The matrix elements are stored in a one-dimensional array, and in order to remember the four single-particle states associated with a particular matrix element we could store the numbers i,l,j and m of the lowest quadruple in similar arrays. This lowest quadruple can be used to generate the complete quadruple group. However, if the original quadruples are ordered as:

(1111), (1112), (1113). ..... (1121), (1122), ... etc.,

then whenever (i,l,j,m) is a lowest quadruple we have

$$i \leq \min(l,j,m).$$

In particular

$$i \leq l ,$$

and so the values of i and l which are stored occur in the sequence

(11), (12), (13), ... (22), (23), ... (33), (3,4) .... .

Because this sequence follows a well-defined pattern it is only necessary to remember at which point in the one-dimensional array of matrix elements the (i,l) pair changes;

it is not necessary to store the i and l indices in separate arrays. It is necessary to store the j and m indices.

In the case of our four shell program this method has been used to store matrix elements between space states. There are 20 such single-particle space states and the number of matrix elements to be stored is 1641. Thus we have 3 arrays of length 1641, one containing matrix elements, another the values of j for the corresponding lowest quadruple, and the third containing the m values for the lowest quadruple. In addition it is necessary to remember the 210 points along these arrays at which the value of i or l changes. This amounts to 5133 storage words and a considerable improvement over the figure 27,720 given earlier.

It has been shown above that it is not necessary to search for particular matrix elements when constructing the average potential, and the order in which they are picked out is immaterial. However when a number is picked out of the storage array it must be remembered that this number is related, in general, to more than one quadruple. So, after the lowest quadruple is recovered from the storage arrays, all the equivalent distinct quadruples must be generated, and the stored matrix element is then used as the matrix element corresponding to each individual quadruple.

APPENDIX 5

SUBROUTINE MINI2

1. Call and parameter list:

CALL MINI2 (FUN, PAM, NDIM, DIRECT, N, STEP, STEPMX, EPS, SHIFT, ICALL, HOP, VAL, WORK, FIN).

2. Specifications:

MINI2 is designed to find the minimum of a function of several variables. The function is called as FUN (PAM) where PAM is an array of length NDIM. The dimensioned parameters with their appropriate dimensions are

PAM (NDIM)

DIRECT (NDIM, NDIM)

HOP (3N + 4)

VAL (3N + 4)

WORK (2NDIM + N)

3. Procedure:

The method has been taken from M. Powell, Computer Journal 7, 155, (1964), though some changes have been made. The subroutine executes one pass of the general procedure and is designed to be called repetitively until convergence is obtained.

For the first call ICALL must be zero, and this parameter is stepped by one internally on each call. When first called (ICALL = 0), MINI2 examines the first N columns of the square matrix DIRECT of side NDIM, these columns being used as directions to search along in the parameter space. The lengths of the directions are stored in WORK and if a zero direction is encountered it is discarded, the remaining columns of DIRECT being shifted down one place, and N is reduced by 1. Also only on the first call a starting value of FUN evaluated at the input parameter values is calculated, on subsequent calls the starting point is remembered from the previous call

On the first and all subsequent calls the following procedure is carried out. Each of the N directions is taken in turn and points are examined along it, using a one dimensional minimization procedure explained below. At each new point the value of FUN is stored in a corresponding place in the array VAL and the distance moved in parameter space is stored in HOP. The result of the one dimensional minimization is to replace the starting PAM array with another one at which the value of FUN is not greater than the starting

value. To ensure this feature the position of the lowest FUN value is always remembered.

When the PAM point in parameter space has been moved along each of the N directions in turn in this way 3N + 1 points have been calculated and stored in VAL and HOP. At this stage a new direction is introduced which is taken from the original PAM point on entry to the subroutine to the most recent PAM point, and if the distance between these two points is d, the new direction is normalized so that one step along it moves a distance of $d/(2\sqrt{N})$. The one of the old directions closest to this new one is now discarded and the new one replaces it in DIRECT. Finally a one dimensional minimization is carried out along this new direction, the best value found for FUN is returned in FIN and the point at which it occurs in PAM, and the net distance moved in this pass is returned in SHIFT.

4. The one dimensional minimization

At the start of this subprocedure the value of FUN (PAM) is given at a point, and a particular direction is given. A step is taken along the direction, which moves the point PAM a distance of STEP multiplied by the length of the direction, and

the value of FUN evaluated. If the new value is lower than the starting value a further step is taken and a third point evaluated, however if the new value of FUN is larger, two steps backward are taken. At this point we have three values of the function evaluated at equal intervals, and a decision is made at this stage. If the function values are f_1, f_2, f_3, and if $f_1-2f_2+f_3>EPS$ then a parabola is fitted through the three f values and the position of the minimum of the parabola is calculated. In this case which may be called the normal case the function is evaluated at the PAM point corresponding to the bottom of the parabola and this point is used as the start of the next one dimensional minimization unless the value of FUN is larger than the lowest one previously found, in which case this previously found point is used instead.

When this normal case is not satisfied (that is $f_1-2f_2+f_3 \leq EPS$) it is decided that the curve is too flat for a parabola to be meaningful or else the parabola has a maximum rather than a minimum. (It should be noted that $f_1-2f_2+f_3$ is proportional to the second derivative averaged over the region of interest.) In this case the subroutine will

either use f_2 as the starting point for the next minimization, if f_2 is smaller than both f_1 and f_3, or else calculate an additional point and make another attempt to fit a parabola to three consecutive points including the new one.

The subroutine will make up to four attempts to fit a parabola in this way, but will not make any attempts after the extra points calculated start to increase in value. In any case where a parabola is not fitted, the lowest value of FUN which has been calculated is used for the next minimization. In cases where more than three points are calculated along a direction only the first and the last two are stored in VAL and HOP.

It should be noted that if the value of EPS is very small or zero the procedure may become unstable particularly around saddle points. On the other hand if EPS is very large the procedure will never fit a parabola and will just take up to 7 steps in each direction remembering always the lowest one, this of course will make convergence very slow.

5. Further comments

None of the parameters need adjustment between calls however, STEP, STEPMX and EPS may be changed

if desired.

EPS should certainly be larger than any rounding error which may occur in the evaluation of FUN, and reasonable values are about the accuracy to which the minimum value is required.

In principle NDIM + 1 passes are needed to find the minimum of a general quadratic function in NDIM variables, however for rather simple functions of 10 variables about 5 passes has been sufficient.

If nothing is known about the function a reasonable initial choice for DIRECT is the unit matrix.

BIBLIOGRAPHY

(1) Y. Abragall, E. Caurier and G. Monsonego, Phys. Letters, 24B (1967) 609

(2) M. Baranger, "Theory of Finite Nuclei", Cargese Lectures in Theoretical Physics, Benjamin 1963

(3) W. Bassichis, I. Kelson and C. Levinson, Phys. Rev., 136 (1964) B380

(4) W. Bassichis, A. Kerman and J. Svenne, Phys. Rev., 160 (1967) 746

(5) J. Bernier and M. Harvey, Nucl. Phys., A94 (1967) 593

(6) H. Bethe, invited lecture, 1966 Gatlinburg Conference

(7) R. Bhaduri and E. Tomusiak, Proc. Phys. Soc., 86 (1965) 451

(8) R. Bhaduri and E. Tomusiak, Nucl. Phys., 88 (1966) 353

(9) P. Bhargava and D. Sprung, Annals of Physics (N.Y.), 42 (1967) 222

(10) B. Brandow, "Theory of the Effective Interaction", Varenna Summer School seminar (1965)

(11) K. Brueckner and W. Wada, Phys. Rev., 103 (1956) 1008

(12) D. Brink and E. Boeker, Nucl. Phys., A91 (1967) 1

(13) T. Brody and M. Moshinsky, Tablas de parentesis de transformacion (Monografias del Instituto de Fisica UNAM, Mexico, 1960)

(14) G. Brown, "Unified Theory of Nuclear Models and Forces", second revised edition 1967

(15) R. Chasman and S. Wahlborn, Nucl. Phys., A90 (1967) 401

(16) S. Das Gupta and M. Harvey, Nucl. Phys., A94 (1967) 602

(17) K. Davies, S. Krieger and M. Baranger, Nucl. Phys., 84 (1966) 545, also: S. Krieger, M. Baranger and K. Davies, Phys. Letters, 22 (1966) 607

(18) J. Elliot and A. Lane, "The Nuclear Shell Model", Encyclopedia of Physics, Vol. XXXIX. Springer Verlag, 1957.

(19) A. Erdelyi, W. Magnus, F. Oberhettinger and F. G. Tricomi, Tables of Integral Transforms, McGraw Hill Book Co., 1954

(20) V. Fock, Z. Physik, 61 (1930) 126, and 62 (1930) 795

(21) J. Goldstone, Proc. Roy. Soc. (London) A239 (1957) 267

(22) D. Hartree, Proc. Cambridge Phil. Soc., 24 (1928) 89

(23) D. Hughes, D. Sprung and A. Volkov, to be published

(24) A. Kallio, Phys. Letters, 18 (1965) 51

(25) A. Kallio and K. Koltveit, Nucl. Phys. 53 (1964) 87

(26) I. Kelson, Phys. Rev., 132 (1963) 2189

(27) I. Kelson and C. Levinson, Phys. Rev., 134 (1964) B269

(28) T. Kuo and G. Brown, Phys. Letters, 18 (1965) 54

(29) T. Kuo and G. Brown, Nucl. Phys., 85 (1966) 40

(30) H. Lamme and E. Boeker, Phys. Letters, 24B (1967) 367

(31) A. Messiah, "Quantum Mechanics", Vols. I and II, third printing 1965

(32) S. Moszkowski and B. Scott, Annals of Physics (N.Y.), 11 (1960) 65

(33) B. Mottelson, in "The Many-Body Problem", Les Houches Summer School (1958), edited by C. DeWitt

(34) R. Muthukrishnan, Nucl. Phys., A93 (1967) 417

(35) S. Nilsson, Mat. Fys. Medd. Dan. Vid. Selsk. 29, No. 16 (1955)

(36) M. Powell, Comp. Journal, 7 (1964) 155

(37) G. Ripka, "Equilibrium Shapes of Light Nuclei", Lectures delivered at the International Centre for Theoretical Physics, Trieste, 1966

(38) D. Vautherin and M. Veneroni, Phys. Letters, 25B (1967) 175

(39) A. Volkov, Nucl. Phys., 74 (1965) 33

(40) A. Volkov, Invited paper on Nuclear Physics, 1967 summer meeting of the American Physical Society, Toronto

(41) C. Wong, Nucl. Phys., A91 (1967) 399

FIGURE CAPTIONS

Figure 1. The radial part of force 2 is shown for two values of λ_r, as indicated. Also shown is a hard-core potential and the long-range part of this, obtained in the Moszkowski-Scott separation technique. The attractive part of the hard-core potential is

$V(r) = -93.5 \exp(-r/1.4)/r$, $r > 0.4$ fm.

Figure 2. λ_r is shown as two functions of the relative wave number, derived by fitting the singlet or triple s-wave phase shifts. Some weighted average points are shown, the weights being the relative singlet and triple strengths, as explained in chapter 3. Also shown is the parabolic fit to these points which is used in force 2. The range of values of k which are used in evaluating matrix elements extends roughly from 0.4 fm^{-1} to 1.6 fm^{-1}, and over this range the parabola is a good fit the the average points.

Figure 3. The binding energy per nucleon in nuclear matter, obtained by a first order perturbation calculation (i.e. a Hartree-Fock calculation), is shown as a function of the Fermi wave number, for forces 1 and 2.

Figure 4. A matrix element of the gaussian potential $\exp(-r^2/\lambda(k)^2)$, where

$$\lambda(k) = \lambda^{\circ}(1 + 0.5\ (k - 1)^2)$$

is shown as a function of the size of the oscillator states. Curve A gives the result

of using the Kallio definition of k^2, given in chapter 3, and using the Moshinsky transformation to separate the relative states. The result of using the definition of k^2, proposed in chapter 3, cannot be separated from curve A on this scale; the two sets of results differ my at most 0.005. Curve B shows the result of using a constant value of k^2 taken from the relative s state. Both curves are normalized to unity at zero size, and so all units are dimensionless. The matrix element evaluated is

$$(000, 002|V|000, 002);$$

other matrix elements examined show very similar behaviour.

Figure 5. The radial density of the ^{16}O configuration 1S, 1P, is shown as ρ_N. Also shown are the two gaussian approximations ρ_I and ρ_{II} defined in chapter 3, and $\alpha r^2 \rho_N$. α is the oscillator constant. All units are dimensionless.

Figure 6. The binding energy obtained for ^{16}O, in the three shell RHF program, is shown as a function of the number of iterations performed. The representation states used have an optimum volume ($a^2b = 0.9186$) determined by a one-dimensional minimization of the energy of the simple configuration 1S, 1P. The deformation of the states is $d = -0.4$.

Figure 7. As for figure 6, the ^{16}O binding energy is shown as a function of the number of iterations. In this case though, the representation states are spherical (i.e. $d = 0$)

and have a volume ($a^2b = 1.00$) which is larger than the optimum volume.

Figure 8. As for figure 6, the ^{16}O binding energy is shown as a function of the number of iterations. In this case, the representation states have their best size and deformation, as determined by a GHA calculation. The large energy scale should be noted.

Figure 9. The binding energy, for the asymmetric ^{24}Mg ground state, is shown as a function of the number of iterations. The representation states have their best parameters, as determined by the corresponding GHA calculation.

Figure 10. The energy of the ^{20}Ne configuration 1S, 1P $(002)^4$, and the energies of the related three and four shell RHF calculations are shown as functions of the deformation d of the representation states. The calculated values are marked with crosses. The representation size ($a^2b = 1.0251$) is chosen to minimize the energy of the pure configuration at zero deformation. On the right hand side the results of the GHA calculation and of the RHF calculation using the GHA parameters are shown.

Figure 11. The dimensionless deformation parameter Q/R^2 for the ^{20}Ne system, as a pure configuration and from three shell RHF calculations, is shown plotted against the deformation d of the representation. d is just the value of Q/R^2 for the (000) orbital.

The size of the representation is given in the figure 10 caption.

Figure 12. The mixing parameters θ_1 and θ_3, for states of the same m and parity and for states of different m but opposite parities respectively, are plotted against the deformation d of the representation. The size of the representation is given in the figure 10 caption. The values obtained in the RHF calculation, which uses the oscillator parameters obtained in the GHA calculation, are shown for comparison on the right. These are marked "RHF".

Figure 13. The kinetic and potential energies of ^{20}Ne configuration 1S, 1P, $(002)^4$ are plotted against the deformation d. The size of the representation is given in the caption for figure 10.

Figure 14. The energies of the ^{8}Be configuration and the related RHF solutions are shown plotted against the deformation d. The format is identical to that of figure 10. The representation size ($a^2b = 1.0504$) has been chosen to minimize the energy of the pure configuration at zero deformation.

Figure 15. The deformation Q/R^2 of the ^{8}Be system, as a pure configuration and from three shell RHF calculations, is plotted against the deformation d of the representation. The representation size is given in the caption for figure 14.

Figure 16. The mixing parameters θ_1 and θ_3 for the RHF calculation, starting with the ^{8}Be configuration 1S, $(001)^4$, are shown as a function of the deformation d. The size of the representation is given in the caption for figure 14.

Figure 17. The kinetic and potential energies of the ^{8}Be configuration 1S, $(001)^4$ are shown plotted against the deformation d of the representation states. The size of the representation is given in the caption for figure 14.

Figure 18. The binding energies of the ^{16}O configuration 1S, 1P, and the related three shell RHF solution are plotted against the deformation d. The GHA result is shown to the right.

The three shell RHF solution using the GHA oscillator parameters cannot be separated from the simpler GHA result on this scale. The four shell RHF solution at zero deformation cannot be separated from the three shell one. The representation size ($a^2b = 0.9186$) is chosen to minimize the energy of the simple configuration at zero deformation.

Figure 19. The deformation Q/R^2 of ^{16}O is shown, for the configuration 1S, 1P and for the related three shell RHF solution, as a function of the deformation d of the representation. It should be noted that, because of the way in which d is defined, the results for the dominant configuration lie on the straight line

$Q/R^2 = d$. The size of the representation is given in the caption for figure 18.

Figure 20. The kinetic and potential energies, of the ^{16}O configuration 1S, 1P, are plotted against the deformation d. The size of the representation states is given in the caption for figure 18.

Figure 21. The energies for the ^{24}Mg configuration 1S, 1P, $(002)^4$, $(011)^4$, and for the related three and four shell RHF solutions are shown as a function of the deformation d. Calculated points are marked with crosses. Only two points have been calculated with the four shell program, and the dashed curve connecting these is necessarily tentative. The constant volume ($a^2b = 1.0414$) is chosen to minimize the energy of the pure configuration at zero deformation. On the right are shown the energies of the cylindrical and cartesian GHA calculations, and of the three shell RHF calculation using the oscillator parameters obtained in the cylindrical GHA calculation.

Figure 22. The deformation parameter Q/R^2 for the ^{24}Mg configuration 1S, 1P, $(002)^4$, $(011)^4$, and for the related three shell RHF solution, is shown as a function of d. Also shown is the asymmetry parameter for the RHF solution. The very small variations in the asymmetry parameter cannot be detected on this scale. The size of the representation states is given in caption for figure 21.

Figure 23. The polar plot of $\cos^2 2\varphi$ gives the variation of the density of the single-particle state

$$\sqrt{\tfrac{1}{2}}[|020) + |0 - 20)]$$

about the z axis. The orthogonal state

$$\sqrt{\tfrac{1}{2}}[|020) - |0 - 20)]$$

has a density dependence which is similar to that shown, but is rotated thorugh 45°.

Figure 24. The single-particle levels for the various ^{8}Be solutions are shown; see chapter 6 and the note below.

Figure 25. As figure 24, for ^{12}C.

Figure 26. As figure 24, for ^{16}O.

Figure 27. As figure 24, for ^{20}Ne.

Figure 28. As figure 24, for ^{24}Mg.

Figure 29. As figure 24, for ^{28}Si.

Figure 30. As figure 24, for ^{32}S.

Figure 31. As figure 24, for ^{36}A.

Figure 32. As figure 24, for ^{40}Ca.

Figure 33. The experimental binding energies per nucleon (corrected for the Coulomb interaction), and those obtained with force 1 are plotted against $A^{-1/3}$. The dashed lines connect the doubly closed shell nuclei ^{4}He, ^{16}O and ^{40}Ca.

Figure 34. The experimental r.m.s. radii and those obtained with force 1 are shown plotted against $A^{1/3}$.

Figure 35. As figure 33, for force 2.

Figure 36. As figure 34, for force 2.

Figure 37. The experimental binding energies per nucleon (corrected for the Coulomb interaction), and those obtained in GHA calculations with force 3 are plotted against $A^{-1/3}$. The two density approximations are marked, and they represent upper and lower bounds for the individual nuclei.

Figure 38. The experimental r.m.s. radii and those obtained in GHA calculations with force 3 are plotted against $A^{1/3}$. The two density approximations are marked, and they represent upper and lower bounds for the individual nuclei.

Figure 39. As figure 37, for force 4.

Figure 40. As figure 38, for force 4.

NOTE: In figures 24 to 32 the degeneracy of a level is indicated by a number in parentheses immediately on the right; if no number appears the degeneracy is fourfold. All levels are symmetrically occupied by neutrons and protons. The levels for GHA solutions are marked with the corresponding cylindrical or cartesial orbital in the notation used throughout the text. The dotted lines connecting various levels are present to facilitate comparison between related spectra. They do not necessarily imply any specific relation between the different single-particle states, though in fact some correspondence often exists. The single-particle states, used in the GHA calculation, (i.e. the

representation states) are split by the spin-orbit force. This splitting breaks the (n m n_z) orbital into two doubly degenerate levels 2m MeV apart. In order to simplify some of the GHA spectra, this splitting is not always shown.

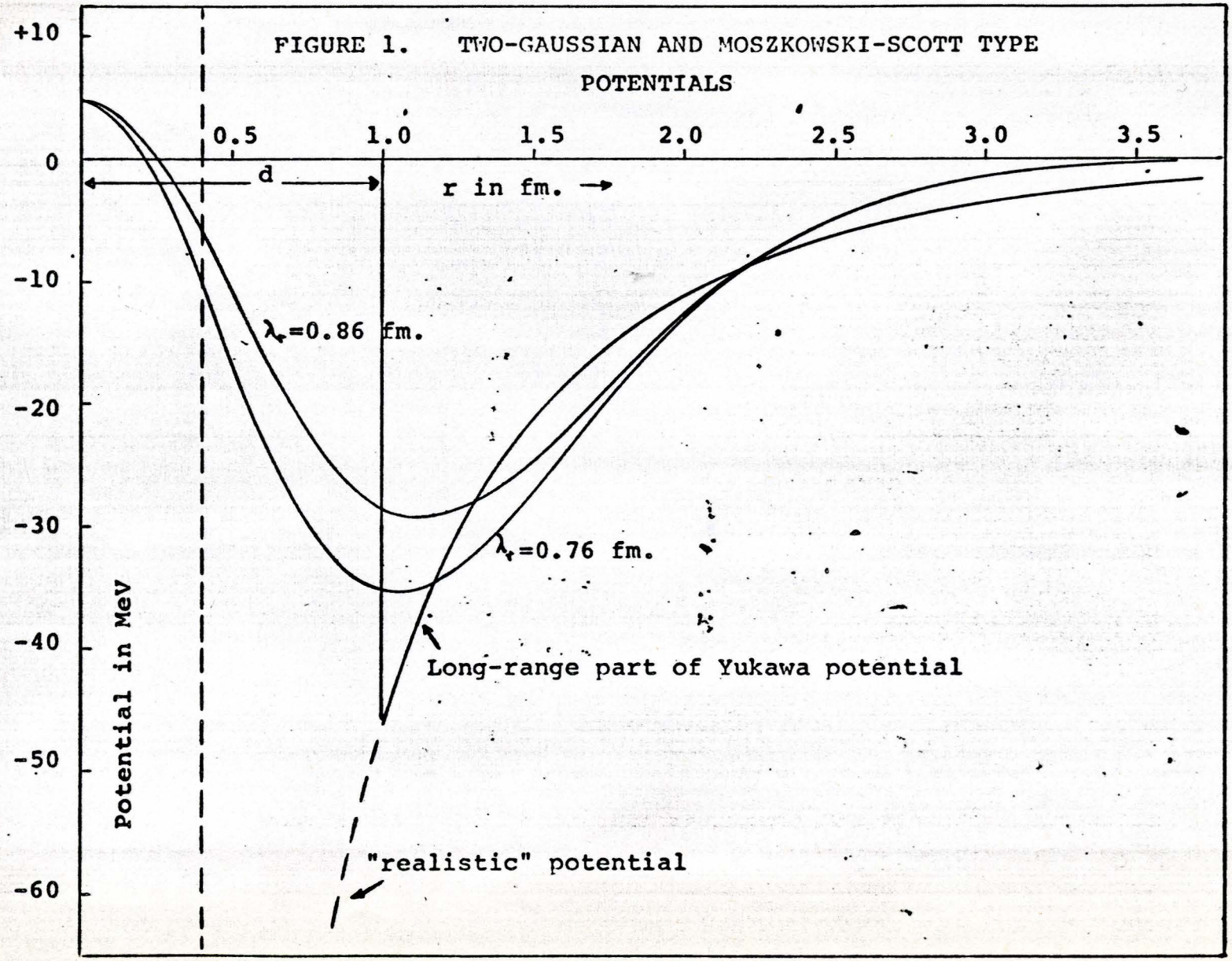
FIGURE 1. TWO-GAUSSIAN AND MOSZKOWSKI-SCOTT TYPE POTENTIALS
+10
0
-10
-20
-30
-40
-50
-60
0.5
1.0
1.5
2.0
2.5
3.0
3.5
d
r in fm. →
λ=0.86 fm.
λ=0.76 fm.
Long-range part of Yukawa potential
"realistic" potential
Potential in MeV

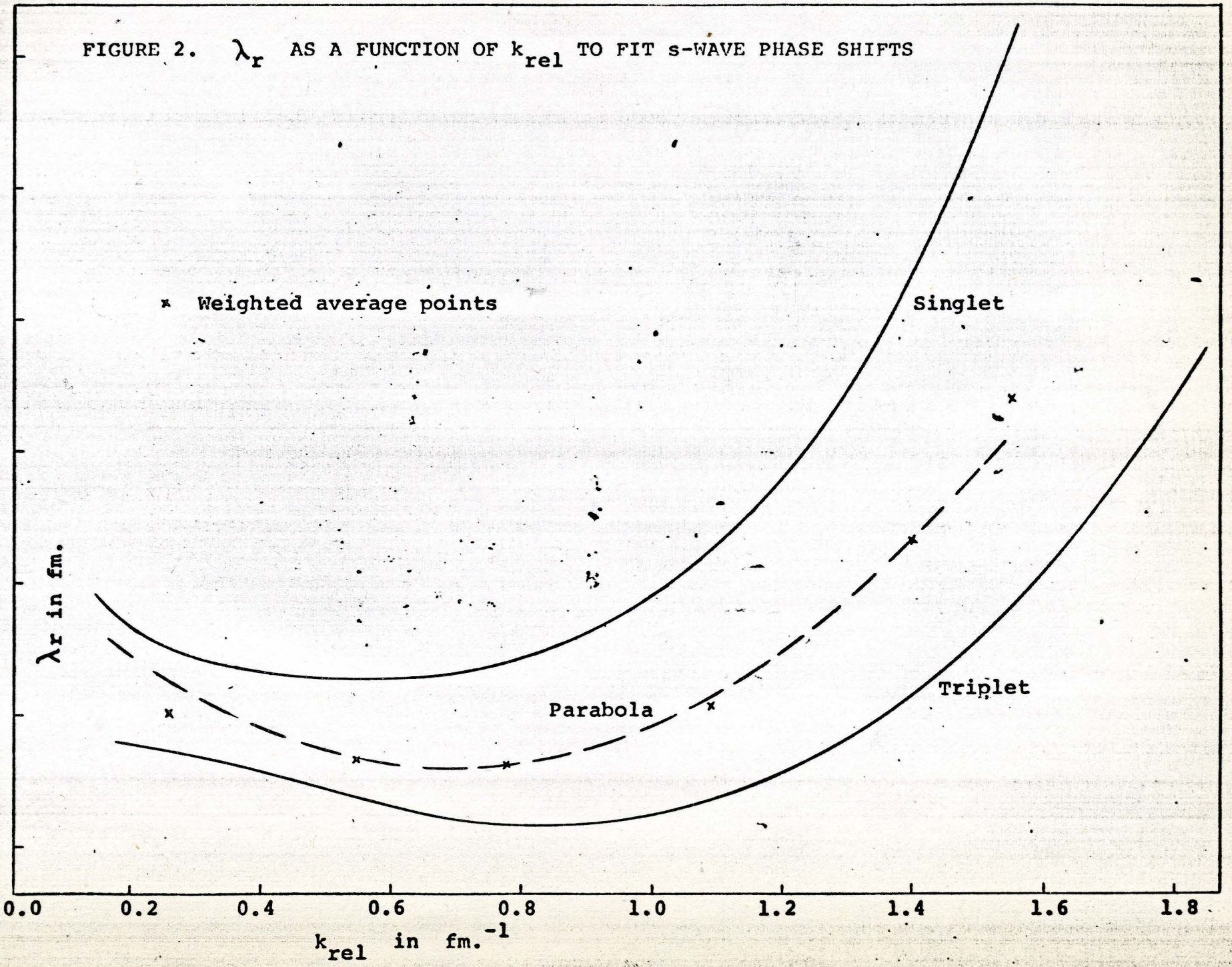
FIGURE 2. λ_r AS A FUNCTION OF k_{rel} TO FIT s-WAVE PHASE SHIFTS
Weighted average points
Singlet
Triplet
Parabola
λ_r in fm.
k_{rel} in fm.$^{-1}$
1.2
1.1
1.0
0.9
0.8
0.7
0.0
0.2
0.4
0.6
0.8
1.0
1.2
1.4
1.6
1.8

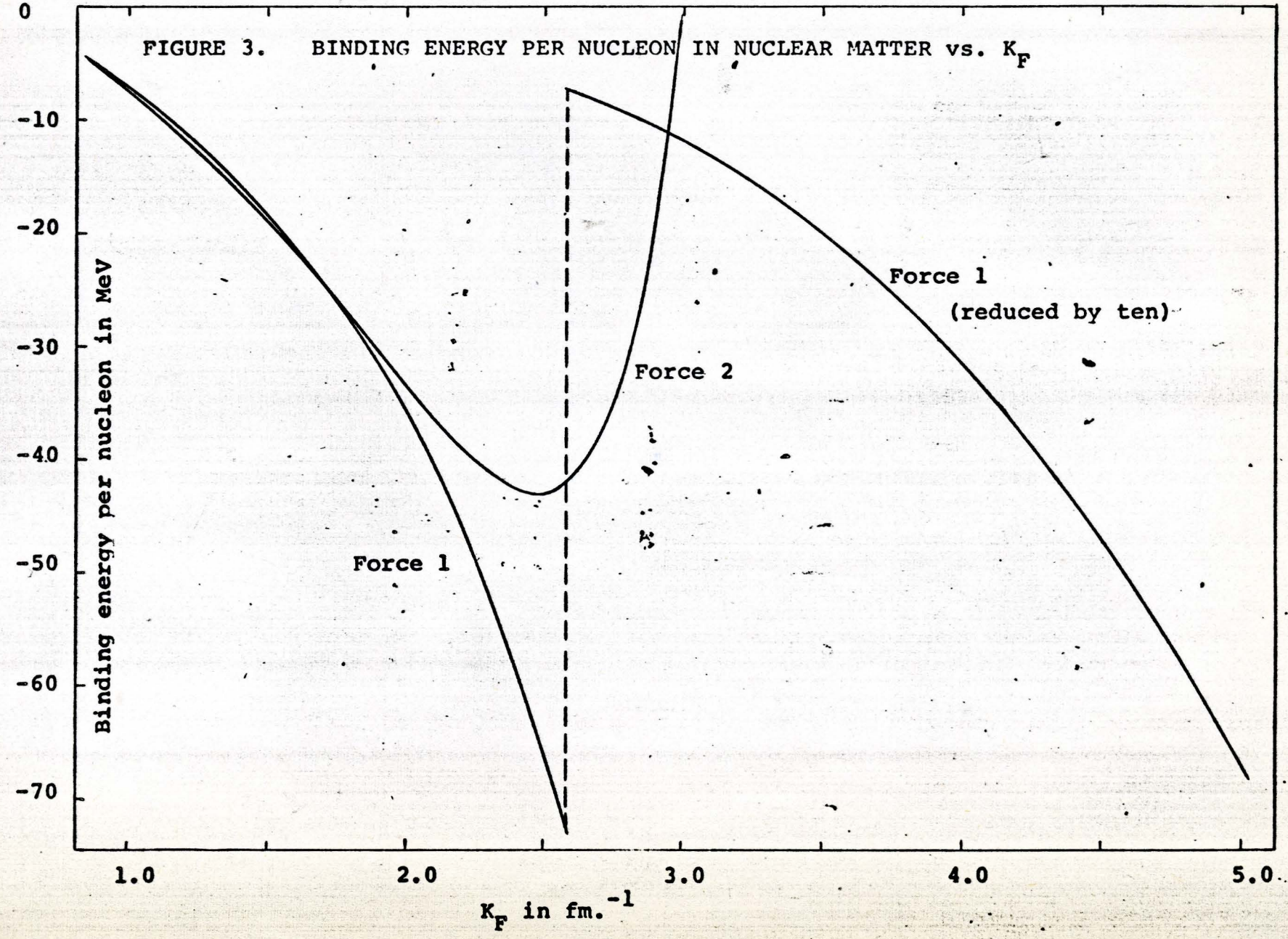
FIGURE 3. BINDING ENERGY PER NUCLEON IN NUCLEAR MATTER vs. K_F
0
-10
-20
-30
-40
-50
-60
-70
Binding energy per nucleon in MeV
Force 1
(reduced by ten)
Force 2
Force 1
1.0
2.0
3.0
4.0
5.0
K_F in fm.$^{-1}$

FIGURE 4. TYPICAL MATRIX ELEMENT OF VELOCITY DEPENDENT POTENTIAL, BY KALLIO AND OTHER TECHNIQUES.

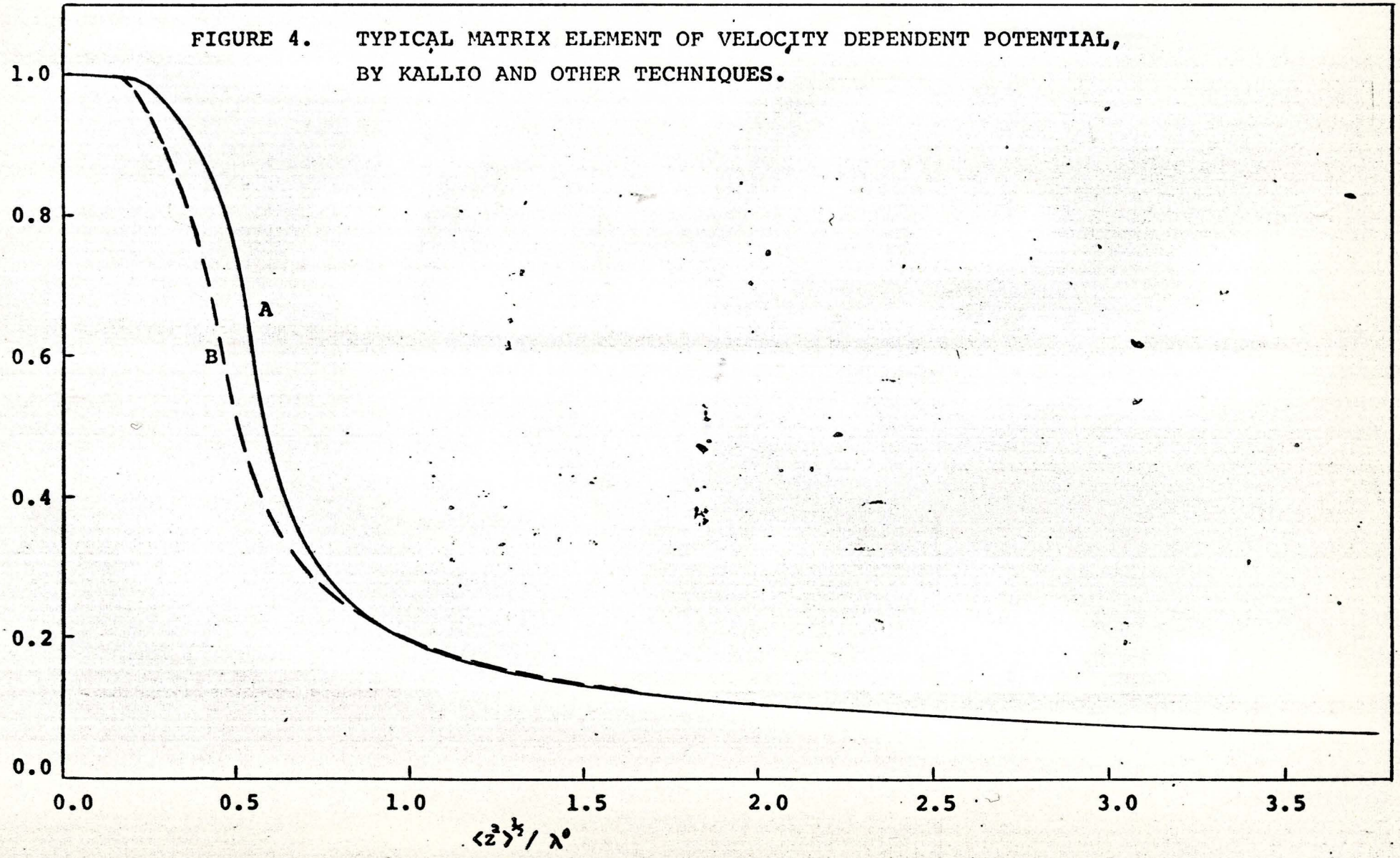

FIGURE 5. TRUE AND APPROXIMATE DENSITIES IN O^{16}

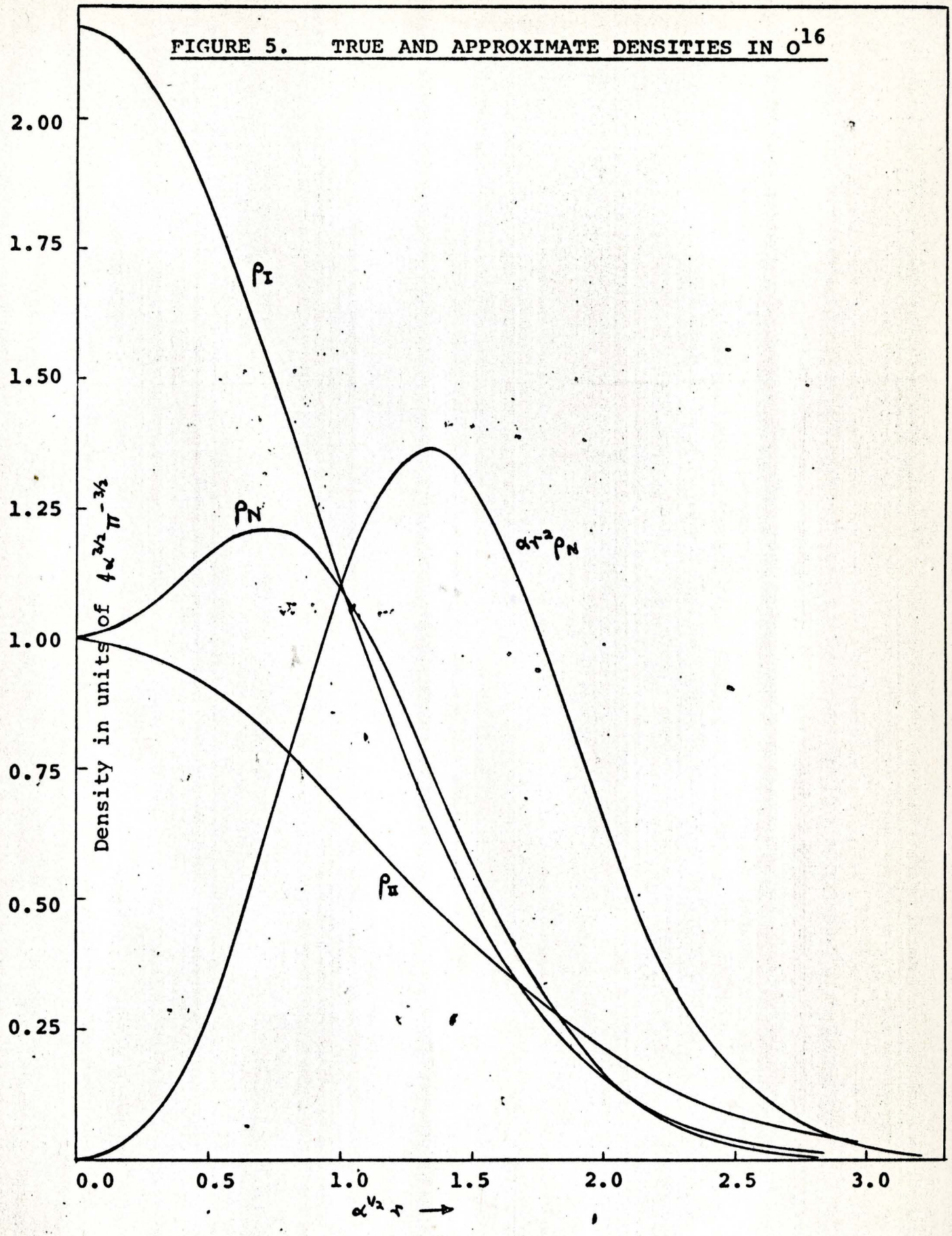

FIGURE 6. CONVERGENCE OF THREE SHELL RHF FOR O^{16} GROUND STATE

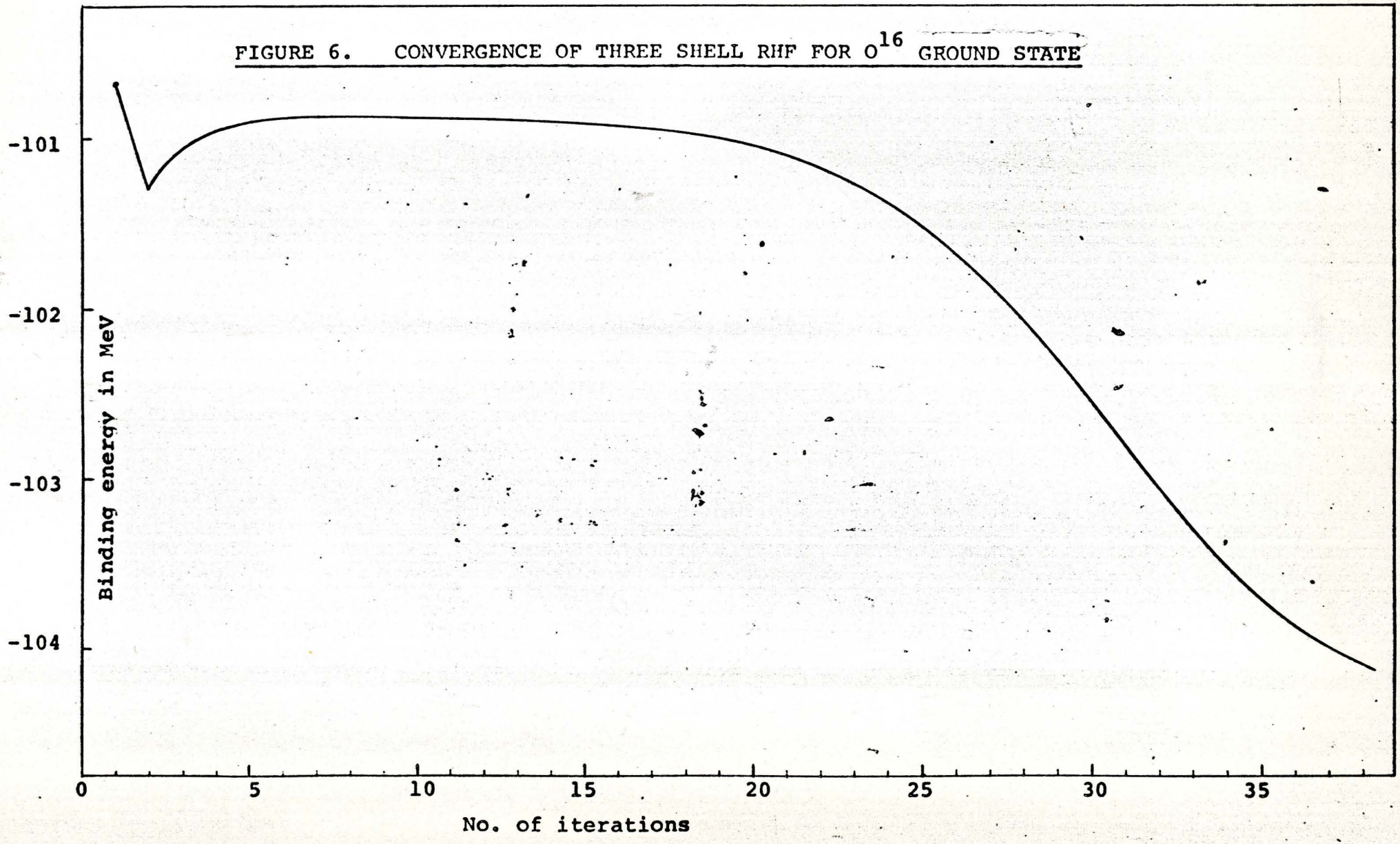

FIGURE 7. CONVERGENCE OF THREE SHELL RHF FOR O^{16} GROUND STATE

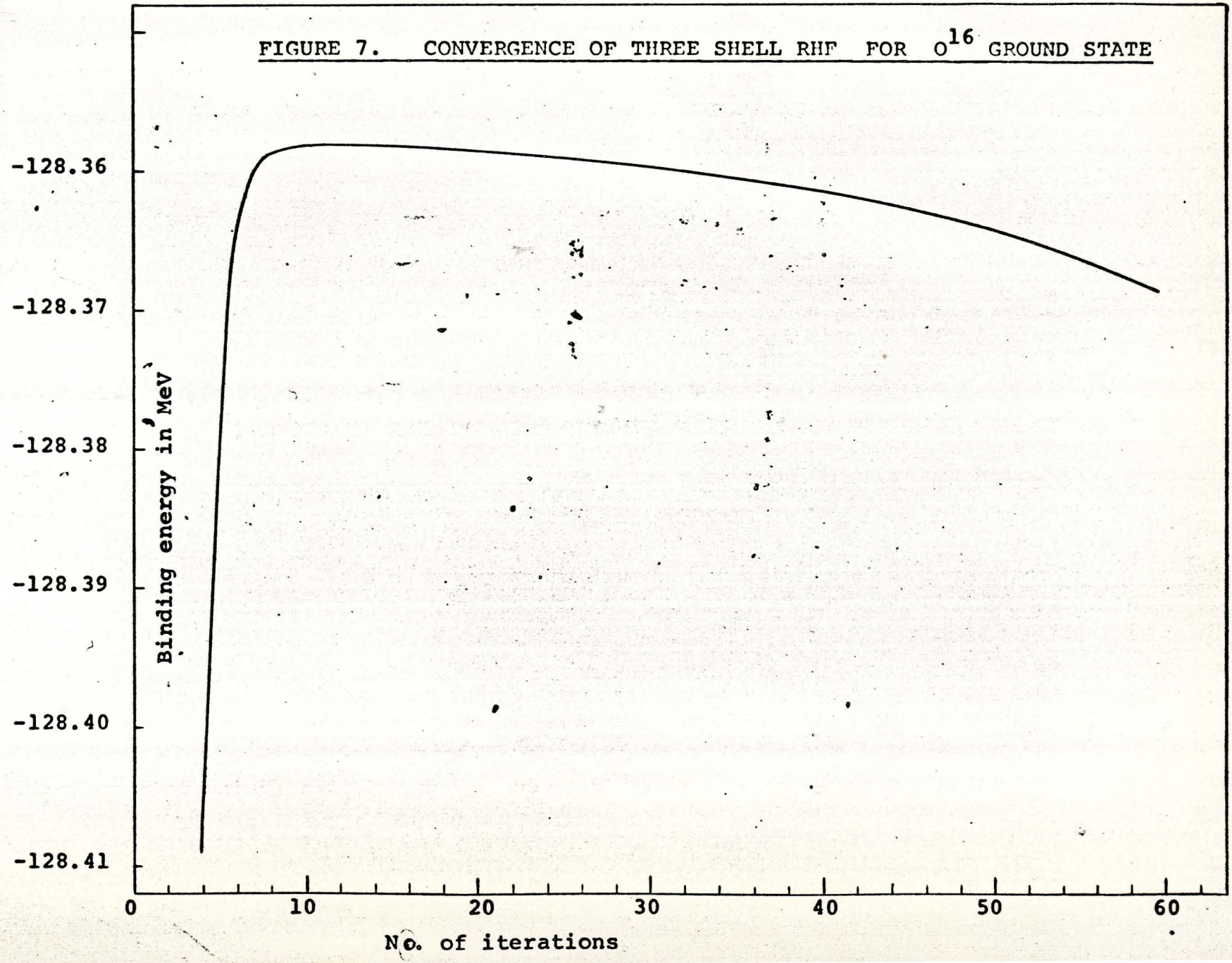

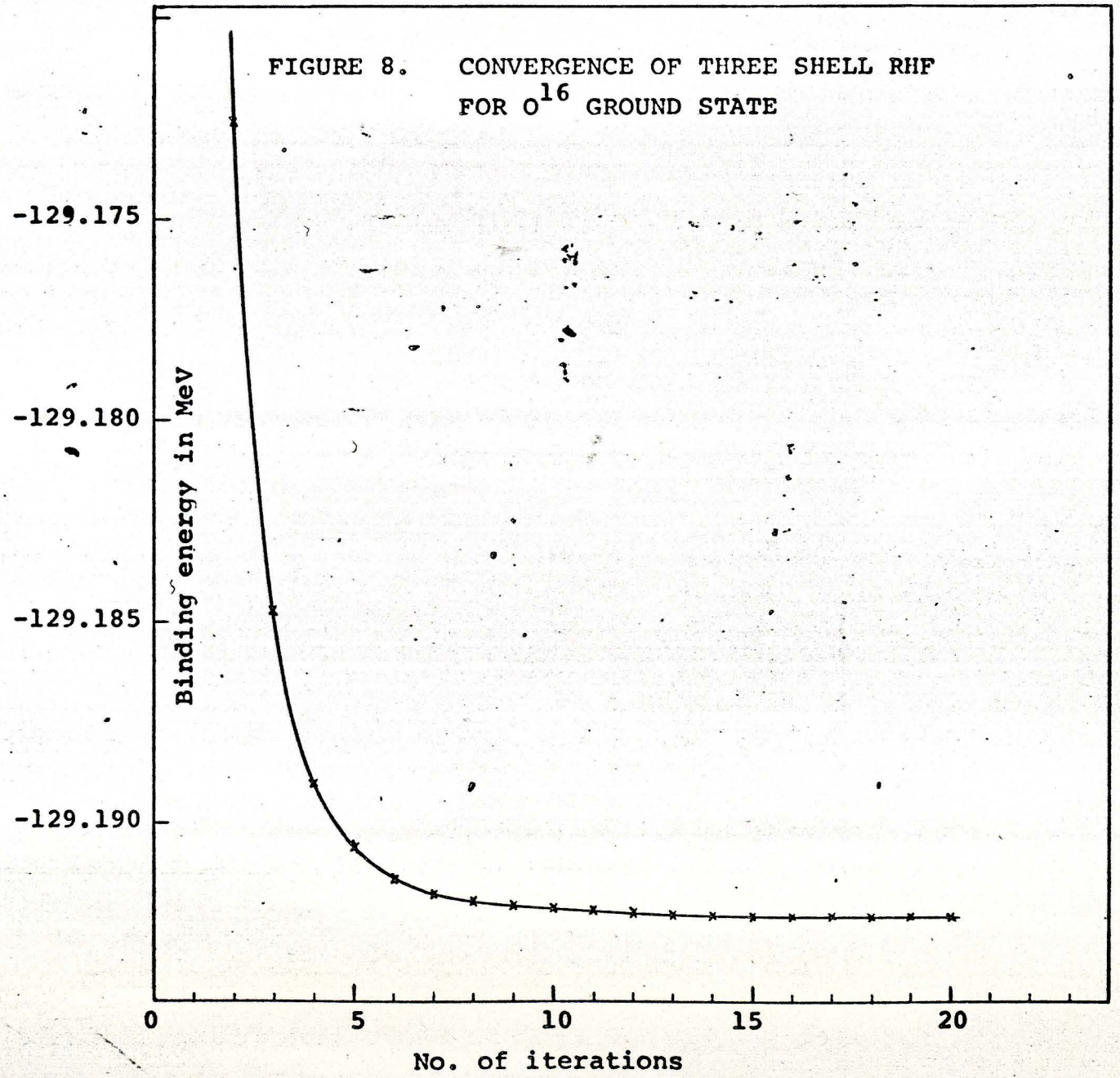

FIGURE 8. CONVERGENCE OF THREE SHELL RHF FOR O^{16} GROUND STATE

FIGURE 9. CONVERGENCE OF THREE SHELL RIIF FOR Mg^{24} GROUND STATE

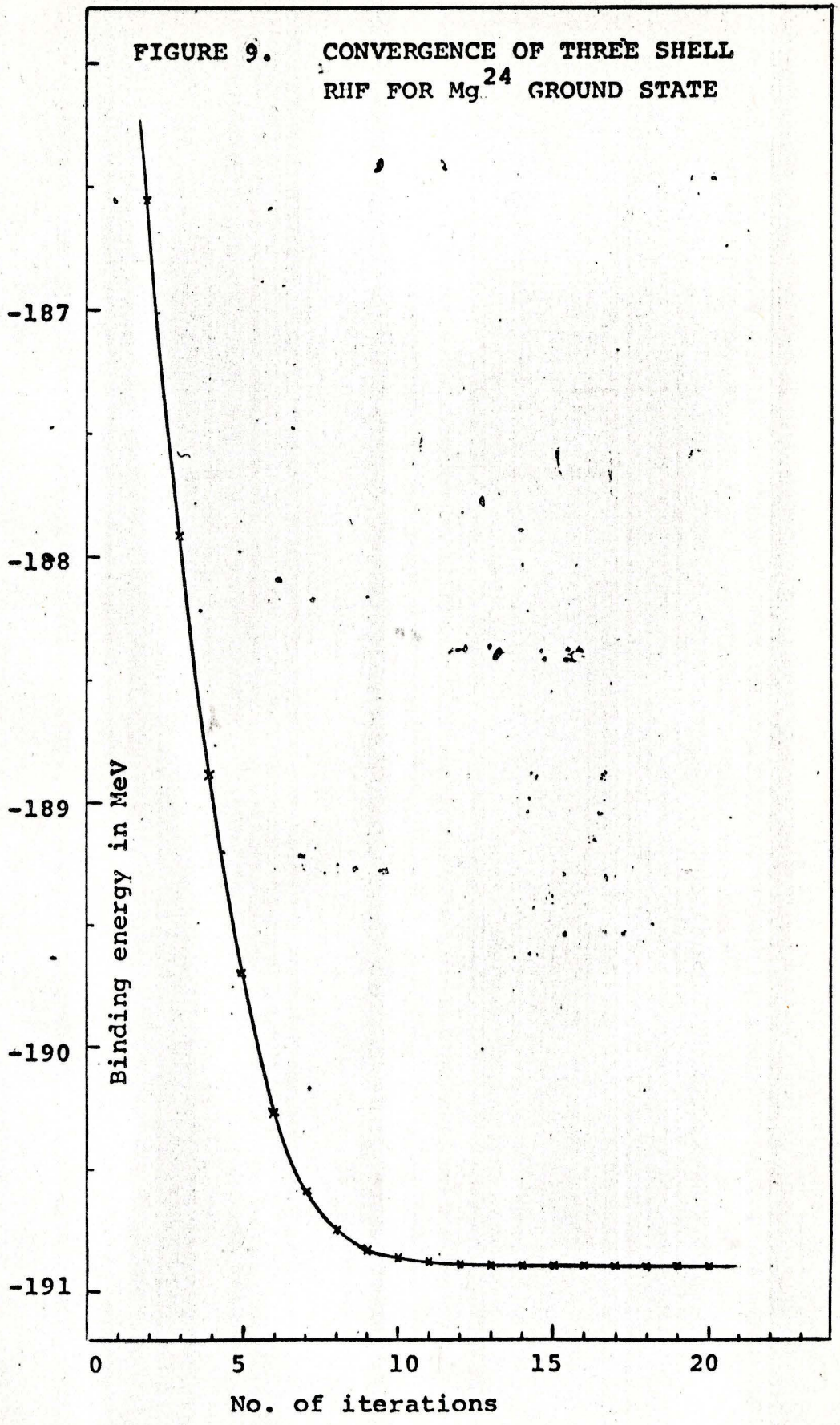

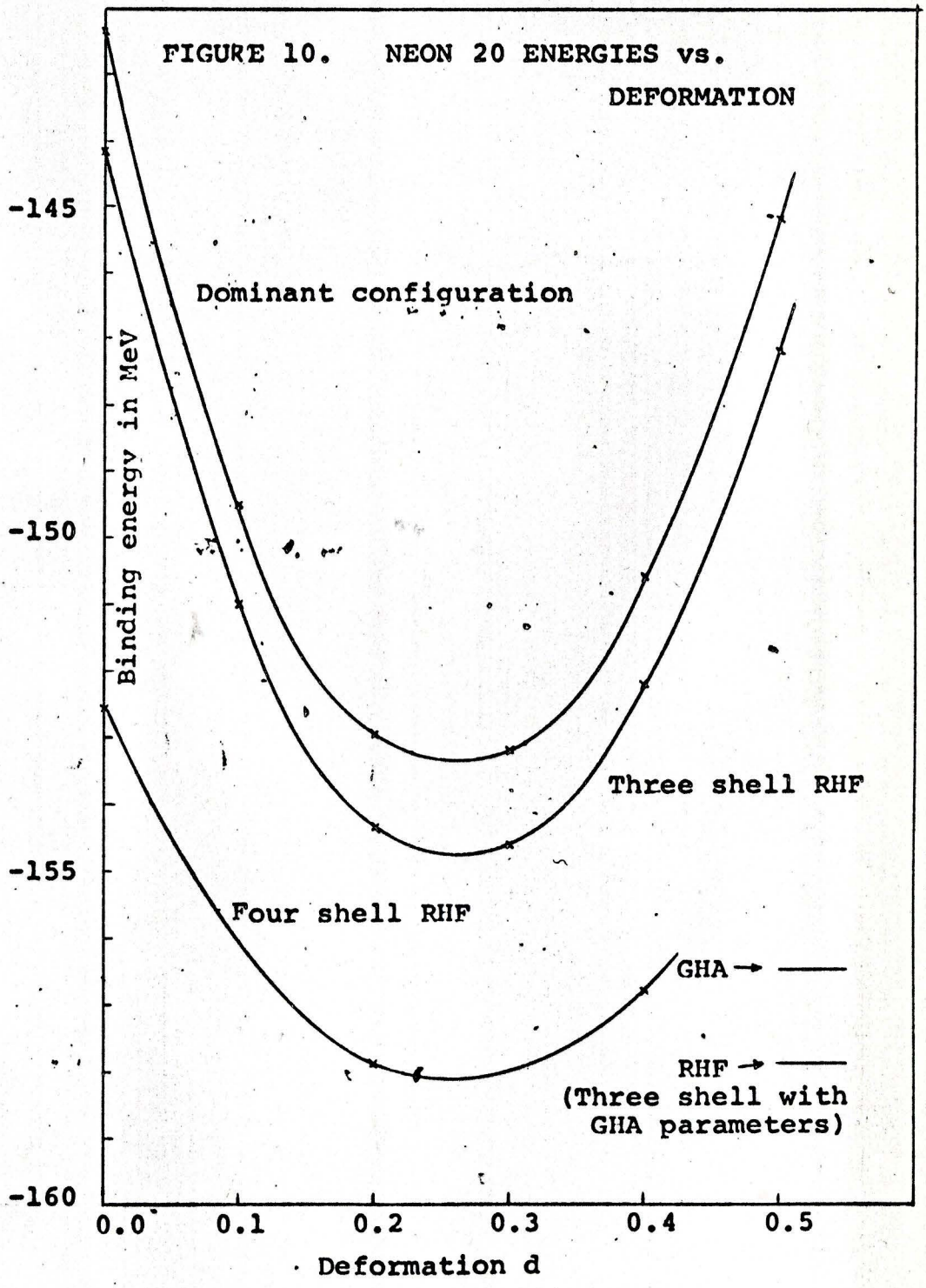
FIGURE 10. NEON 20 ENERGIES vs. DEFORMATION
-145
-150
-155
-160
Binding energy in MeV
Dominant configuration
Three shell RHF
Four shell RHF
GHA →
RHF →
(Three shell with GHA parameters)
0.0
0.1
0.2
0.3
0.4
0.5
Deformation d

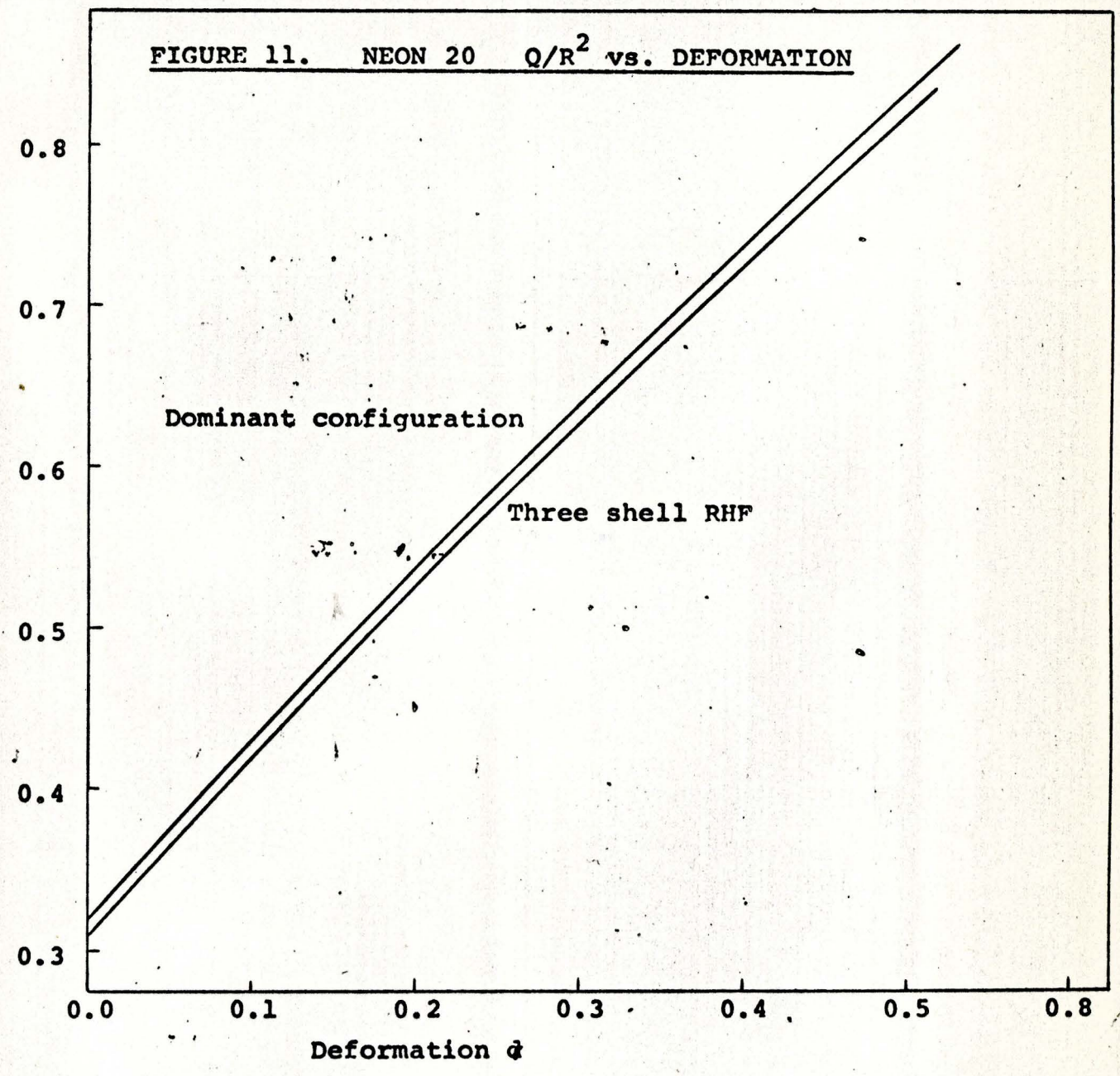
FIGURE 11. NEON 20 Q/R^2 vs. DEFORMATION
0.8
0.7
0.6
0.5
0.4
0.3
Dominant configuration
Three shell RHF
0.0
0.1
0.2
0.3
0.4
0.5
0.8
Deformation d

FIGURE 12. NEON 20 MIXING PARAMETERS vs. DEFORMATION

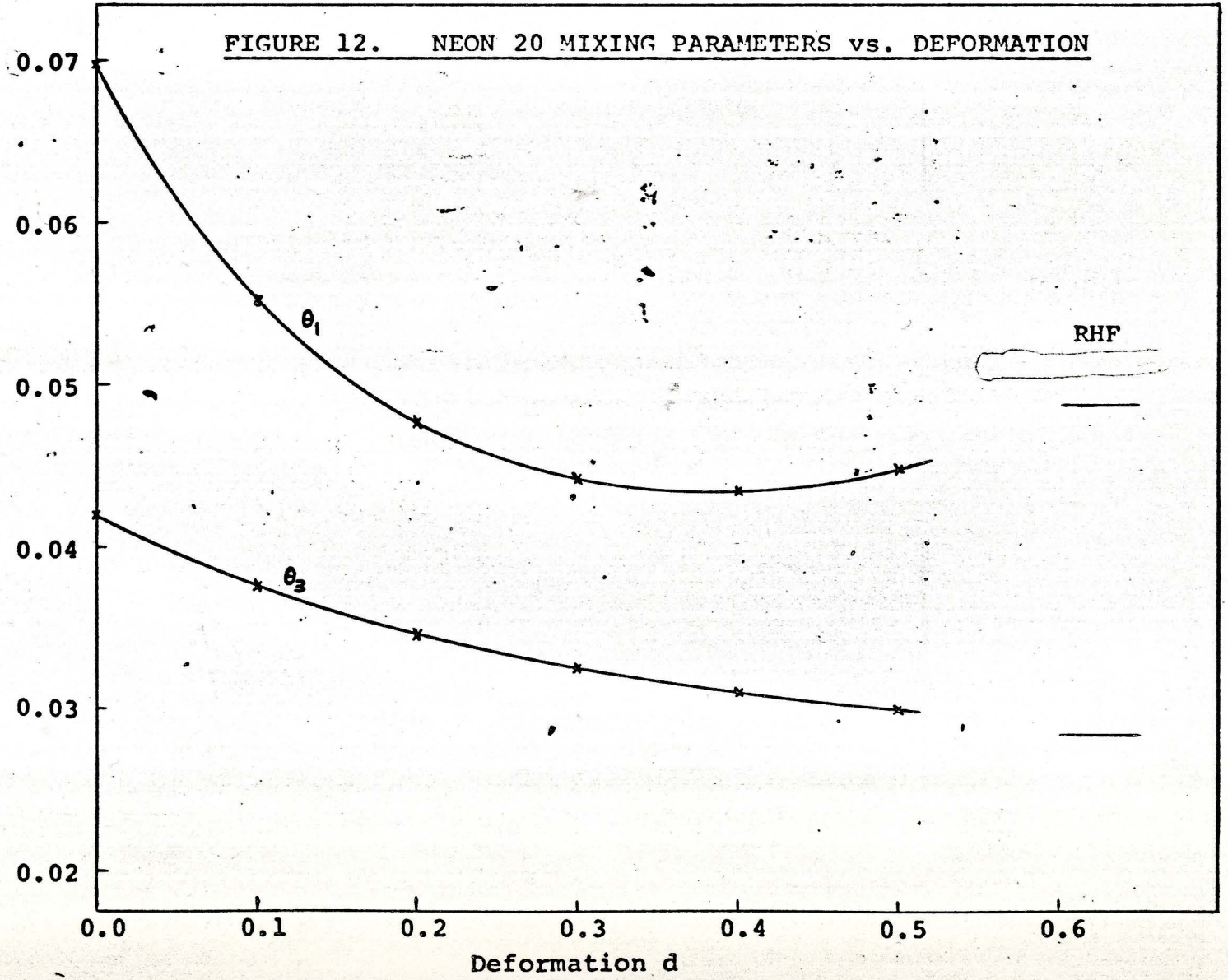

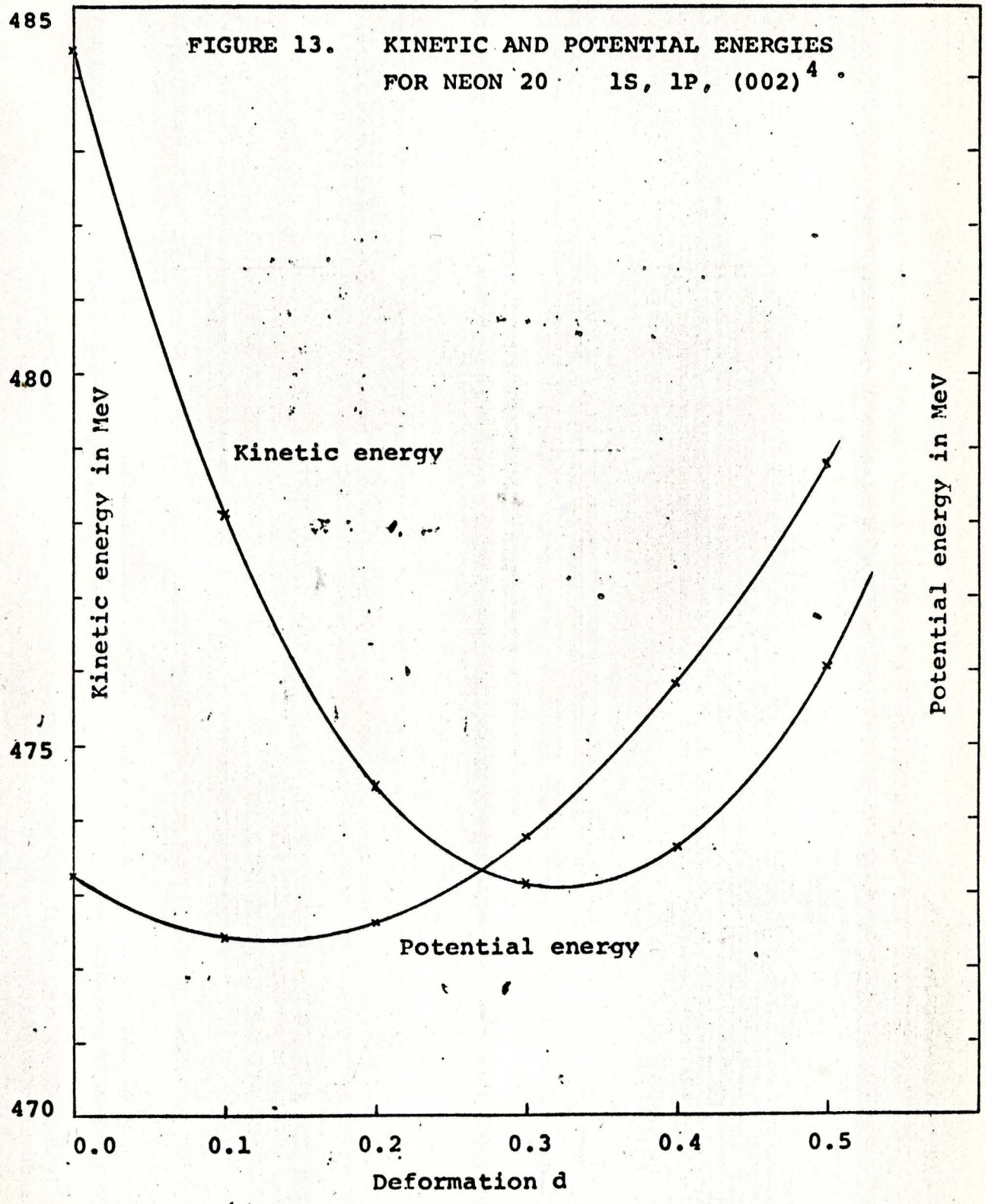

FIGURE 13. KINETIC AND POTENTIAL ENERGIES FOR NEON 20 1S, 1P, $(002)^4$.

FIGURE 14. BERYLLIUM 8 ENERGY vs. DEFORMATION

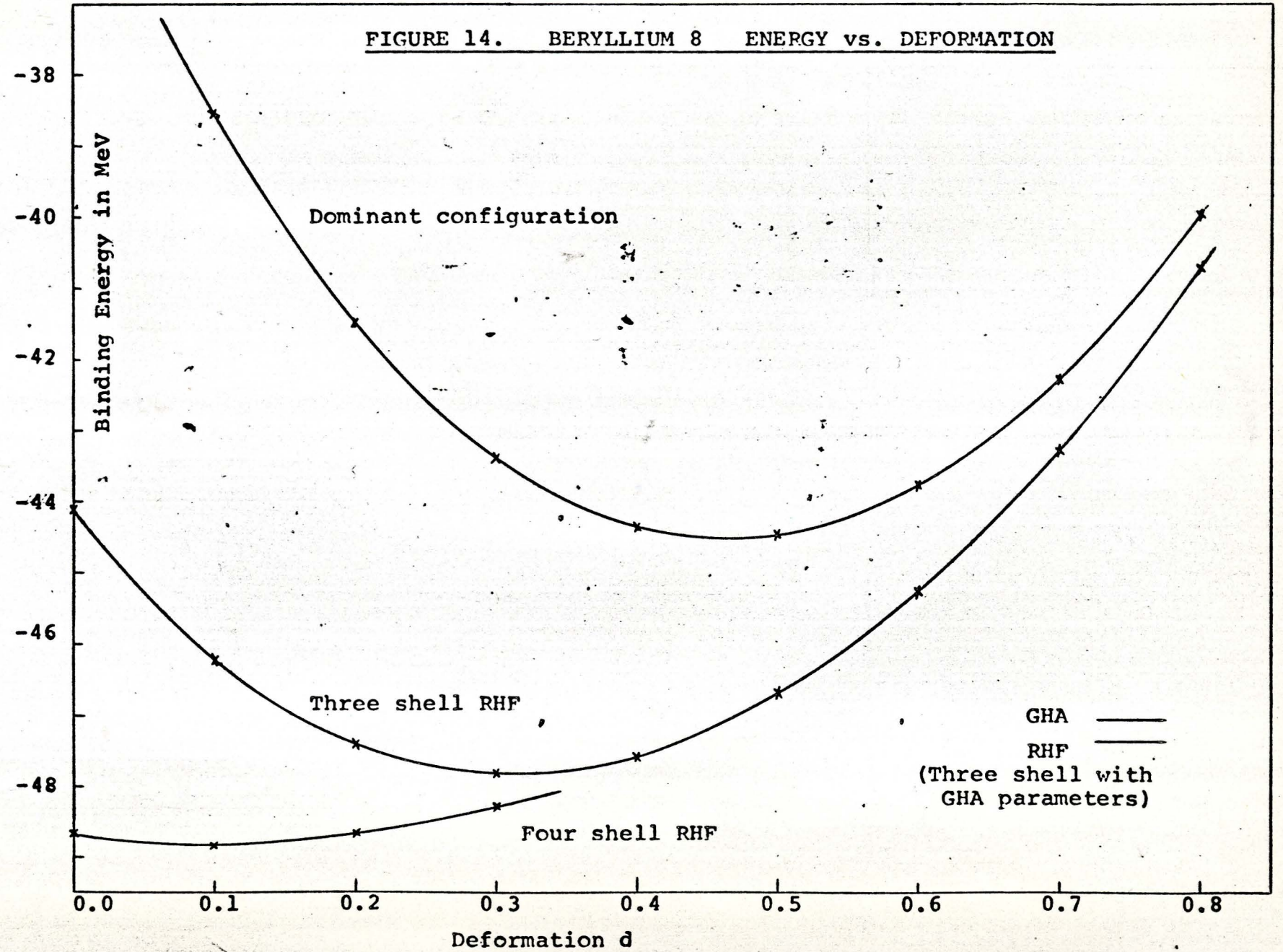

FIGURE 15. BERYLLIUM 8 Q/R^2 vs. DEFORMATION

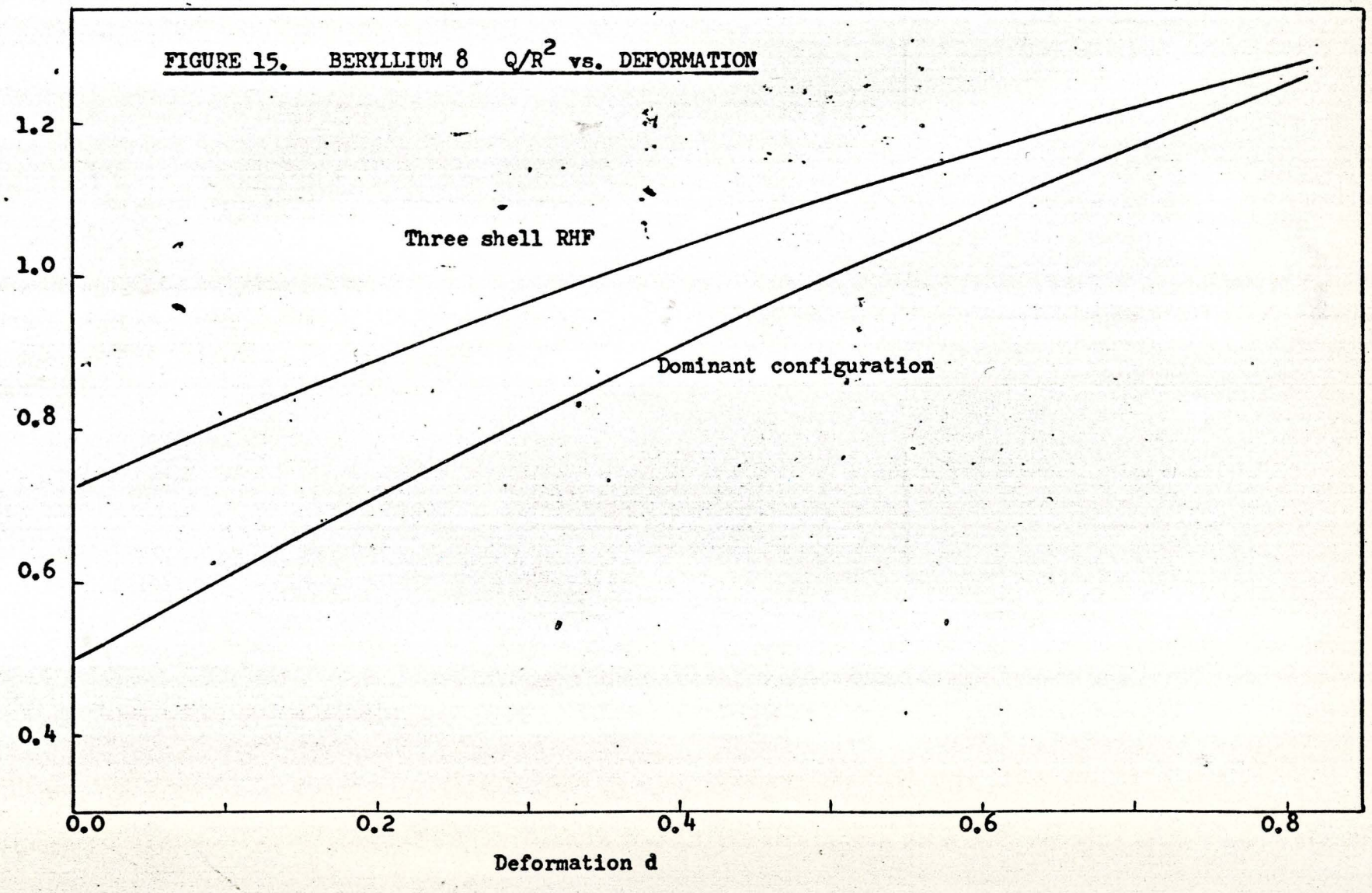

FIGURE 16. BERYLLIUM 8 MIXING PARAMETERS vs. DEFORMATION

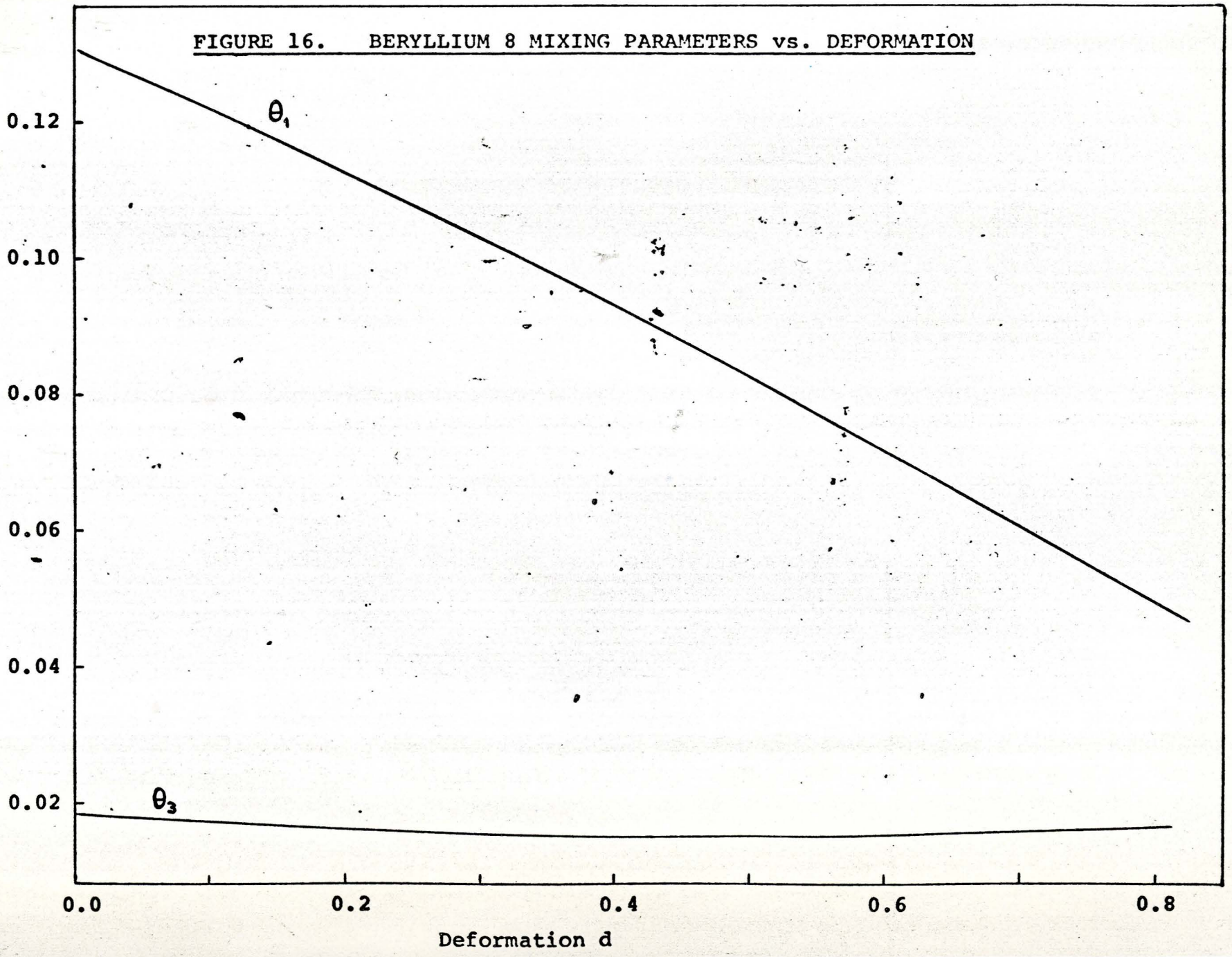

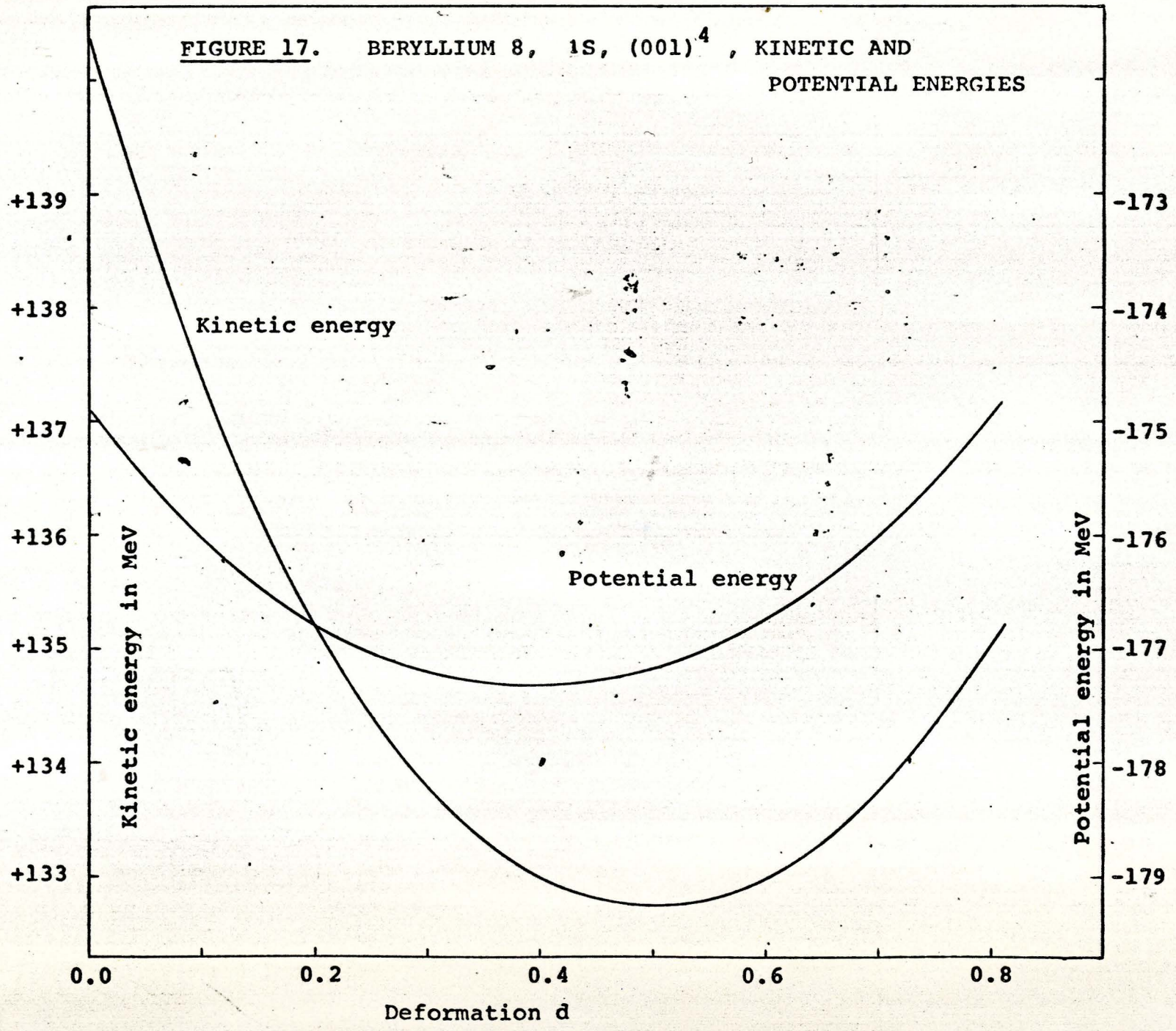
FIGURE 17. BERYLLIUM 8, 1S, (001)^4, KINETIC AND POTENTIAL ENERGIES
Kinetic energy
Potential energy
+139
+138
+137
+136
+135
+134
+133
-173
-174
-175
-176
-177
-178
-179
Kinetic energy in MeV
Potential energy in MeV
0.0
0.2
0.4
0.6
0.8
Deformation d

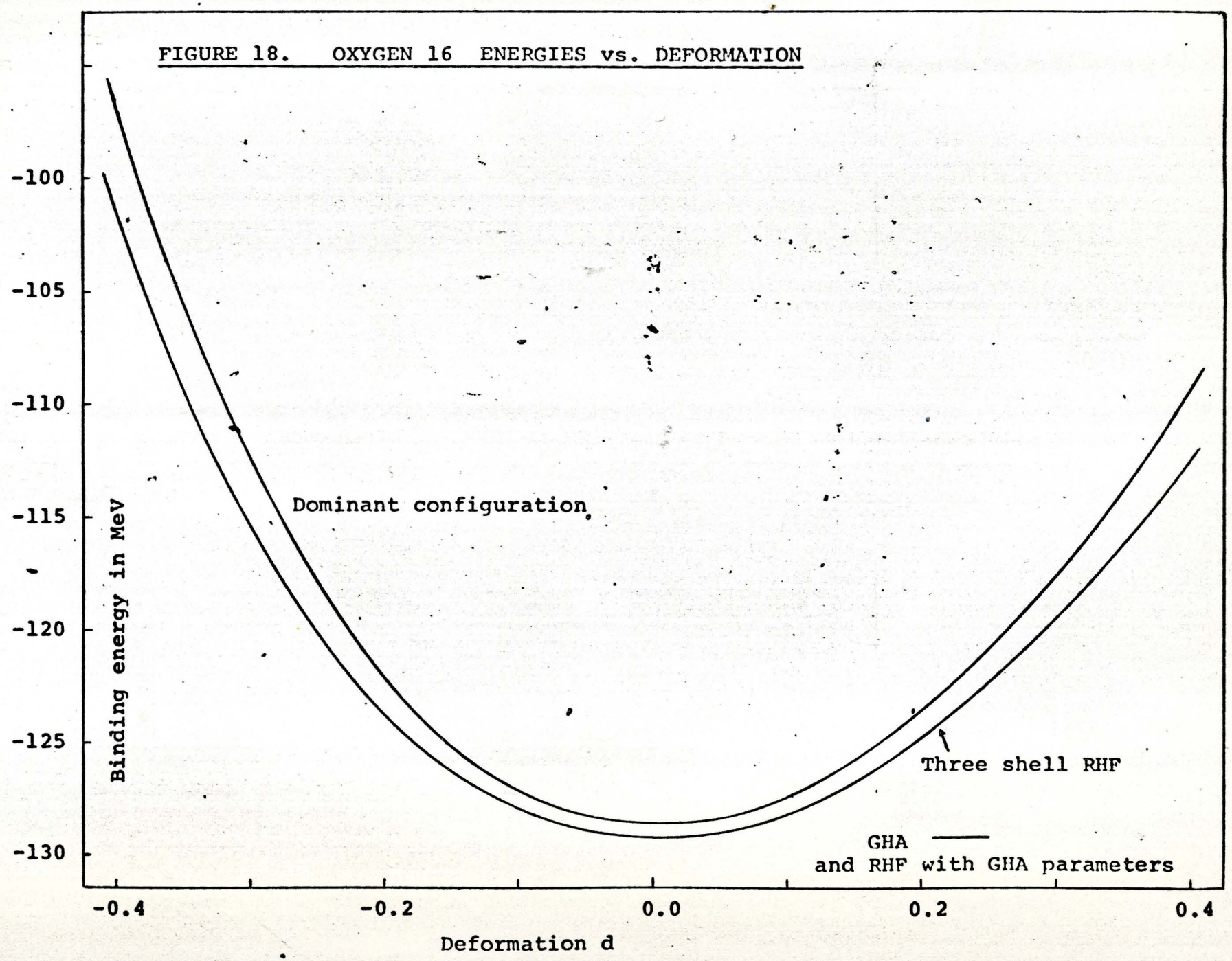
FIGURE 18. OXYGEN 16 ENERGIES vs. DEFORMATION
-100
-105
-110
-115
-120
-125
-130
Binding energy in MeV
Dominant configuration
Three shell RHF
GHA
and RHF with GHA parameters
-0.4
-0.2
0.0
0.2
0.4
Deformation d

FIGURE 19. OXYGEN 16 Q/R^2 vs. DEFORMATION

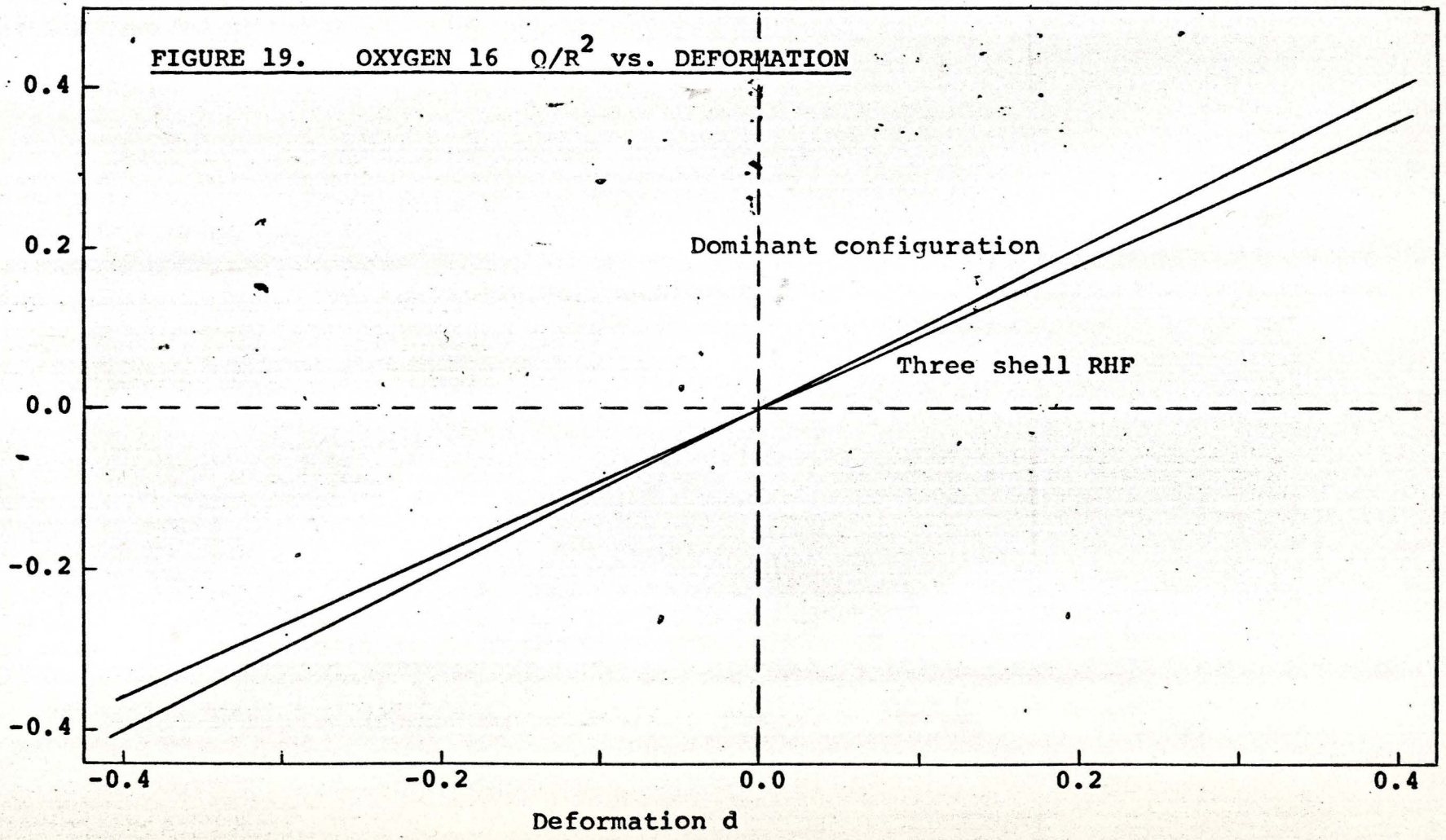

FIGURE 20. OXYGEN 16 (1S, 1P,) KINETIC AND POTENTIAL ENERGIES

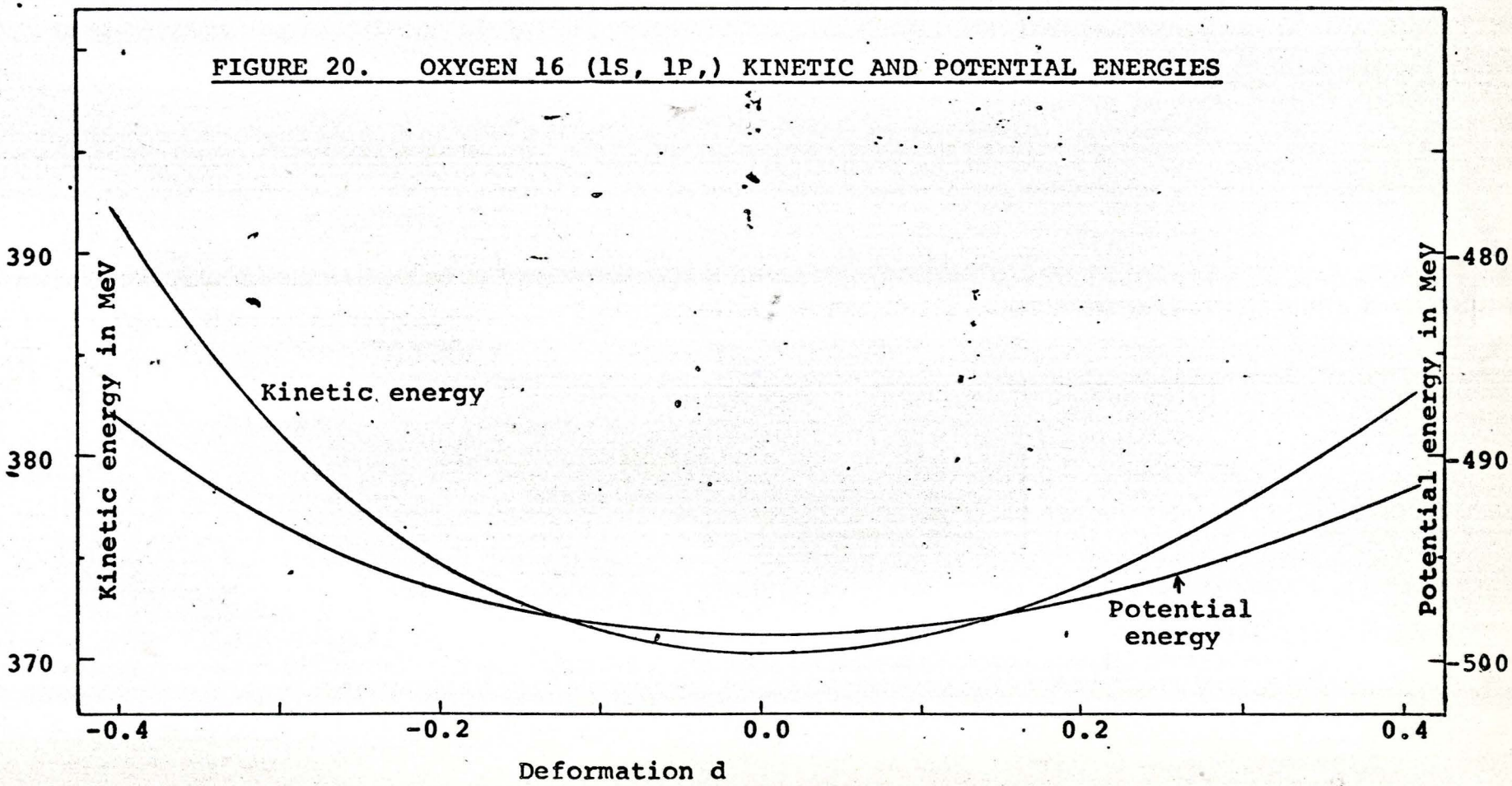

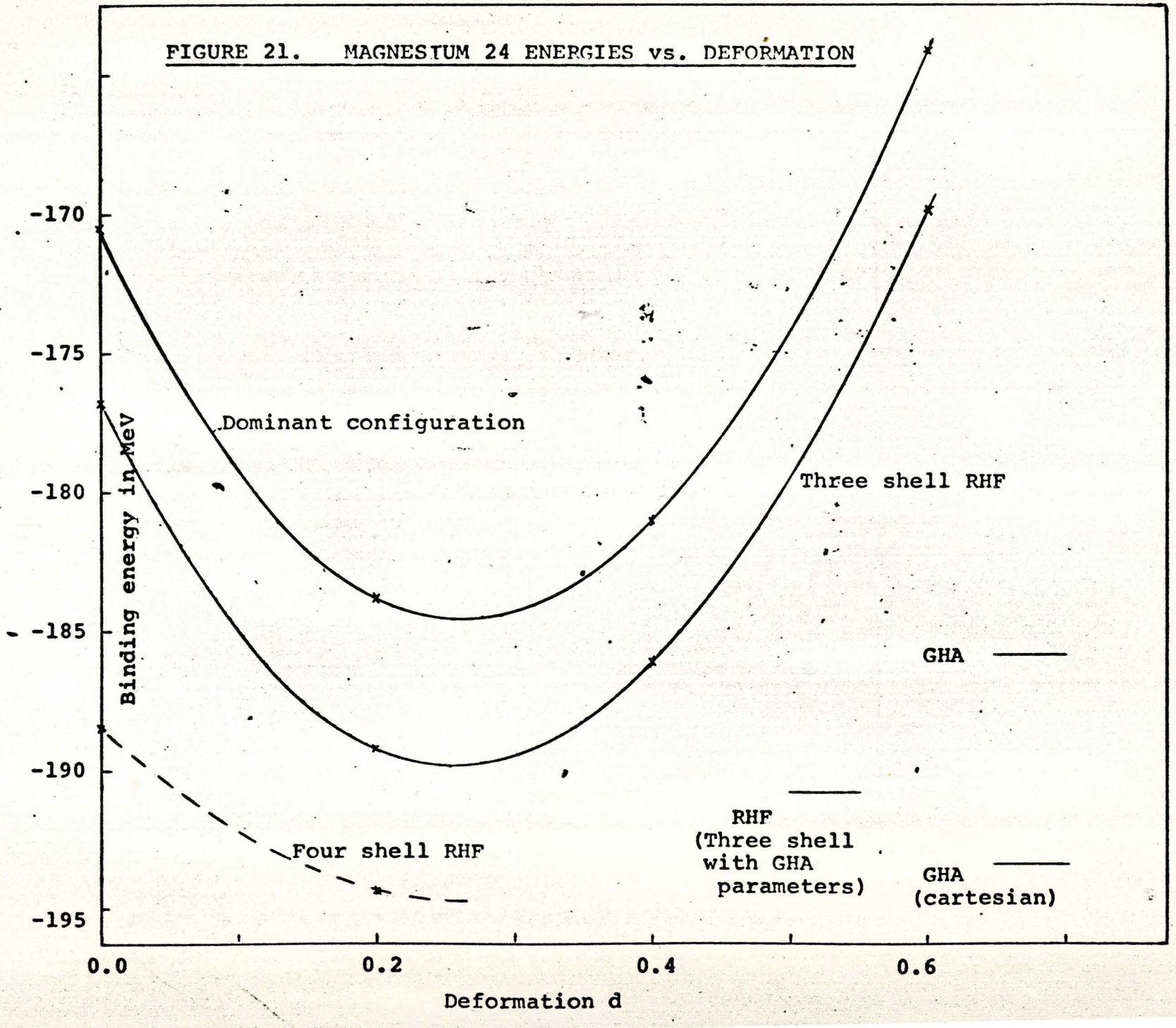
FIGURE 21. MAGNESIUM 24 ENERGIES vs. DEFORMATION
-170
-175
-180
-185
-190
-195
Binding energy in MeV
Dominant configuration
Three shell RHF
GHA
Four shell RHF
RHF
(Three shell
with GHA
parameters)
GHA
(cartesian)
0.0
0.2
0.4
0.6
Deformation d

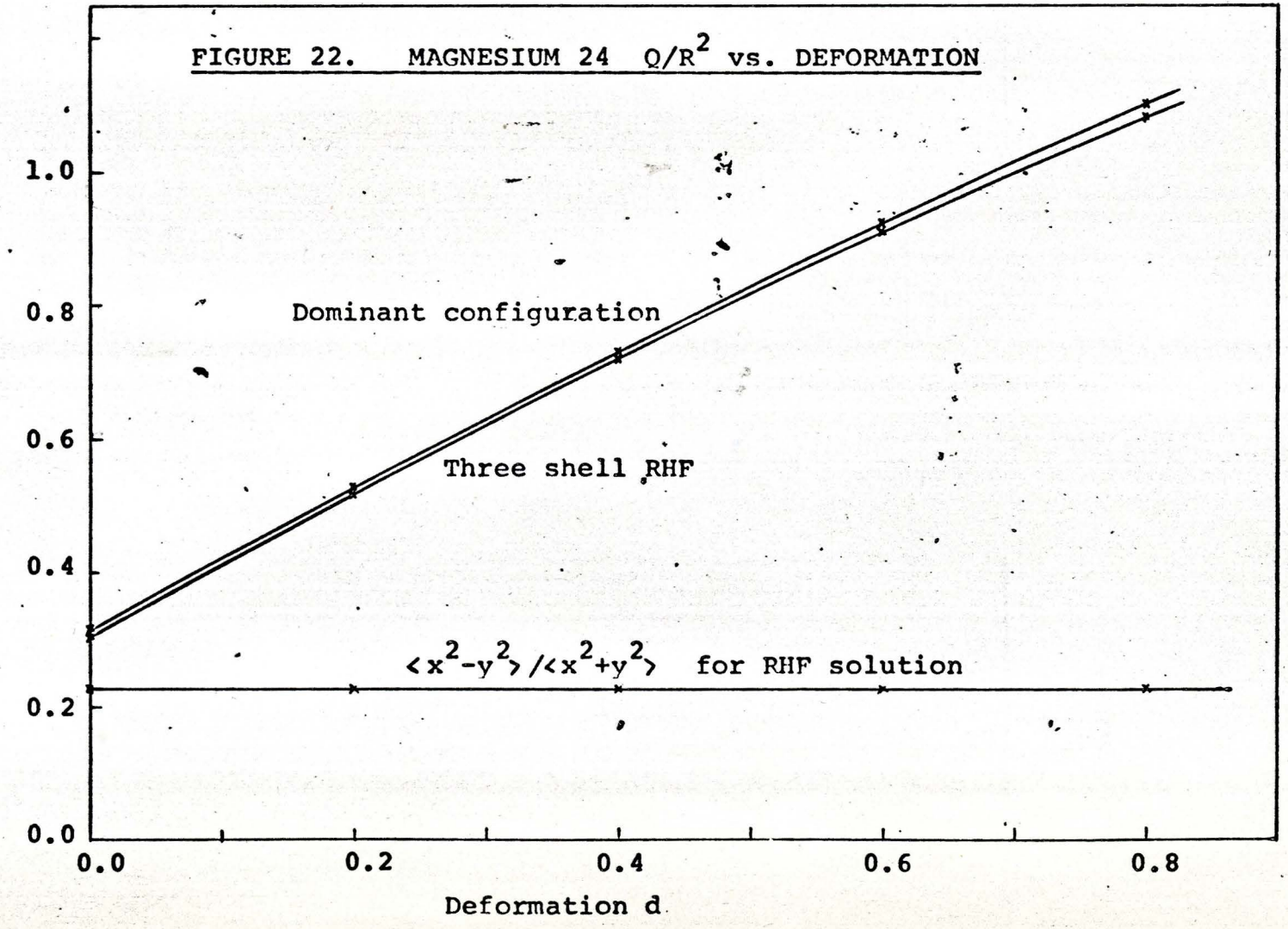
FIGURE 22. MAGNESIUM 24 Q/R^2 vs. DEFORMATION
1.0
0.8
0.6
0.4
0.2
0.0
Dominant configuration
Three shell RHF
$\langle x^2-y^2\rangle / \langle x^2+y^2\rangle$ for RHF solution
0.0
0.2
0.4
0.6
0.8
Deformation d

FIGURE 23. $\cos^2 2\varphi$

POLAR PLOT

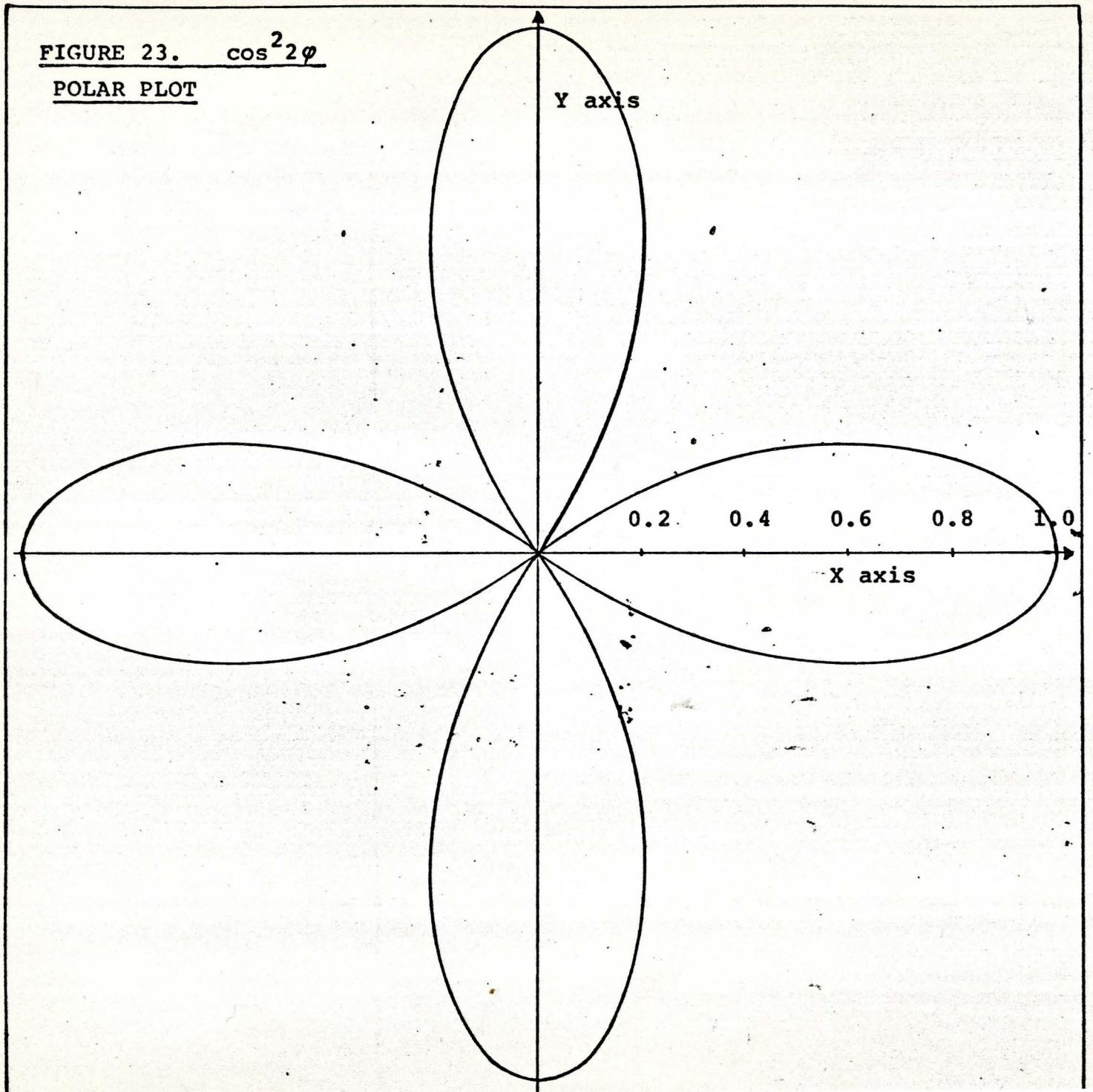

FIGURE 24. BERYLLIUM 8 SINGLE PARTICLE LEVELS

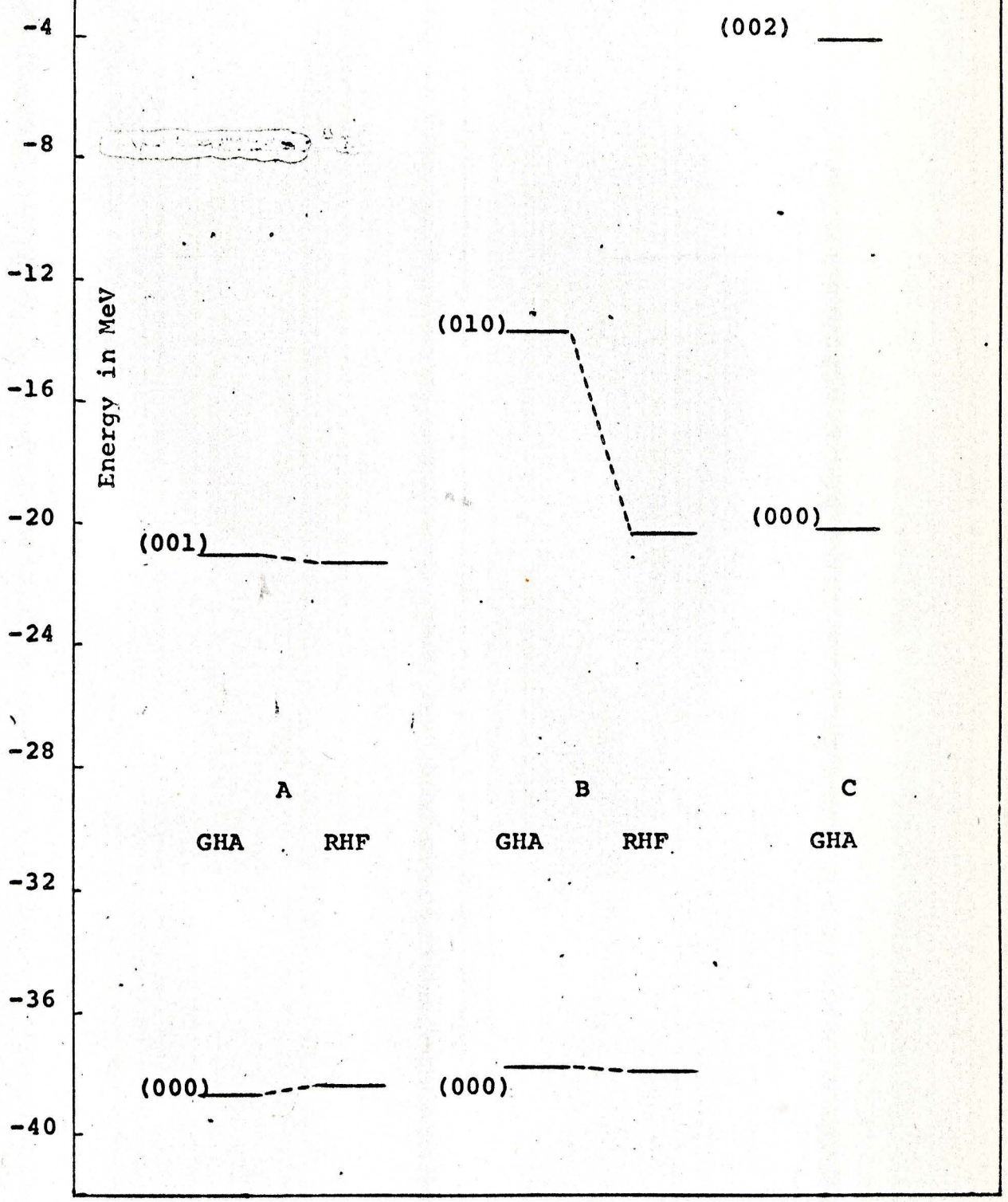

FIGURE 25. CARBON 12 SINGLE PARTICLE LEVELS

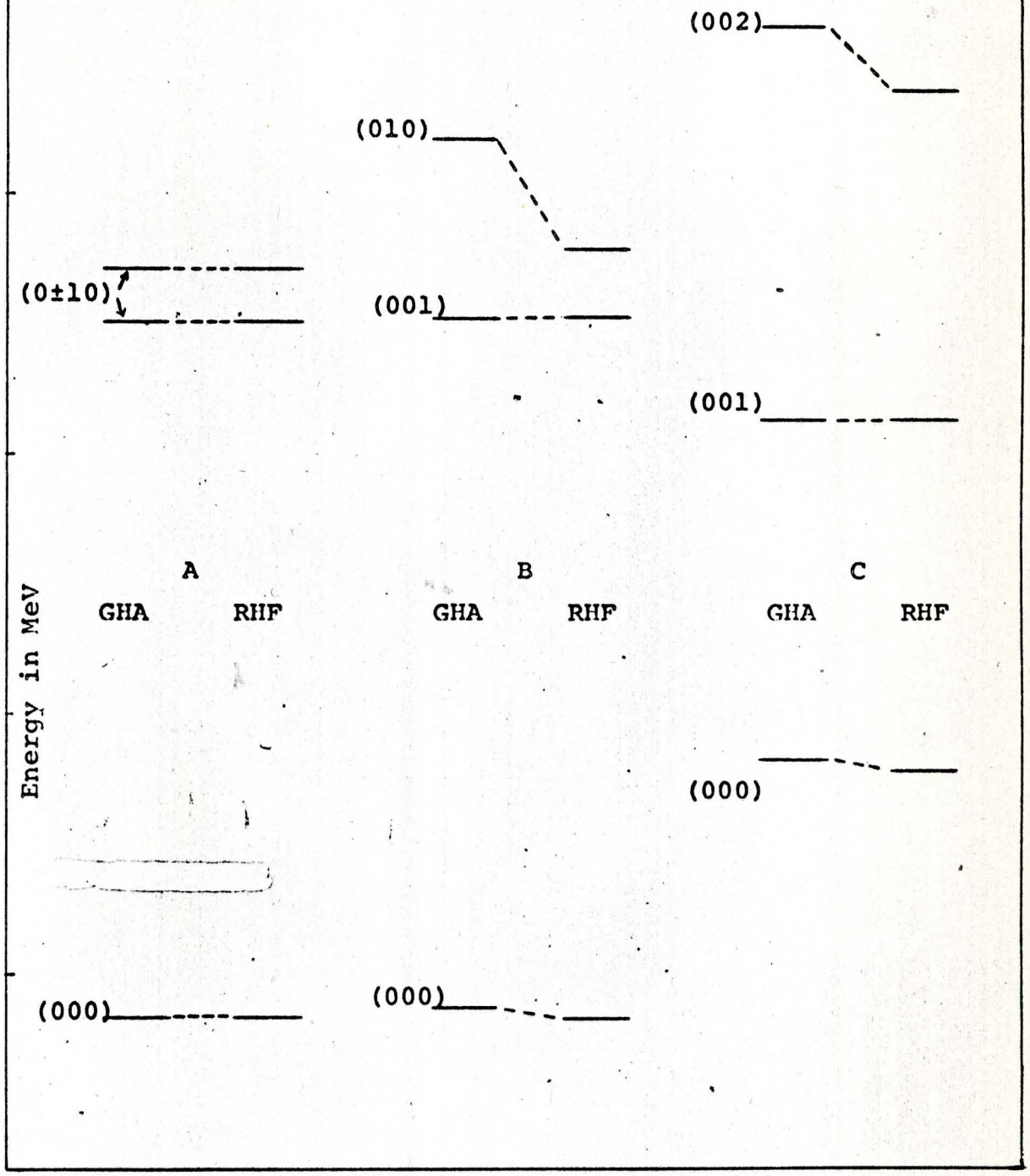

FIGURE 26. OXYGEN 16 SINGLE PARTICLE LEVELS

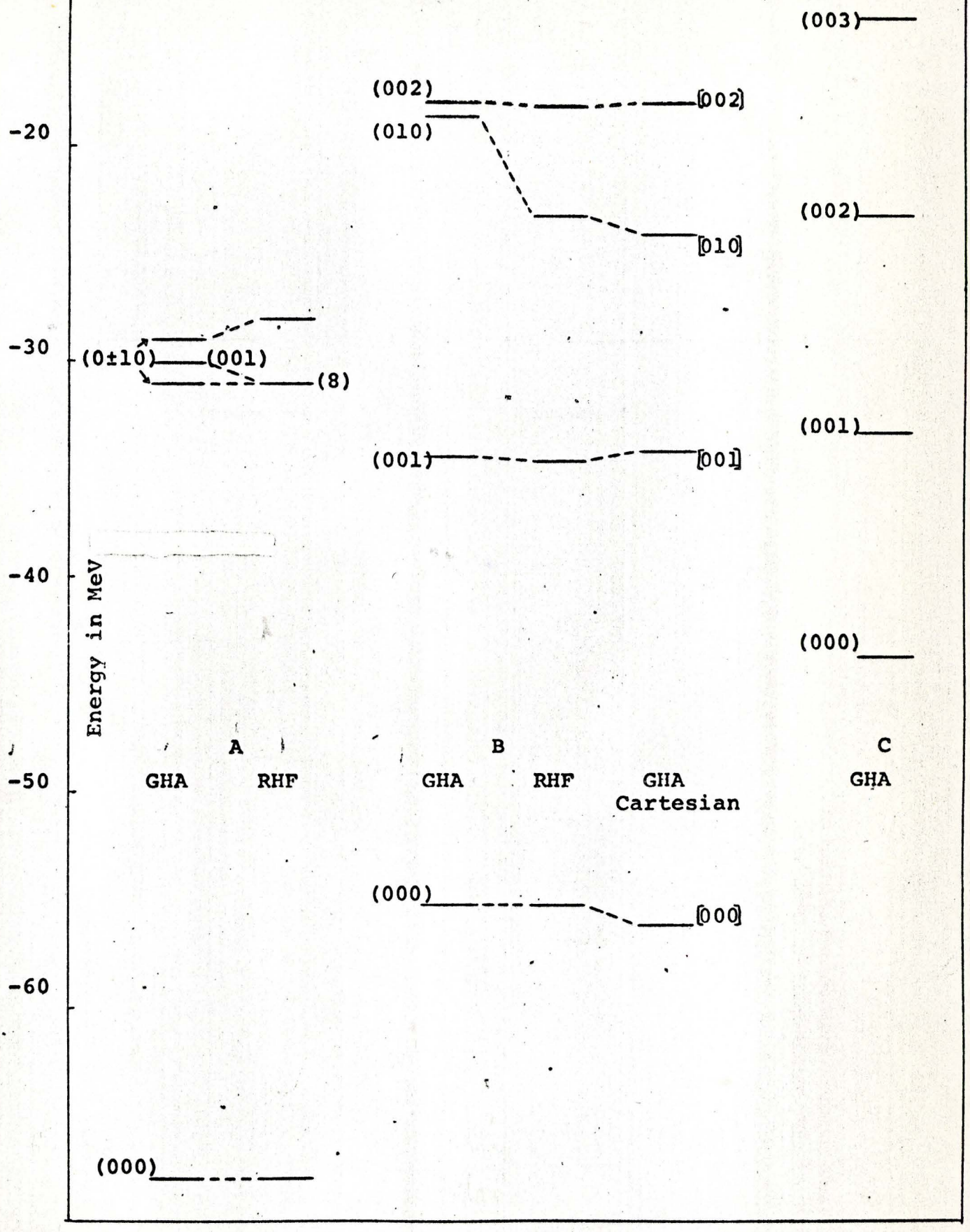

FIGURE 27. NEON 20 SINGLE PARTICLE LEVELS

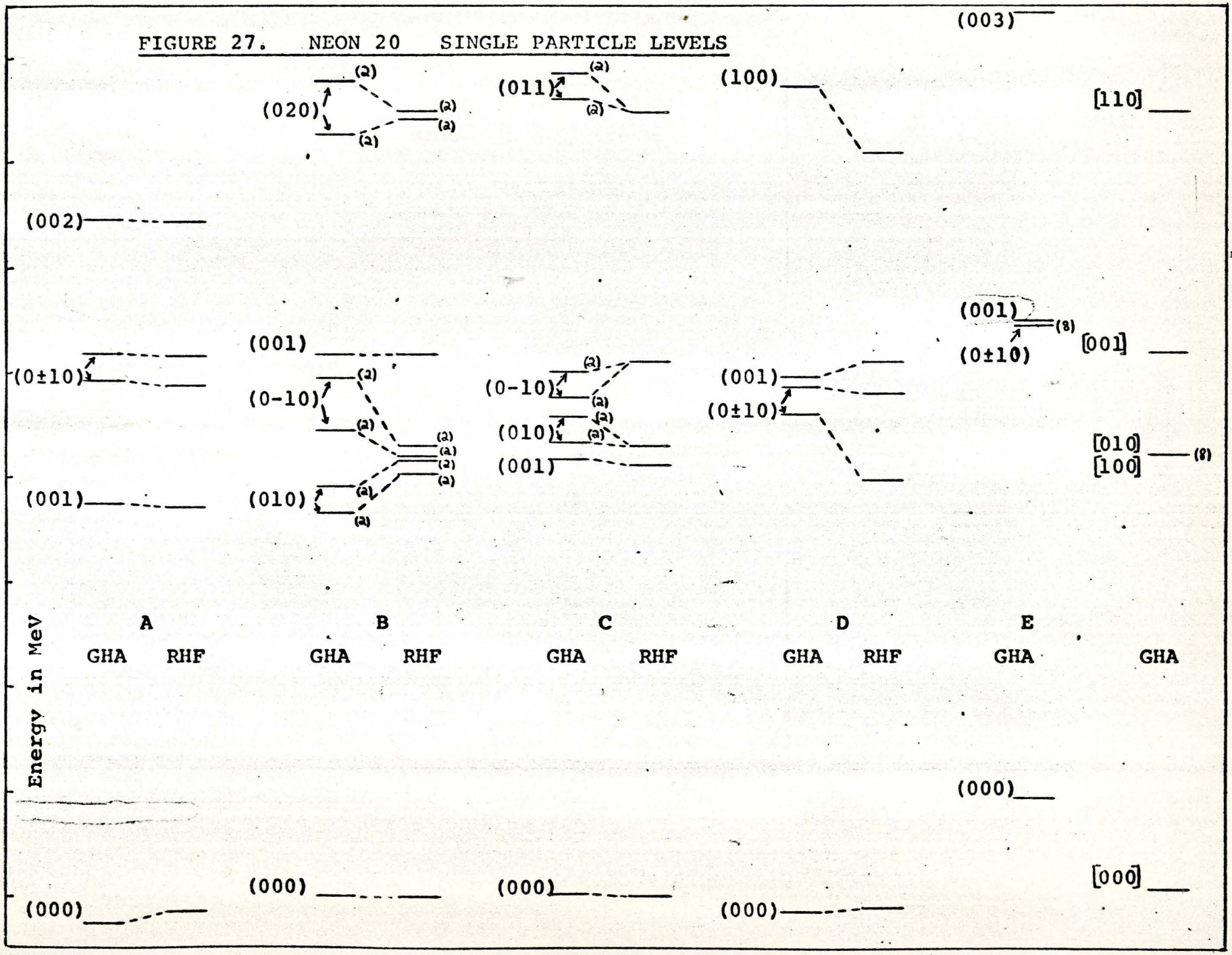

FIGURE 28. MAGNESIUM 24 SINGLE PARTICLE LEVELS

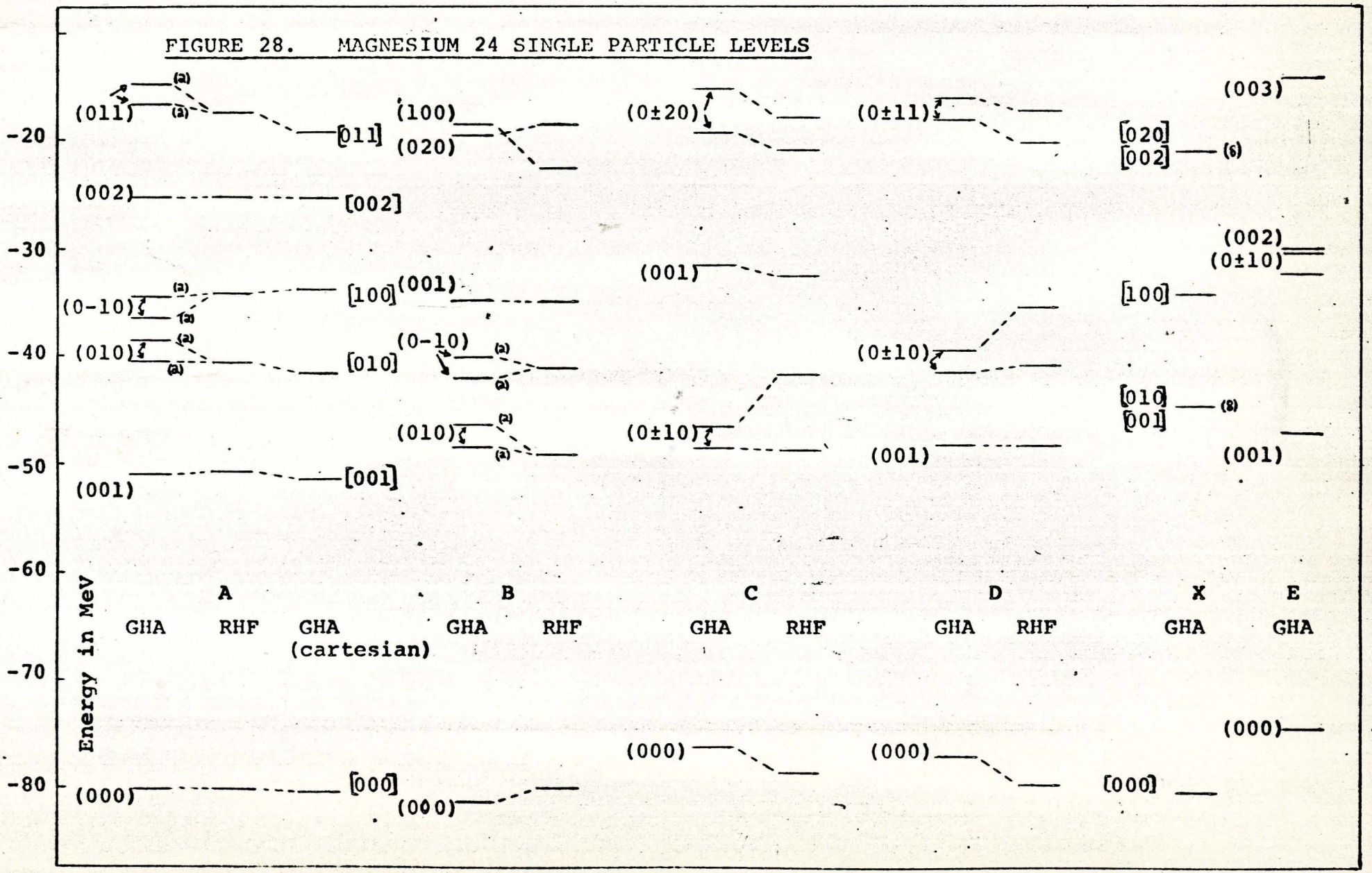

FIGURE 29. SILICON 28 SINGLE PARTICLE LEVELS

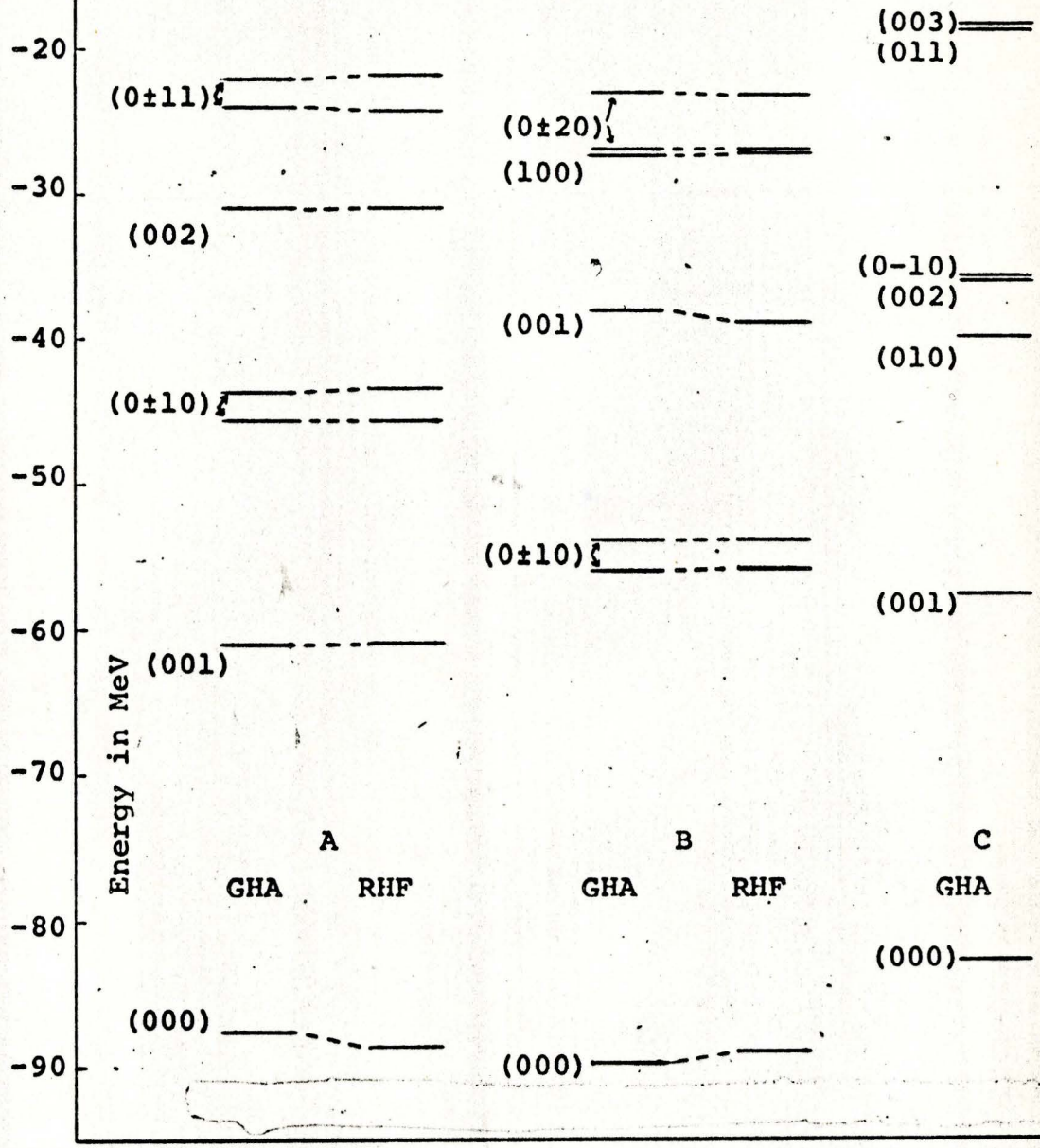

FIGURE 30. SULPHUR 32 SINGLE PARTICLE LEVELS

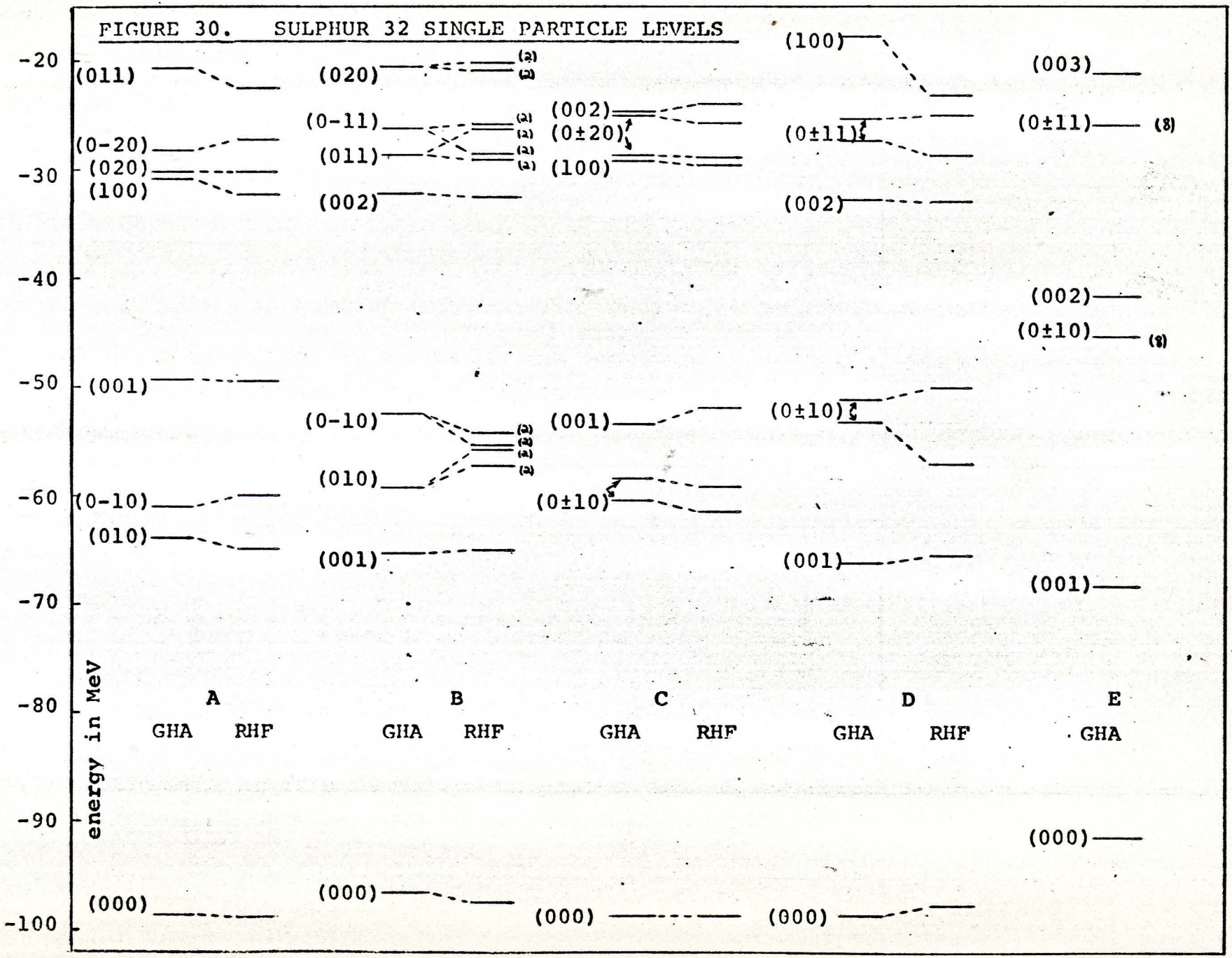

FIGURE 31. ARGON 36 SINGLE PARTICLE LEVELS

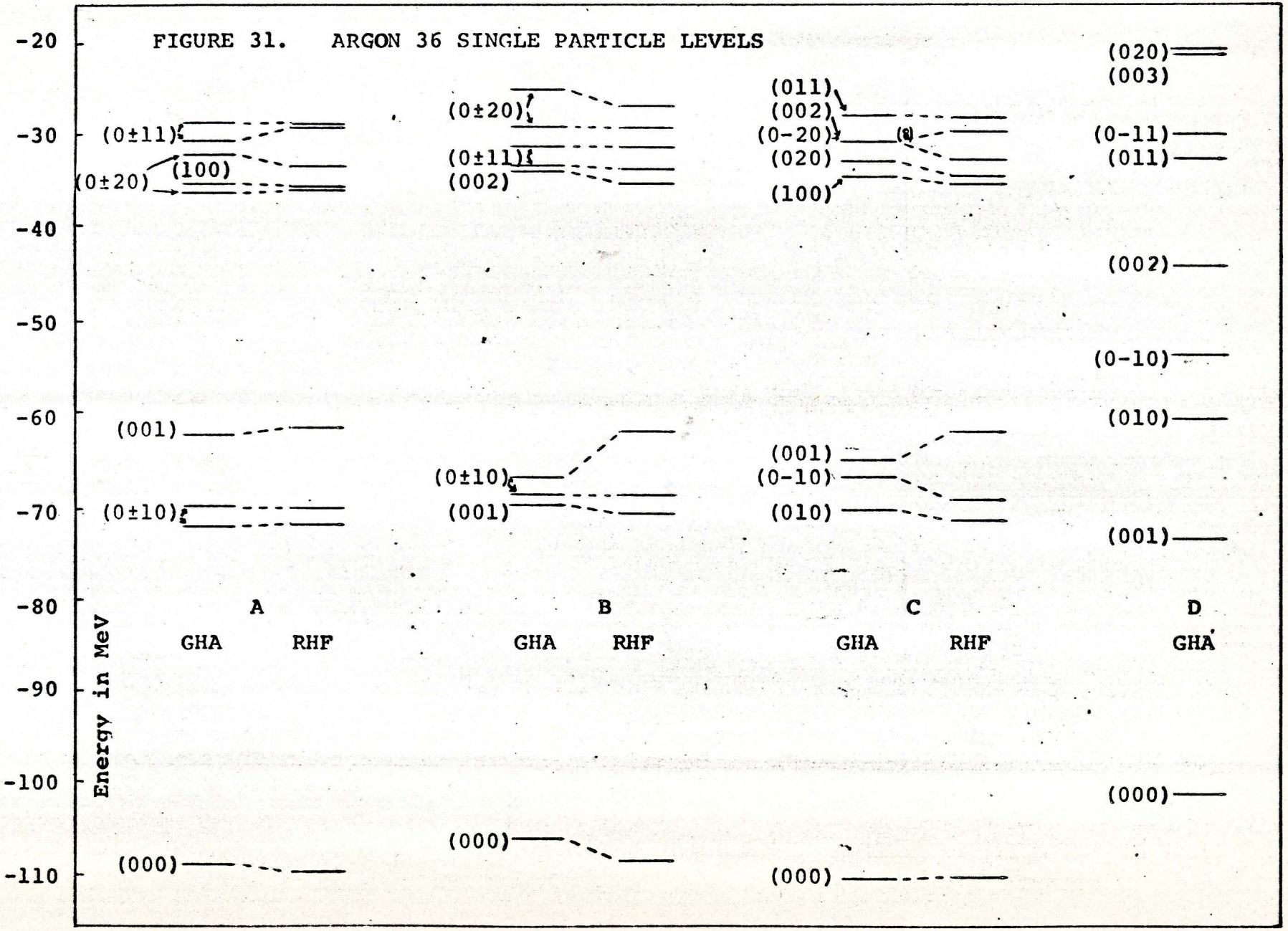

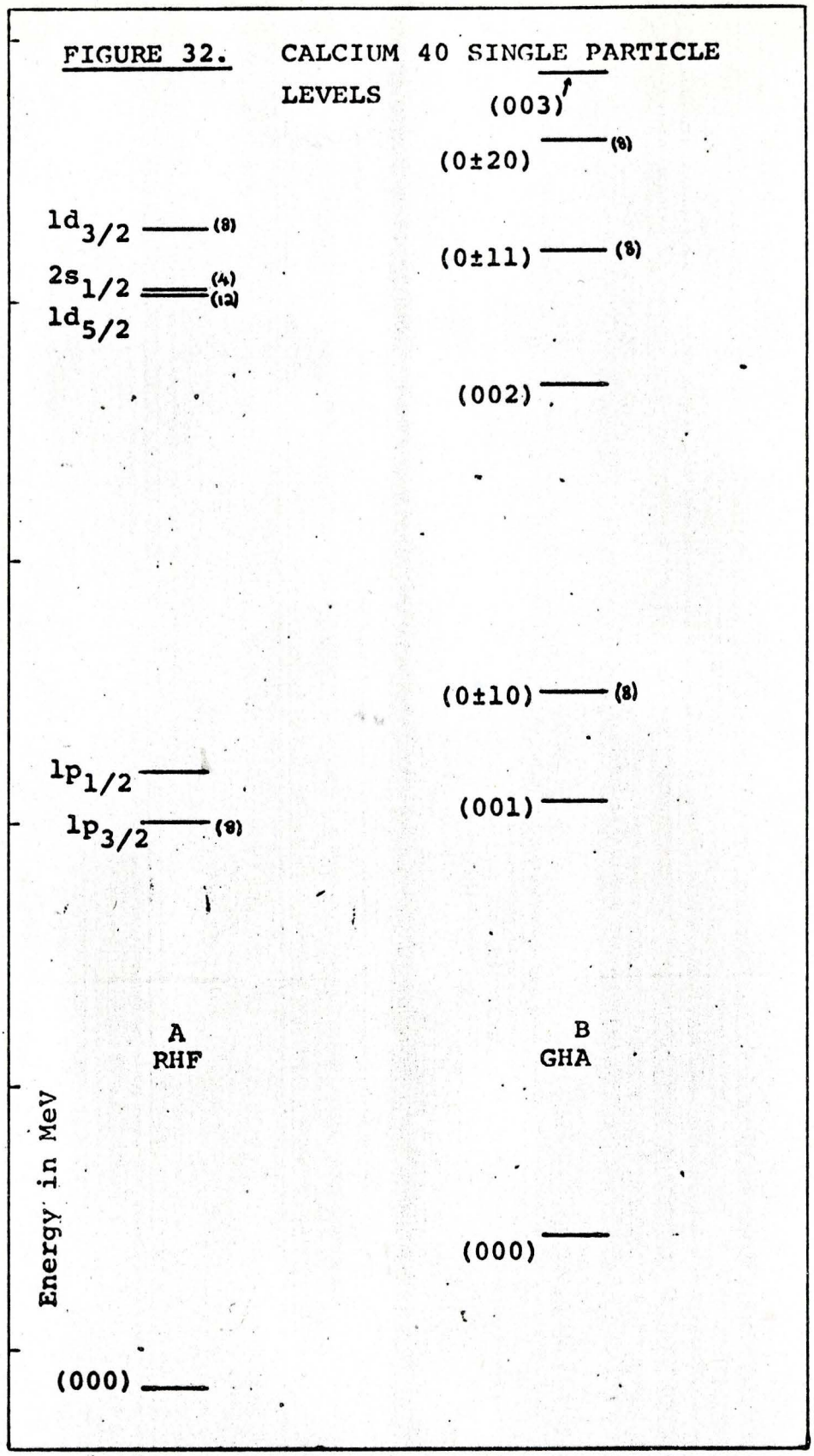
FIGURE 32. CALCIUM 40 SINGLE PARTICLE LEVELS
(003)
(0±20)
(8)
1d3/2
(8)
(0±11)
(8)
2s1/2
(4)
(12)
1d5/2
-40
(002)
-60
(0±10)
(8)
1p1/2
(001)
-80
1p3/2
(8)
A
RHF
B
GHA
-100
Energy in MeV
(000)
-120
(000)

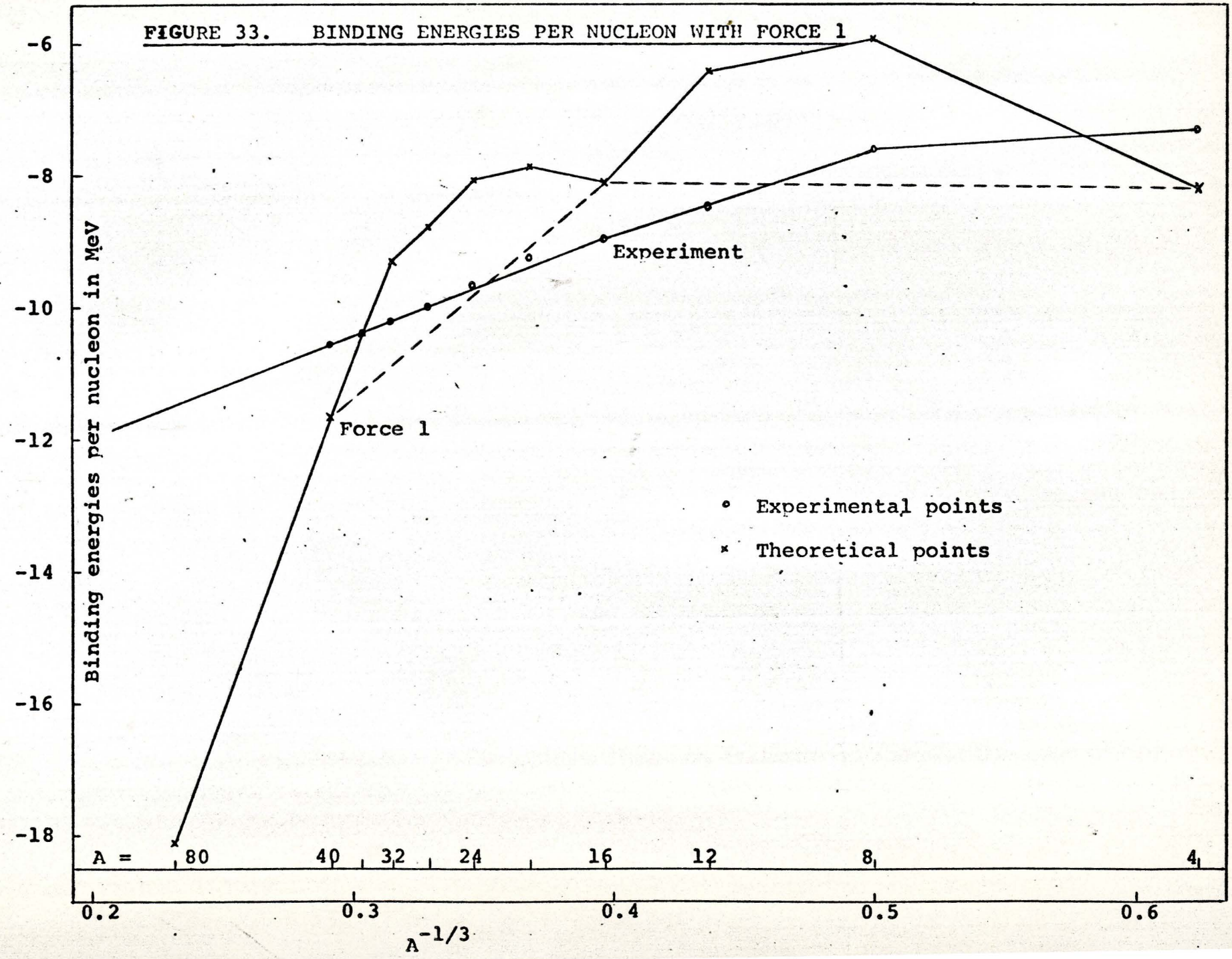
FIGURE 33. BINDING ENERGIES PER NUCLEON WITH FORCE 1
-6
-8
-10
-12
-14
-16
-18
Binding energies per nucleon in MeV
Experiment
Force 1
Experimental points
Theoretical points
A = 80 40 32 24 16 12 8 4
0.2 0.3 0.4 0.5 0.6
$A^{-1/3}$

FIGURE 34. RMS RADII WITH FORCE 1

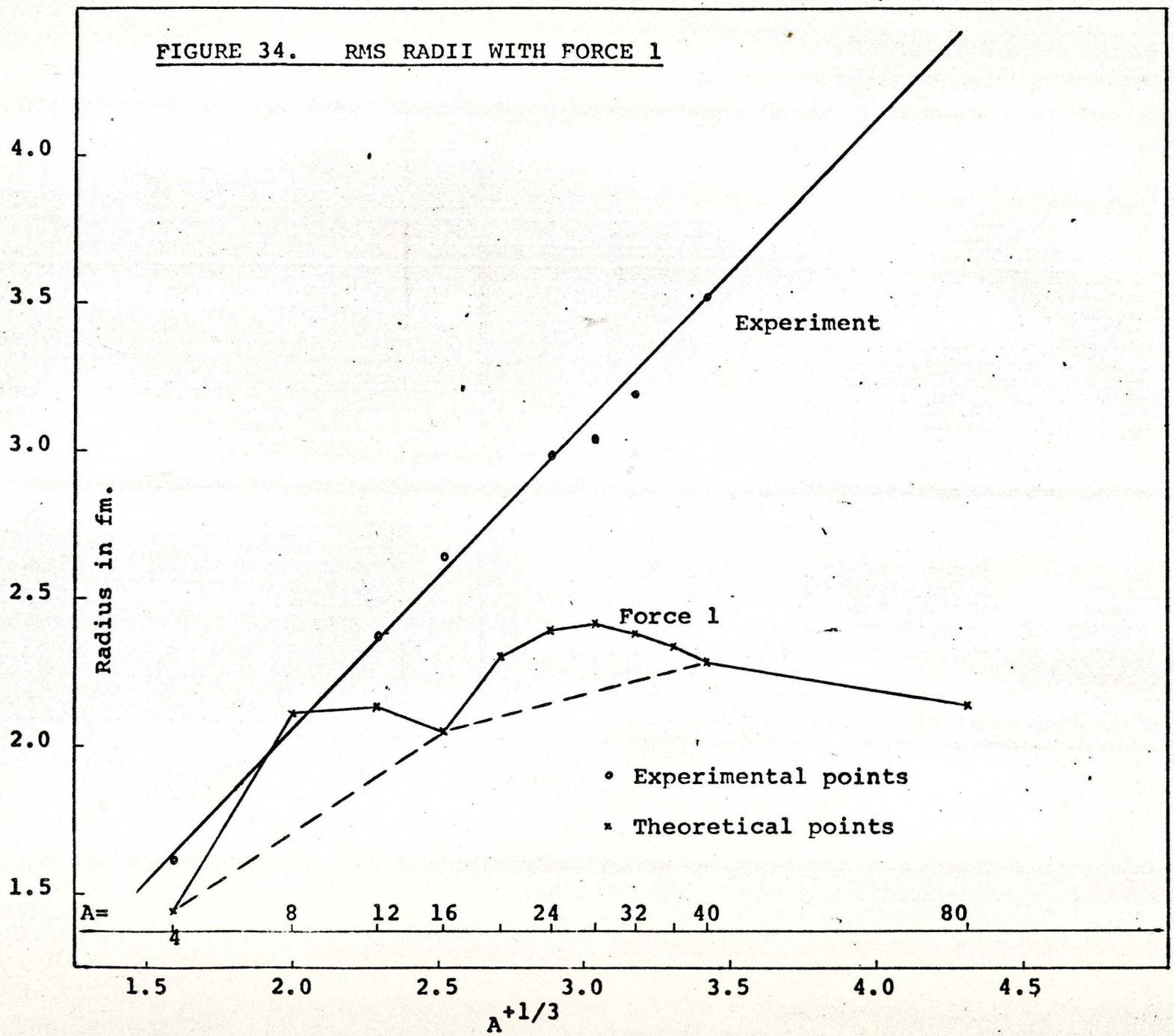

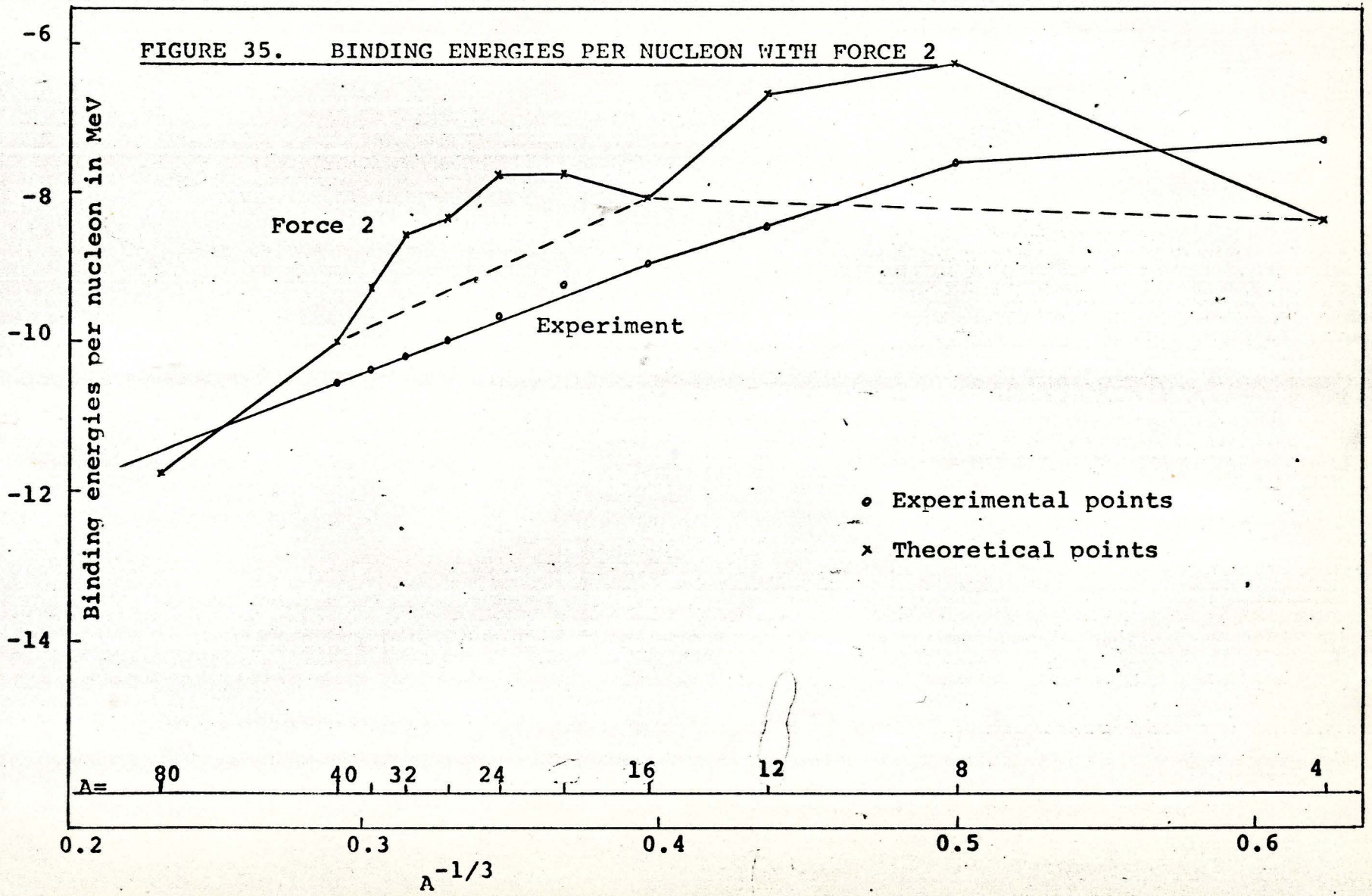
FIGURE 35. BINDING ENERGIES PER NUCLEON WITH FORCE 2
Binding energies per nucleon in MeV
-6
-8
-10
-12
-14
Force 2
Experiment
Experimental points
Theoretical points
A=
80
40
32
24
16
12
8
4
0.2
0.3
0.4
0.5
0.6
$A^{-1/3}$

FIGURE 36. RMS RADII WITH FORCE 2

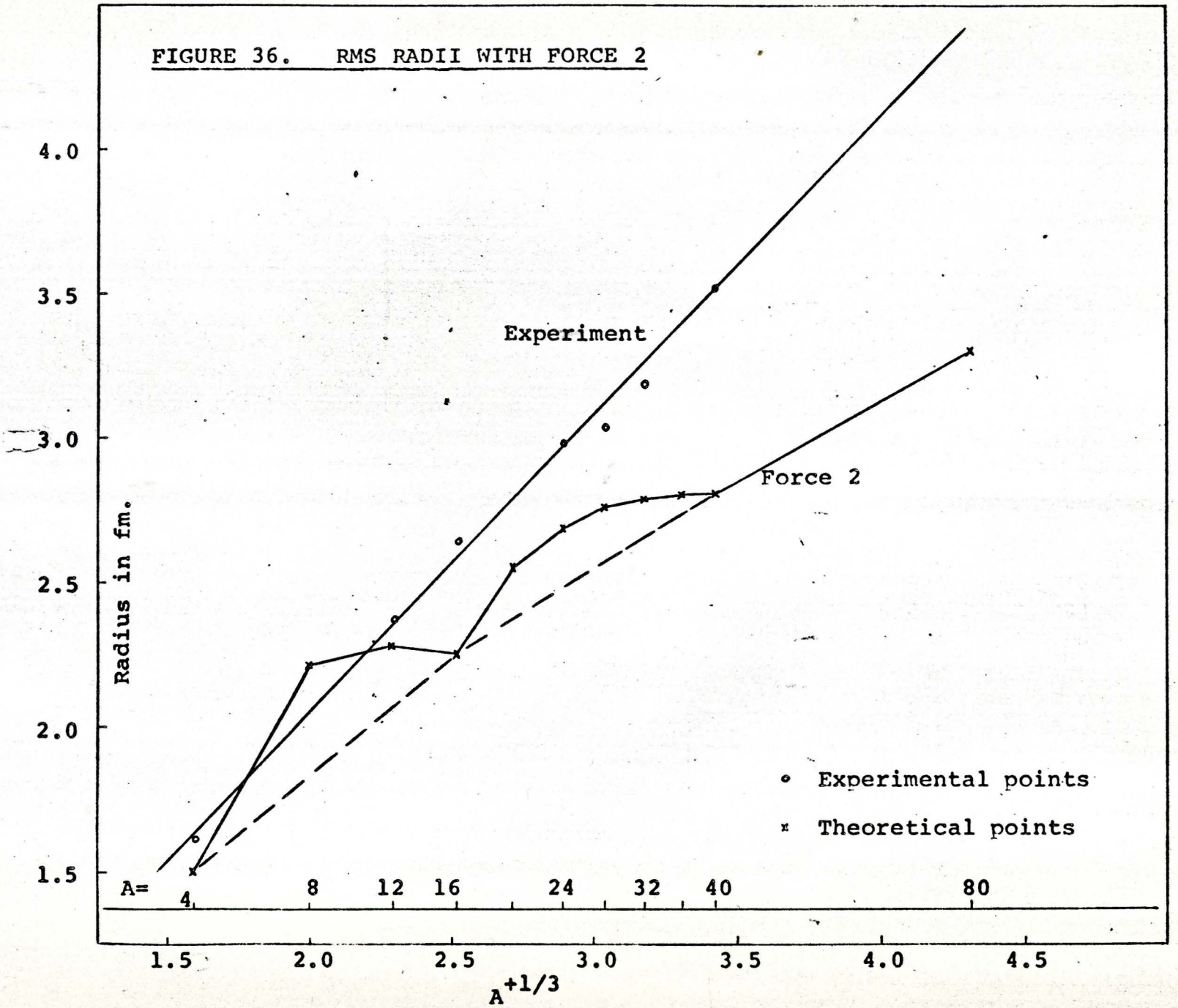

FIGURE 37. BINDING ENERGIES PER NUCLEON WITH FORCE 3

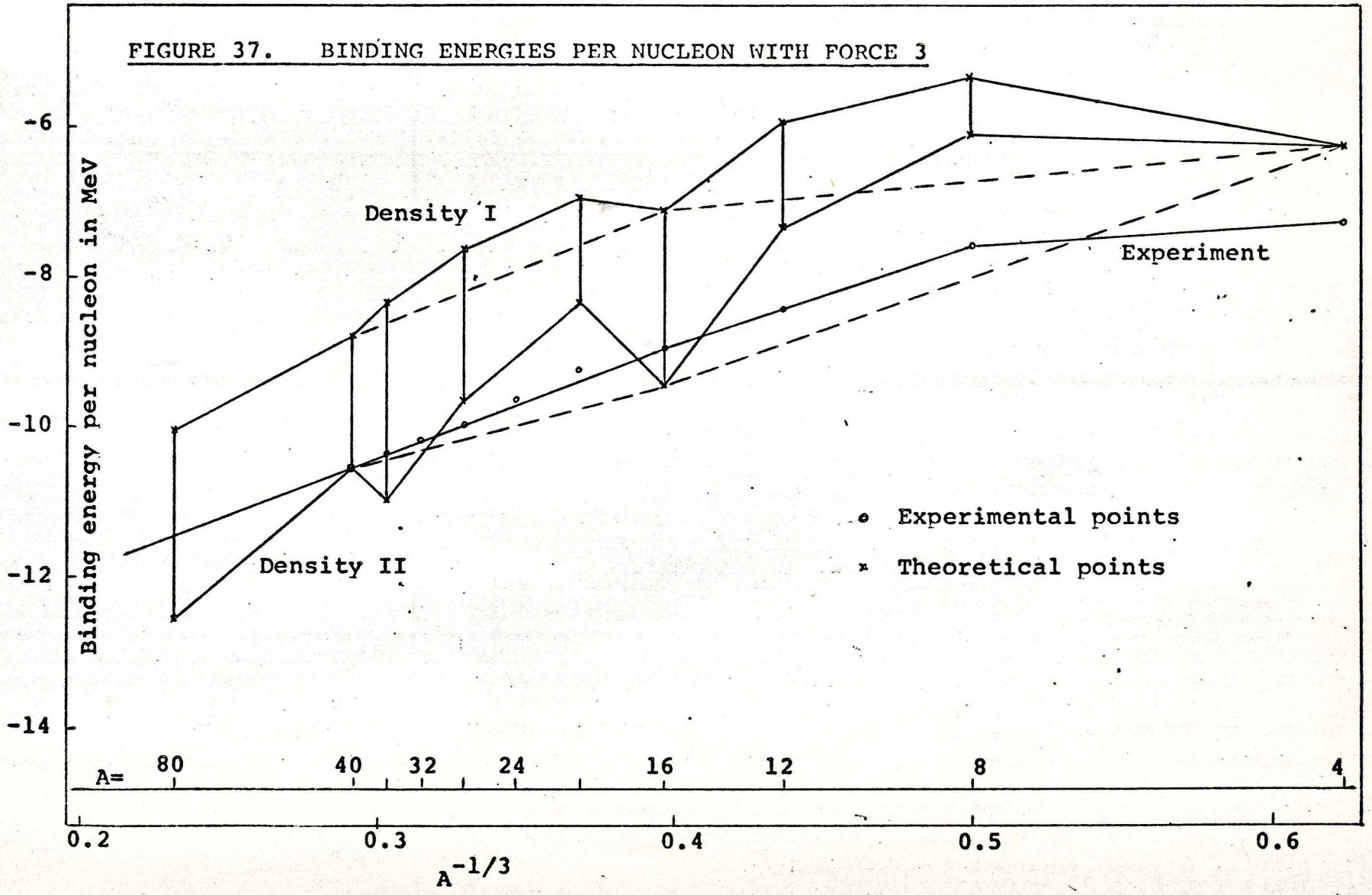

FIGURE 38. RMS RADII WITH FORCE 3

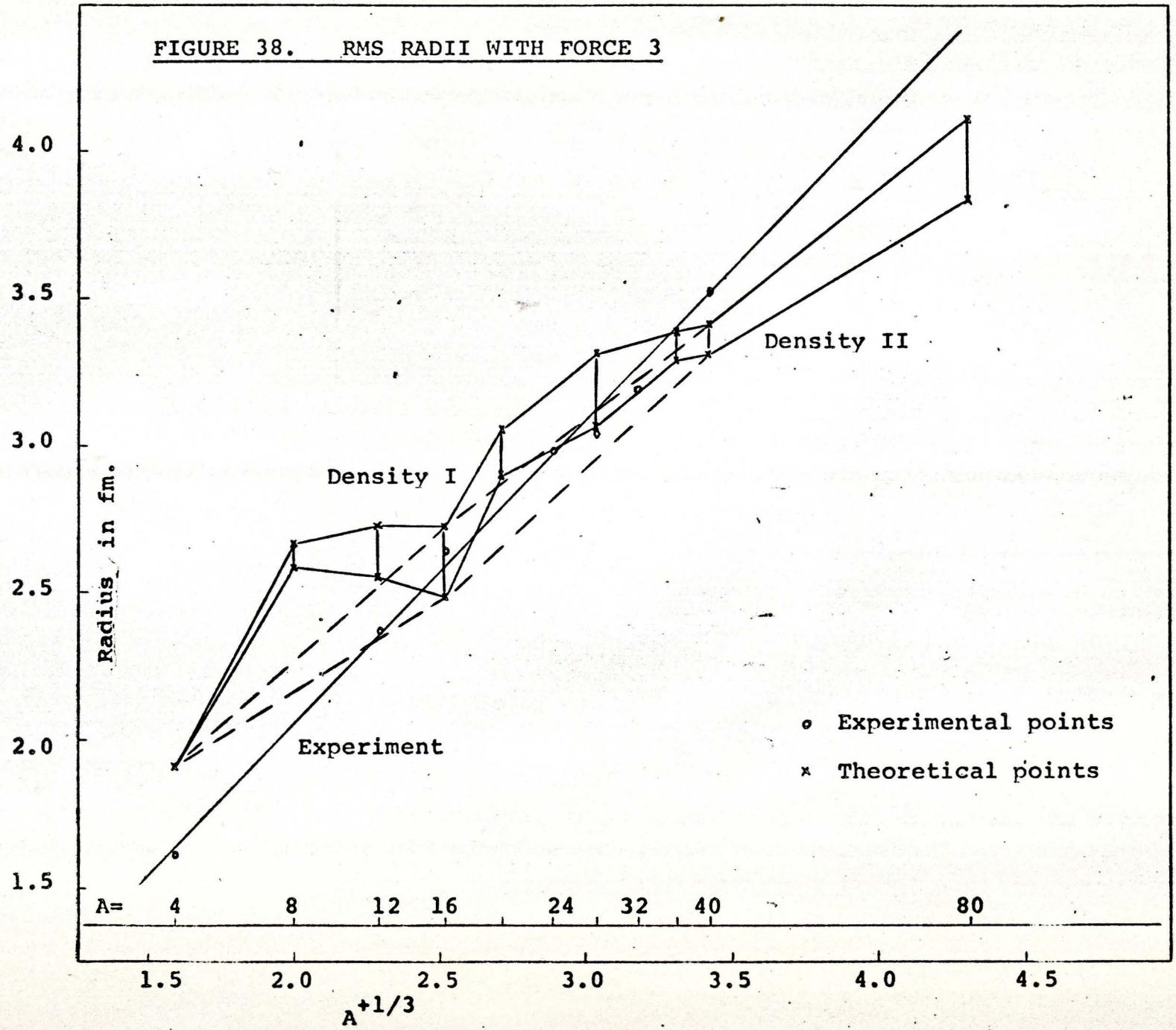

FIGURE 39. BINDING ENERGIES PER NUCLEON WITH FORCE 4

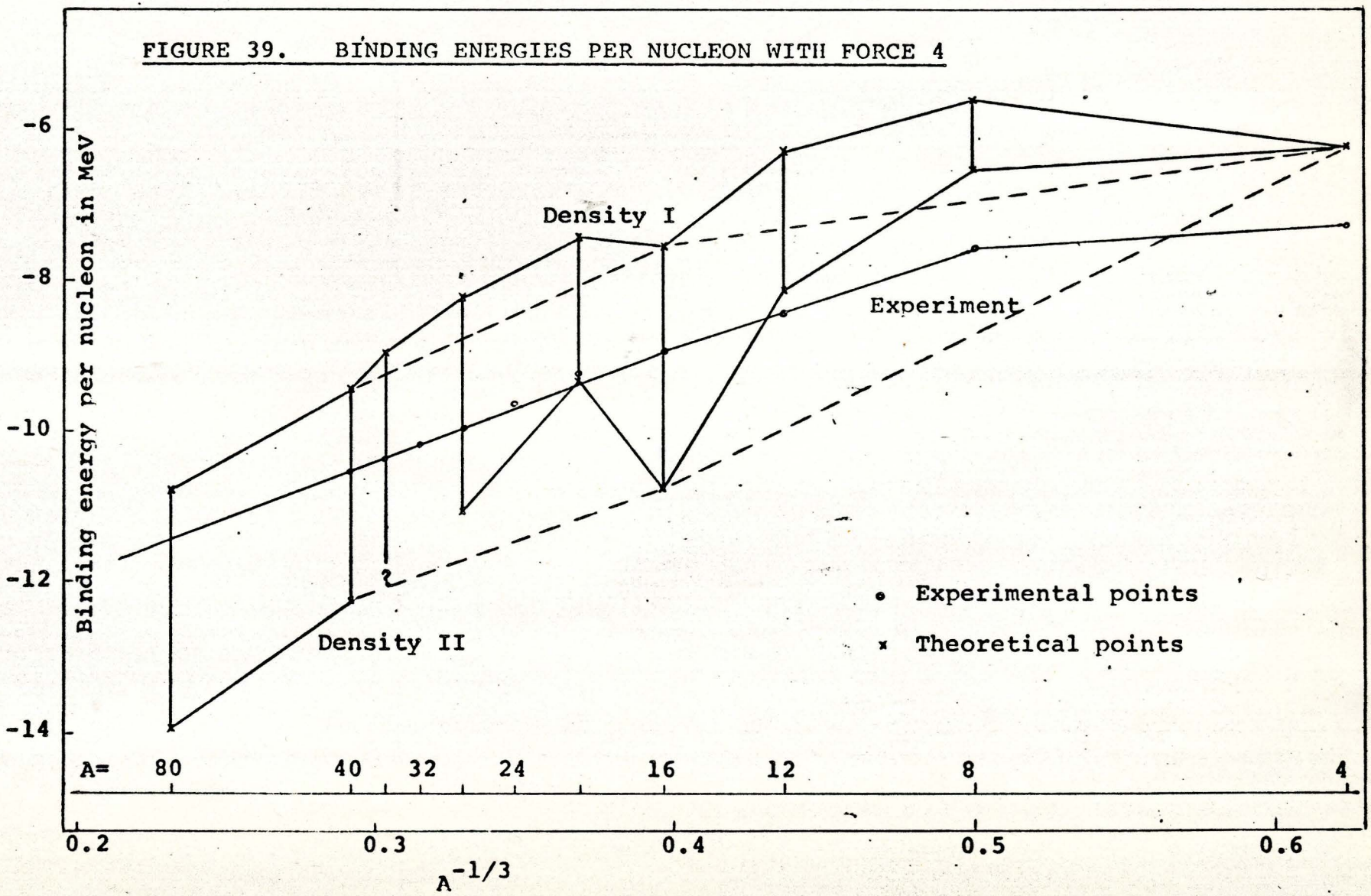

FIGURE 40. RMS RADII WITH FORCE 4